

S-1 MPC

S1-A Annual Performance Report for 2015

Reference: MPC-0139
Nomenclature: DI-MPC-APR
Issue: 1.0
Date: 2016, Mar.29

CLS (siège)
8-10 rue Hermès
Parc technologique du Canal
31520 Ramonville Saint-Agne
FRANCE

Tél. : +33 (0)5 61 39 47 00
Fax : +33 (0)5 61 75 10 14
Mél. : info@cls.fr
Web : www.cls.fr

CLS Brest Le Ponant
Avenue La Pérouse
29280 Plouzané
FRANCE

Tél. : +33 (0)2 98 05 76 80
Fax : +33 (0)2 98 05 76 90





Chronology Issues:

Issue:	Date:	Reason for change:	Author
1.0	29.03.16	Initial release	G.Hajduch P.Meadows

People involved in this issue:

Written by (*):	Peter Meadows	Date + Initials:(visa or ref)
Checked by (*):	G.Hajduch	Date + Initial:(visa ou ref) [Checker]
Approved by (*):	G.Hajduch	Date + Initial:(visa ou ref) [Approver]
Application authorized by (*):		Date + Initial:(visa ou ref)

**In the opposite box: Last and First name of the person + company if different from CLS*

Index Sheet:

Context:	Sentinel-1 Mission Performance Centre
Keywords:	Sentinel-1, Mission Performance Centre, Annual Report
Hyperlink:	

Distribution:

Company	Means of distribution	Names
CLS ESA	Notification	



List of tables and figures

List of tables:

Table 1 Radar Data Base Changes History. 5

Table 2 List of products affected by mis-synchronization 6

Table 3 Estimated PG trends: period APR 2014 - MAY 2015 (co-pol) 7

Table 4 Estimated PG trends : period APR 2014 - MAY 2015 (cross-pol) 8

Table 5 Noise power stability (3-sigma): period JAN 2015 - DEC 2015 (co-pol) 10

Table 6 Average bitrate for each acquisition mode. 13

Table 7 Elevation pointing verification..... 14

Table 8 SM Azimuth and Slant Range Spatial Resolutions 16

Table 9 IW Azimuth and Slant Range Spatial Resolutions 16

Table 10 EW Azimuth and Slant Range Spatial Resolutions 17

Table 11 SM & IW Sidelobe Ratios 17

Table 12: SM ENL & RR Measurements 18

Table 13: IW ENL & RR Measurements..... 18

Table 14: EW ENL & RR Measurements 18

Table 15: Azimuth Ambiguity Ratios 21

Table 16: SLC Relative Radar Cross-Section for the DLR transponders (dB) 25

Table 17: SM SLC Relative Radar Cross-Section for the DLR transponders (dB)..... 26

Table 18: IW & EW SLC Relative Radar Cross-Section for the DLR transponders (dB) 27

Table 19: IW SLC Relative Radar Cross-Section for the DLR transponders (dB) 27

Table 20: EW SLC Relative Radar Cross-Section for the DLR transponders (dB) 27

Table 21: Gain Imbalance using the DLR transponders 33

Table 22: Gain Imbalance using the DLR transponders 34

Table 23: Phase Imbalance using the DLR transponders 35

Table 24 Polarimetric Calibration Measurements..... 36

Table 25: SLC Cross-talk 38

List of figures:

Figure 1 PG gain trend over time (HH and VV) 3

Figure 2 Gain (*left*) and phase (*right*) stability of the SAR antenna tiles (average of the error matrixes in RX, over rows). The intermittent Tile#5 failure events can be recognized (cyan dots). 4

Figure 3 Burst synchronization statistics. 5

Figure 4 PG gain trend over time (HH and VV) 7

Figure 5 PG gain trend over time (VH and HV) 7

Figure 6 PG gain trend over time (closer view May-September 2015) 8



Figure 7 Analysis of the single cal pulses gain over time. *Top*: TX cal, *Mid*: RX-EPDN cal, *Bottom*: TA-APDN cal. 9

Figure 8 Noise power versus time (IW mode). 11

Figure 9 I/Q channel imbalance. 12

Figure 10 Elevation pointing verification with notch acquisitions over Amazon rain forest..... 13

Figure 11 Doppler Centroid versus time. Average on a data-take basis (dots) and daily average (red line). The star-trackers reconfigurations events are marked by the vertical black lines..... 14

Figure 12 SM Azimuth and Slant Range Spatial Resolutions 16

Figure 13 IW Azimuth and Slant Range Spatial Resolutions..... 16

Figure 14 EW Azimuth and Slant Range Spatial Resolutions..... 17

Figure 15: SM SLC Early Azimuth Ambiguity, ESTEC Transponder IRF and Late Ambiguity 19

Figure 16: IW Early Azimuth Ambiguity, ESTEC Transponder IRF and Late Ambiguity (A indicates nominal ambiguity locations and S are ships - the non-nominal ambiguities are between the ambiguities and the IRF mainlobe) 20

Figure 17: EW Early Azimuth Ambiguity, ESTEC Transponder IRF and Late Ambiguity (A indicates nominal ambiguity locations and S are ships - the non-nominal ambiguities are between the ambiguities and the IRF mainlobe) 21

Figure 18: IW Image of SE England (showing the location of the BAE Corner Reflector) and N France with the location of two regions of range ambiguities indicated (acquisition 2nd November 2014, 17:40:53 UT). 22

Figure 19: Extract of middle ambiguity region showing various range ambiguities plus other point targets. 23

Figure 20: Detail of middle ambiguity region (left) and the source of the ambiguity in Rotterdam (right). 23

Figure 21: Detail of middle ambiguity region (left) and the source of the ambiguity in Rotterdam (right). 24

Figure 22: Detail of right ambiguity region (left) and the source of the ambiguity in Waalwijk (right)..... 24

Figure 23: SM SLC Relative Radar Cross-Section for the DLR transponders..... 26

Figure 24: IW SLC Relative Radar Cross-Section for the DLR transponders 26

Figure 25: EW SLC Relative Radar Cross-Section for the DLR transponders 27

Figure 26: IW SLC Relative Radar Cross-Section for the BAE Corner Reflector 28

Figure 27: Example Australian Corner Reflector and Impulse Response 28

Figure 28: Australian CR relative RCS (top, middle) and RCS standard deviation (bottom). 29

Figure 29 Permanent Scatter Calibration Time Series for Stripmap S6 over Chicago 30

Figure 30 Permanent Scatter Calibration Time Series for TopSAR IW over Milan 30

Figure 31: ALE estimates for StripMap and IW SLC product time series using precise state vectors (AUX_POEORB) shortly after the calibration phase and after May 2015. In (a) and (c), each point represents a single SM SLC product over Torny-le-Grand (green) or Dübendorf (black). In (b), red and blue points represent single targets at Torny-le-Grand, while in (d) the points represent single products. Atmospheric path delay correction was applied by UZH in all cases. Bistatic residual correction was applied by UZH in (c) and (d), and the SWST (range) bias, taken from (a), was applied within the S1A processor beginning in May 2015, as can be seen in (c) and (d). 32

Figure 32: Gain Imbalance using the DLR transponders. 34

Figure 33: Phase Imbalance using the DLR transponders. 34



Figure 34: SLC Co-registration Examples 36

Figure 35: SLC Cross-talk Examples 38

Figure 36 Example Updated Azimuth Antenna Pattern..... 39

Figure 37: NESZ measures for SM. Blue is the measured NESZ and the red lines are the predicted NESZ at minimum and maximum orbital altitudes. 43

Figure 38: NESZ measures for IW. Blue is the measured NESZ and the red lines are the predicted NESZ at minimum and maximum orbital altitudes. 44

Figure 39: NESZ measures for EW. Blue is the measured NESZ and the red lines are the predicted NESZ at minimum and maximum orbital altitudes. 45

Figure 40: NESZ measures for WV. Blue is the measured NESZ and the red lines are the predicted NESZ at minimum and maximum orbital altitudes. 47

Figure 41: An example of Radio Frequency Interference..... 47

Figure 42: An example of Radarsat-2/Sentinel1-A Interference 48

Figure 43: An unusual user anomaly..... 49

Figure 44: Detail of an unusual user anomaly 49

Figure 45: SAR Wind speed compared with reference wind speed for IW mode VV polarization. 51

Figure 46: Significant wave height for the long waves performances for December 2015 in Wave Mode 1 (left) and Wave Mode 2 (right). The model outputs from WW3 are considered as reference here. This is only valid from a statistical point of view. 52

Figure 47: Monthly performances for WV1 (top-left) and WV2 (top-right) and number of acquisitions co-located to reference data for validation for WV1 (bottom-left) and WV2 (bottom-right). Thick solid lines stand for the mean difference between Sentinel-1 and WW3 model significant wave height..... 53

Figure 48: Geophysical Doppler as included in the Level 2 products as a function of radial wind speed (wind speed projected in the line of sight of the radar) for WV1 (left) and WV2 (right). The colour code indicates the latitude. 54

Figure 49: Doppler bias as a function of latitude estimated over ocean (blue) and land (brown). 55

Figure 50: Geometric Doppler, data Doppler, and EM Doppler differences between wv1 and wv2 acquired over rain forest areas in VV (left) and HH (right) polarizations. 55

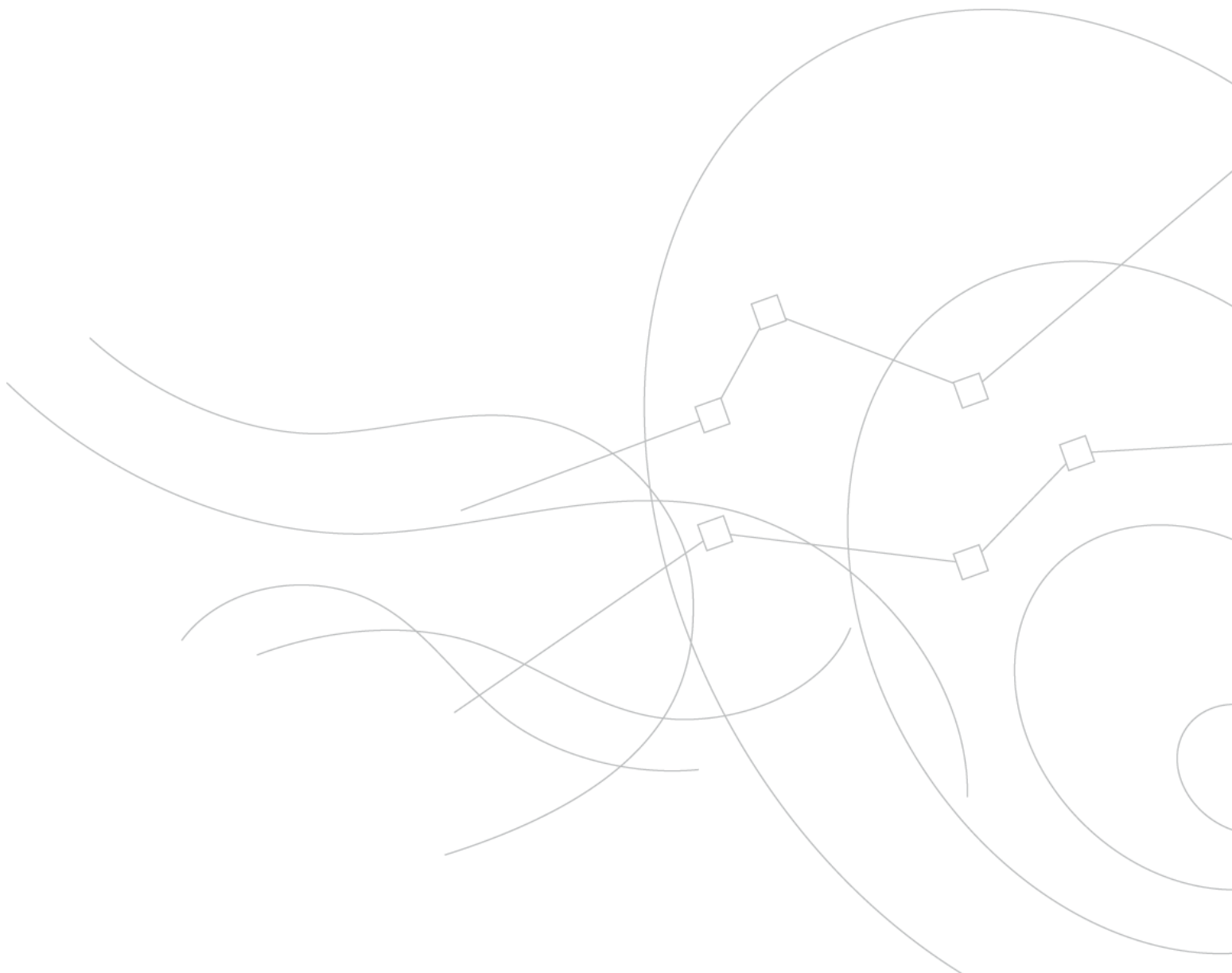
Figure 51: Radial velocity field from Sentinel 1A IW RVL product acquired over Agulhas in ascending mode. Here land areas are used to calibrate the Doppler anomaly before computing the radial velocity. A clear signature of the Agulhas current is observed as well as wind/wave induced velocity..... 56

Figure 52: Left: EM doppler offset computed from antenna model with error matrix corresponding to the day of acquisition. Right: Doppler offset computed from rain forest data. Upper panel is S1A IW mode and lower panel is EW mode. 57

Figure 53: RVL product Doppler offset in azimuth before (black) and after (red) de-scalloping for each swath of IW mode. The data are acquired over rainforest, and the azimuth profiles area obtained by averaging in range. 57

Applicable documents

- [AD-01] Sentinel-1 Product Specification, S1 RS-MDA-52-7441, Issue 3/1, October 2015
- [AD-02] Sentinel-1 Product Definition, S1-RS-MDA-57-7440, Issue 2/6, July 2015
- [AD-03] Sentinel-1 IPF Detailed Algorithm Definition, S1-TN-MDA-52-7445, Issue 1/6, November 2014
- [AD-04] Sentinel-1 IPF Auxiliary Product Specification, S1-RS-MDA-52-7443, Issue 3/0, July 2015





Reference documents

- [S1-RD-01] S1-A MPC Commissioning Phase Report DI-MPC-CPR MPC-0184, Issue 1.3, March 2015.
- [S1-RD-02] Sentinel-1 A Instrument Processing Facility and Operational Product Status After One Year of Operation. Nuno Miranda, Peter Meadows, Adrian Schubert, Alan Pilgrim, David Small, Davide Giudici, Riccardo Piantanida & Guillaume Hajduch. Proceedings of the CEOS SAR Workshop, October 27-29, 2015, ESTEC, Noordwijk, The Netherlands.
(<http://sarvc.ceos.org/documents/doc/154/>).
- [S1-RD-03] Sentinel-1A Radiometric Calibration. Peter Meadows, Alan Pilgrim, Riccardo Piantanida, Davide Riva & Nuno Miranda. Proceedings of the CEOS SAR Workshop, October 27-29, 2015, ESTEC, Noordwijk, The Netherlands.
(<http://sarvc.ceos.org/documents/doc/156/>).
- [S1-RD-04] Calibration with Trihedral Corner Reflectors: A Case Study using Satellite-based X, C and L- Band Frequency Synthetic Aperture Radar Data over Queensland, Australia. Medhavy Thankappan, Matthew Garthwaite, Peter Meadows, Nuno Miranda, Adrian Schubert and David Small. Proceedings of the CEOS SAR Workshop, October 27-29, 2015, ESTEC, Noordwijk, The Netherlands.
(<http://sarvc.ceos.org/documents/doc/193/>).
- [S1-RD-05] Joint Investigations on Radarsat-2,/Sentinel-1 A Mutual RFI. Bjorn Rommen, Itziar Barat, Marielle Chabot, Casey Lambert, Dan Williams. Proceedings of the CEOS SAR Workshop, October 27-29, 2015, ESTEC, Noordwijk, The Netherlands.
- [S1-RD-06] Schubert, A., D. Small, N. Miranda, D. Geudtner, E. Meier. Sentinel-1A Product Geolocation Accuracy: Commissioning Phase Results. Remote Sens. 2015, 7, 9431–9449. doi: 10.3390/rs70709431.
- [S1-RD-07] Schubert, A., D. Small, N. Miranda, D. Geudtner, E. Meier. Sentinel-1A Product Geolocation Accuracy: Beyond the Calibration Phase. Presented at CEOS SAR Calibration & Validation Workshop; Noordwijk, The Netherlands, 2015.
- [S1-RD-08] Small, D., A. Schubert. Guide to ASAR Geocoding, UZH technical note for ESA-ESRIN, Contract No. 20907/07/I-EC, RSL-ASAR-GC-AD, Iss. 1.01; University of Zurich: Zurich, Switzerland, 2008, 36p.
- [S1-RD-09] GMES Sentinel-1 Team. GMES Sentinel-1 System Requirements Document, Ref. S1-RS-ESA-SY-0001, Iss. 3, Rev. 3, 2010.
- [S1-RD-10] Pietro Guccione, Michele Belotti, Davide Giudici, Andrea Monti Guarnieri, Ignacio Navas-TraverSentinel-1A: Analysis of FDBAQ Performance on Real Data, IEEE TRANSACTIONS ON GEOSCIENCE AND REMOTE SENSING, 2015.
- [S1-RD-11] Harald Johnsen, Fabrice Collard, "Sentinel-1 ocean swell wave spectra (OSW) algorithm development", [S1-AD-20]-S1-TN-NRT-52-7450, Issue 1, Revision 1, November 2010.

List of Contents

1. Introduction	1
1.1. Purpose of the document	1
1.2. Structure of the document	1
2. Executive Summary	2
3. Instrument Status	3
3.1. Antenna Status	3
3.2. Instrument Unavailability	4
3.3. Auxiliary Data File Updates	4
3.4. Radar Data Base Updates	4
3.5. Orbit Manoeuvres	5
3.6. Burst synchronization	5
3.7. Internal Calibration	7
3.7.1. Noise power monitoring	10
4. Products Status	12
4.1. Level 0 Products	12
4.1.1. Timeline and missing lines	12
4.1.2. I/Q statistics	12
4.1.3. FDBAQ	12
4.1.4. Instrument Pointing	13
4.2. Level 1 Products	14
4.2.1. Level 1 Processor Updates	14
4.2.2. Image Quality	15
4.2.2.1. Spatial Resolution	16
4.2.2.2. Sidelobe Ratios	17
4.2.2.3. ENL and Radiometric Resolution	17
4.2.2.4. Ambiguity Analysis	18
4.2.2.4.1. Azimuth Ambiguities	18
4.2.2.4.2. Unexpected Azimuth Ambiguities	18
4.2.2.4.3. Range Ambiguities	22
4.2.3. Radiometric Calibration	24
4.2.3.1. IW/EW Re-Calibration	25
4.2.3.2. Absolute Radiometric Calibration	25
4.2.3.3. Permanent Scatter Calibration	29
4.2.4. Geometric Calibration	31
4.2.5. Polarimetric Calibration	33
4.2.5.1. Gain Imbalance	33



- 4.2.5.2. Phase Imbalance 34
- 4.2.5.3. Coregistration 35
- 4.2.5.4. Cross-talk..... 37
- 4.2.6. Elevation Antenna Patterns 38**
- 4.2.7. Azimuth Antenna Patterns 38**
- 4.2.8. Noise Equivalent Radar Cross-section..... 39**
- 4.2.9. Summary of Anomalies 47**
 - 4.2.9.1. Radio Frequency Interference47
 - 4.2.9.2. Radarsat-2/Sentinel1-A Mutual Interference48
 - 4.2.9.3. Other Anomalies48
- 4.2.10. Quality Disclaimers 49**
- 4.3. Level 2 products 50**
 - 4.3.1. Wind measurement..... 50**
 - 4.3.1.1. Image Mode (SM-IW-EW)50
 - 4.3.2. Swell Measurement..... 52**
 - 4.3.2.1. Wave Mode52
 - 4.3.3. Radial Velocity Measurement 53**
 - 4.3.3.1. Wave Mode53
 - 4.3.3.2. TOPS Mode55
- Appendix A - List of Acronyms 59**
- Appendix B - S1-A Orbit Cycles and N-Cyclic Reports 60**
- Appendix C - ESA S1-A Technical Reports..... 61**
- Appendix D - S1-A Transmit Receive Module Failures 62**
- Appendix E - S1-A Instrument Unavailability 63**
- Appendix F - S1-A Auxiliary Data Files 65**
- Appendix G - S1-A Orbit Manoeuvres 69**
- Appendix H - S1-A Quality Disclaimers 72**
- Appendix I - S1-A Antenna Pointing 73**



1. Introduction

1.1. Purpose of the document

The purpose of this document is to provide the status on the S1-A instrument and product performance during 2015.

1.2. Structure of the document

The outline of this report is given below:

- Chapter 1 : this introduction
- Chapter 2 : Executive Summary
- Chapter 3 : Instrument Status
- Chapter 4 : Products Status

The following appendices are also provided:

- Appendix A : List of Acronyms
- Appendix B : S1-A Orbit Cycles and N-Cyclic Reports
- Appendix C : ESA S1-A Technical Reports
- Appendix D : S1-A Transmit Receive Module Failures
- Appendix E : S1-A Instrument Unavailability
- Appendix F : S1-A Auxiliary Data Files
- Appendix G : S1-A Orbit Manoeuvres
- Appendix H : S1-A Quality Disclaimers
- Appendix I : S1-A Antenna Pointing



2. Executive Summary

This report gives the status of the Sentinel1-A instrument and products during 2015, the first full year of routine operations since the launch of the satellite in April 2014 and the subsequent commission phase. A summary of this status can also be found in a paper presented at the CEOS SAR workshop at ESTEC in October 2015 (see [S1-RD-02]).

As will be seen in Chapters 3 and 4 many aspects of the instrument and products are considered with the aim of ensuring user's receive high quality products.



3. Instrument Status

Here the status of the S1-A instrument during 2015:

3.1. Antenna Status

The Antenna status is routinely monitored using the dedicated RFC calibration mode. The RFC products are processed in order to generate the Antenna Error Matrix from which it is possible to retrieve the failure and drift of each TRM.

The Figure below shows the antenna Transmit/Receive Module (TRM) status at the end of 2015. Ten (10) failures are counted in total among TX-RX and H-V. A full list of all TRM failures during 2015 is given in Appendix D.

The impact of the failures on the antenna patterns shape is modelled by the antenna model and the data products are compensated accordingly within the level-1 processor.

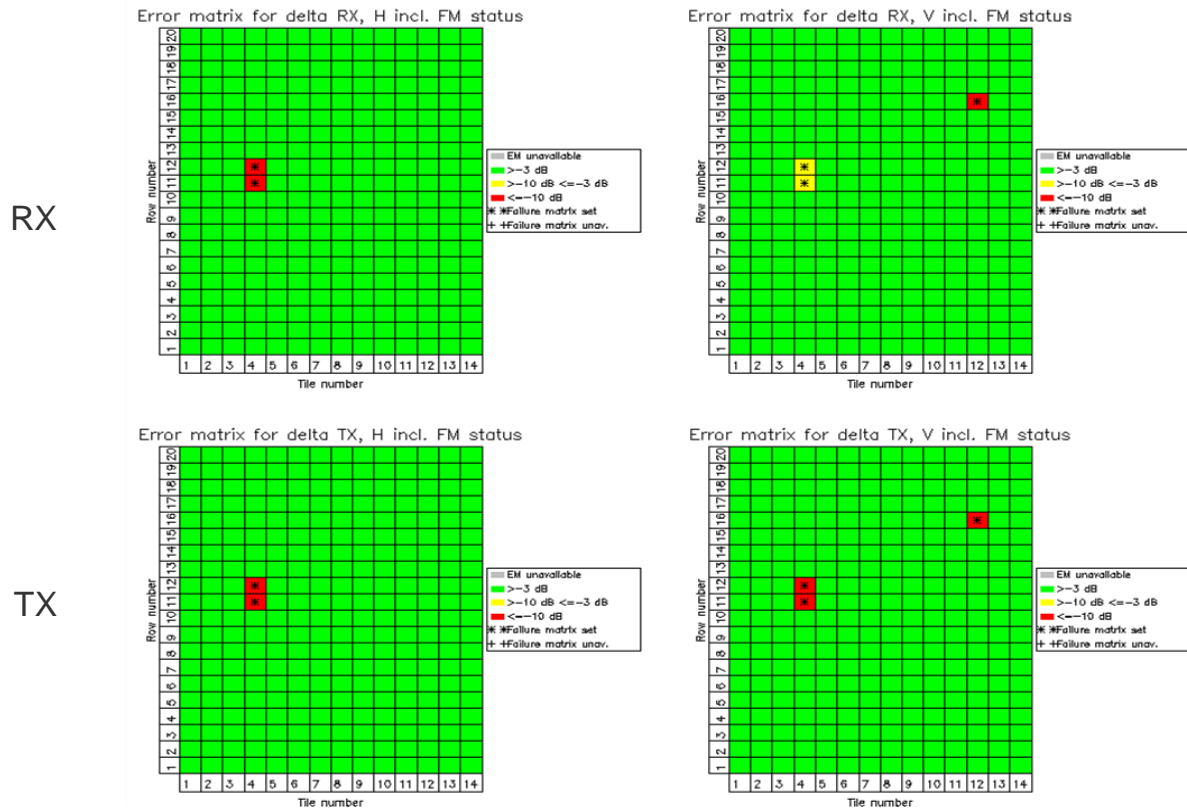


Figure 1 PG gain trend over time (HH and VV)

As reported in Appendix D, Tile #5 showed an intermittent failure in the period October 2014 - July 2015.

The non-nominal behaviour of the tile amplifier (TA) was responsible of power drops (in receive only, both polarizations) affecting the full tile (see Figure 2).

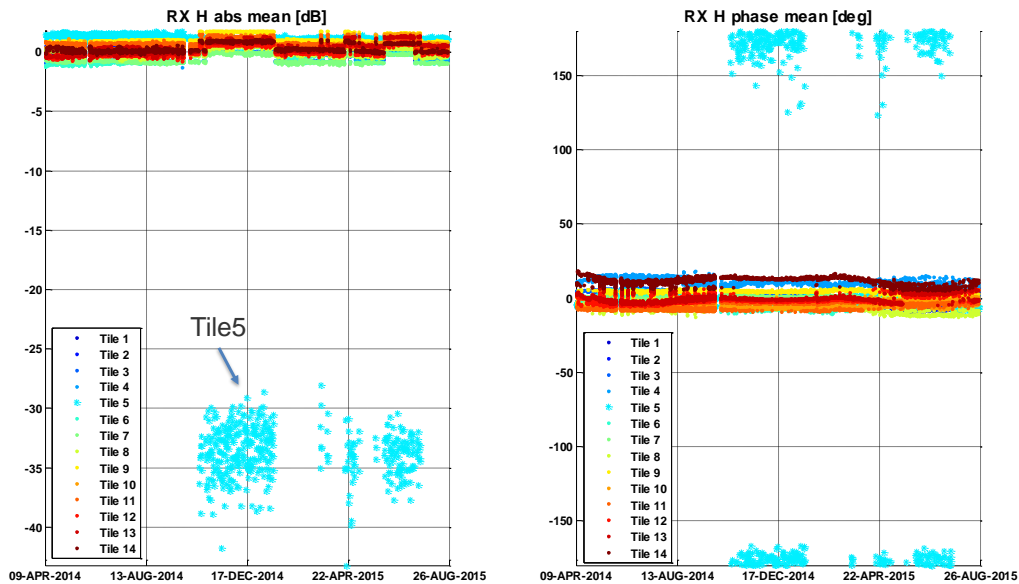


Figure 2 Gain (*left*) and phase (*right*) stability of the SAR antenna tiles (average of the error matrixes in RX, over rows). The intermittent Tile#5 failure events can be recognized (cyan dots).

The tile was switched to redundancy on the 22nd July 2015 and the intermittent failure has disappeared ever since. The Radar Data Base (RDB) ID was set to 5 to mark the switching to redundancy.

Excluding the failed TRMs, the antenna shows overall a stable behaviour: 0.4 dB of average temporal stability for the gain and 5° for the phase have been computed.

3.2. Instrument Unavailability

A summary of the S1-A instrument unavailability during the reporting period is provided together with an explanation is provided. A full list of all instrument unavailabilities during 2015 is given in Appendix E.

3.3. Auxiliary Date File Updates

A summary of S1-A Auxiliary Data Files (ADFs) updates during the reporting period is provided together with an explanation of the updates. A full list of all ADF updates since the S1-A launch is given in Appendix F.

3.4. Radar Data Base Updates

A summary of S1-A Radar Data Base (RDB) updates during 2015 is provided in the following Table.

RDB ID	Date of endorsement	Update reason
RDB #1	4 April 2014	Launch version
RDB #2	16 June 2014	Corrected an error in ECC2 and ECC19



RDB #3	15 September 2014	New instrument gain settings and ADC FSR
RDB #4	17 June 2015	New reference frame for quaternions (ECI 2000)
RDB #5	22 July 2015	Switch to redundancy of antenna tile #5

Table 1 Radar Data Base Changes History.

3.5. Orbit Manoeuvres

A summary of S1-A orbit manoeuvres during the reporting period is provided. A full list of all S1-A orbit manoeuvres since launch is given in Appendix G.

3.6. Burst synchronization

The burst synchronization between repeat pass interferometric acquisitions is relevant for the TOPSAR modes (IW and EW) to provide an indication of the quality of the interferometric phase that can be expected. The SAR acquisition start time is planned over a discrete set of points round orbit with precision down to milliseconds. The performance of the synchronization is monitored by the PDGS OBS tool.

Figure 3 shows the burst synchronization over time for IW and EW mode. Each dot represents a repeat pass acquisition, considering as reference cycle number 43 (10-22 March 2015). It can be noticed that the synchronization is always very high, with the 98.9% of the IW data takes and 96.8% of the EW data takes showing a synchronization better than the 99% of the burst length.

The mis-synchronization event happened on the 18th and 19th of May 2015 is highlighted in the figure. This event was due to a temporary issue that has rapidly been understood and corrected. The list of affected products is reported in Table 2.

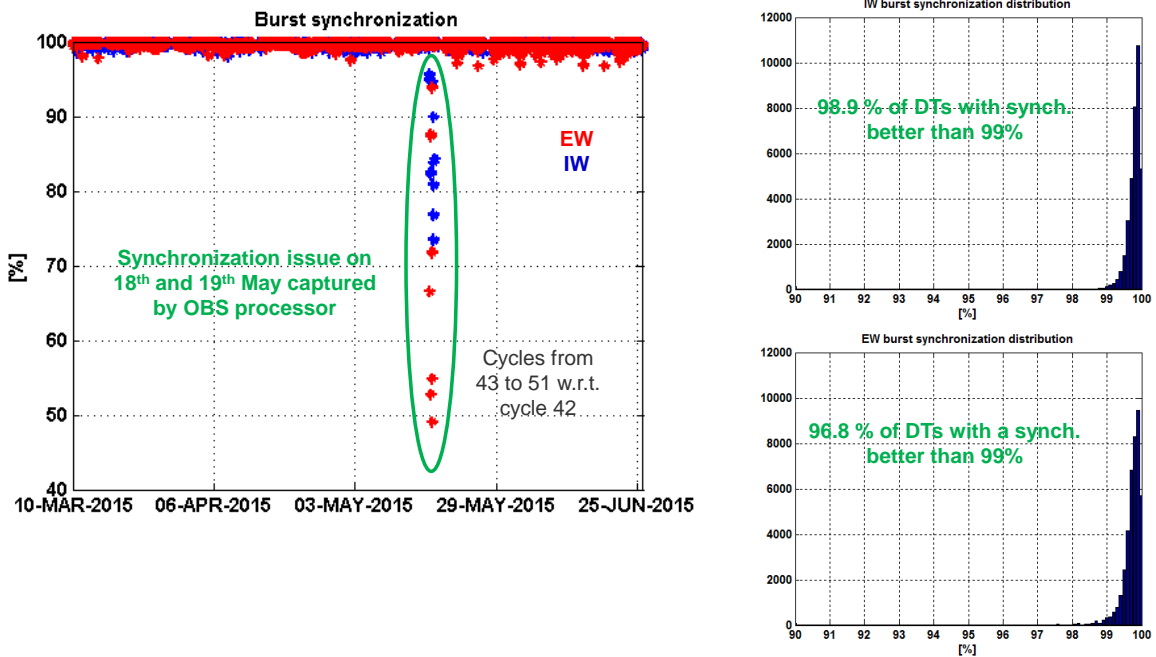


Figure 3 Burst synchronization statistics.



LOA Product name	Mode	Pol.	Start time (GPS)	Stop time (GPS)	Orbit number	Data Take ID
S1A_IW_RAW__0ADV_20150517T073253_20150517T073350_005958_007AD8_5C8C.SAFE	IW	DV	17/05/2015 07:32:53	17/05/2015 07:33:50	005958	007AD8
S1A_EW_RAW__0ASH_20150517T081938_20150517T082310_005958_007ADA_2B7E.SAFE	EW	SH	17/05/2015 08:19:38	17/05/2015 08:23:10	005958	007ADA
S1A_EW_RAW__0ADH_20150517T104733_20150517T105032_005960_007AE2_D470.SAFE	EW	DH	17/05/2015 10:47:33	17/05/2015 10:50:32	005960	007AE2
S1A_IW_RAW__0ASV_20150517T120452_20150517T121119_005961_007AE4_5E5C.SAFE	IW	SV	17/05/2015 12:04:52	17/05/2015 12:11:19	005961	007AE4
S1A_EW_RAW__0ADH_20150517T135501_20150517T140114_005962_007AE9_D97A.SAFE	EW	DH	17/05/2015 13:55:01	17/05/2015 14:01:14	005962	007AE9
S1A_EW_RAW__0ASH_20150517T181216_20150517T181503_005964_007AF4_37AC.SAFE	EW	SH	17/05/2015 18:12:16	17/05/2015 18:15:03	005964	007AF4
S1A_EW_RAW__0ADH_20150517T185122_20150517T185338_005965_007AF7_0169.SAFE	EW	DH	17/05/2015 18:51:22	17/05/2015 18:53:38	005965	007AF7
S1A_EW_RAW__0ADH_20150517T185525_20150517T185728_005965_007AF8_93EE.SAFE	EW	DH	17/05/2015 18:55:25	17/05/2015 18:57:28	005965	007AF8
S1A_EW_RAW__0ASH_20150517T195104_20150517T195427_005965_007AFA_2D52.SAFE	EW	SH	17/05/2015 19:51:04	17/05/2015 19:54:27	005965	007AFA
S1A_IW_RAW__0ASV_20150518T014706_20150518T015037_005969_007B19_6C5D.SAFE	IW	SV	18/05/2015 01:47:06	18/05/2015 01:50:37	005969	007B19
S1A_EW_RAW__0ADV_20150518T020053_20150518T020358_005969_007B1A_0867.SAFE	EW	DV	18/05/2015 02:00:53	18/05/2015 02:03:58	005969	007B1A
S1A_IW_RAW__0ADV_20150518T032350_20150518T032933_005970_007B1E_0640.SAFE	IW	DV	18/05/2015 03:23:50	18/05/2015 03:29:33	005970	007B1E
S1A_IW_RAW__0ASV_20150518T033250_20150518T033521_005970_007B1F_E543.SAFE	IW	SV	18/05/2015 03:32:50	18/05/2015 03:35:21	005970	007B1F
S1A_EW_RAW__0ASH_20150518T040317_20150518T040408_005970_007B20_DCB8.SAFE	EW	SH	18/05/2015 04:03:17	18/05/2015 04:04:08	005970	007B20
S1A_EW_RAW__0ADH_20150518T144130_20150518T144410_005977_007B4B_F7C9.SAFE	EW	DH	18/05/2015 14:41:30	18/05/2015 14:44:10	005977	007B4B

Table 2 List of products affected by mis-synchronization



3.7. Internal Calibration

The instrument gains and phase stability over time is monitored through the gain and phase of the PG-product. Figure 4 below shows the PG-gain over time, for the HH and VV polarization cases. Figure 5 shows the PG trend for the cross-pol cases (VH and HV).

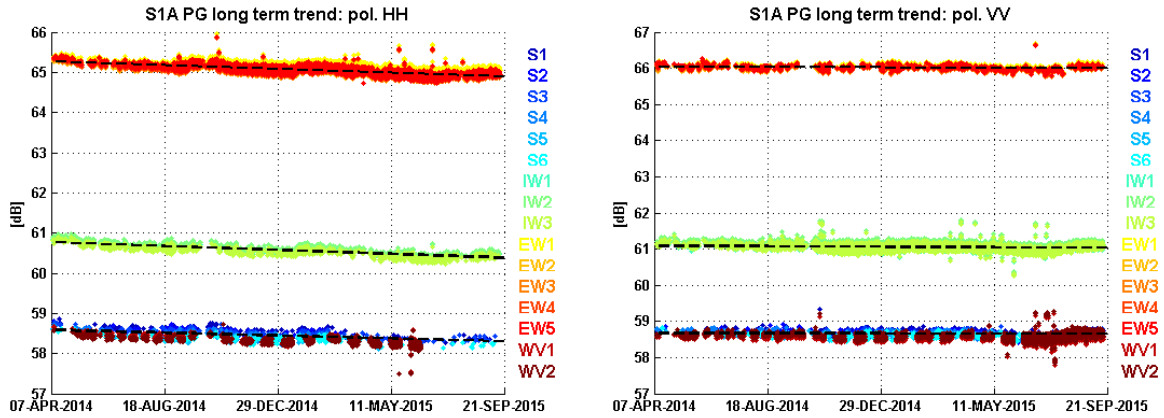


Figure 4 PG gain trend over time (HH and VV)

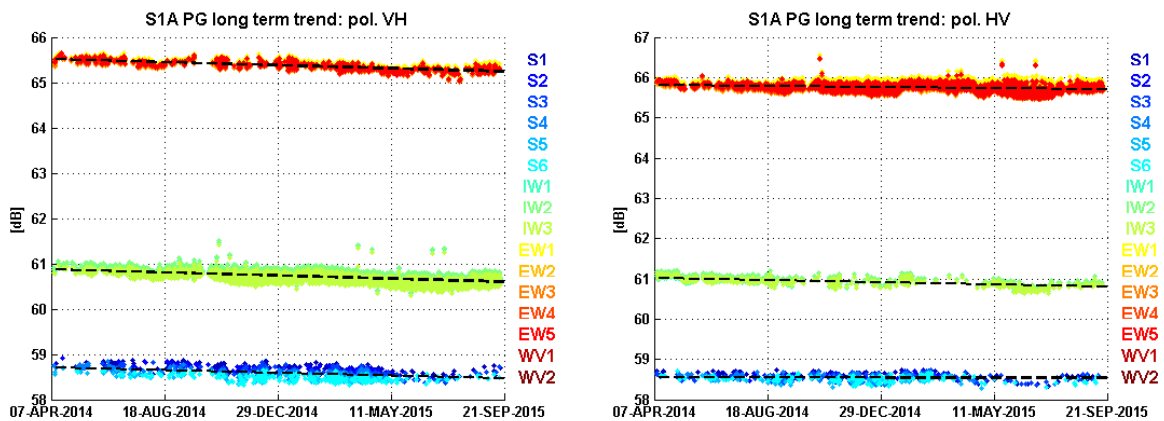


Figure 5 PG gain trend over time (VH and HV)

In the HH case, a linear decay over time can be observed, common to all the swaths. The decay is not visible for the VV case instead. The estimated values of the slope are reported in Table 3 below.

Acquisition Mode	HH	VV
SM	-0.20 dB/year	-0.01 dB/year
IW	-0.26 dB/year	-0.04 dB/year
EW	-0.25 dB/year	-0.02 dB/year
WV	-0.21 dB/year	-0.02 dB/year

Table 3 Estimated PG trends: period APR 2014 - MAY 2015 (co-pol)



A linear decay, similar to the HH case, is noticeable in the VH case. The values of the estimated slopes are reported in Table 4 below.

Acquisition Mode	VH	HV
SM	-0.16 dB/year	-0.01 dB/year
IW	-0.19 dB/year	-0.09 dB/year
EW	-0.18 dB/year	-0.07 dB/year

Table 4 Estimated PG trends : period APR 2014 - MAY 2015 (cross-pol)

The slope of the linear decay appears stable with time up to May 2015, when a change in the slope is observed and the decay ceases. A closer view of the May 2015 - September 2015 period is shown in figure below. The reason of the changed behaviour has been found to be related to an increase of the instrument temperature, in turn related to increased operational use, starting from March 2015.

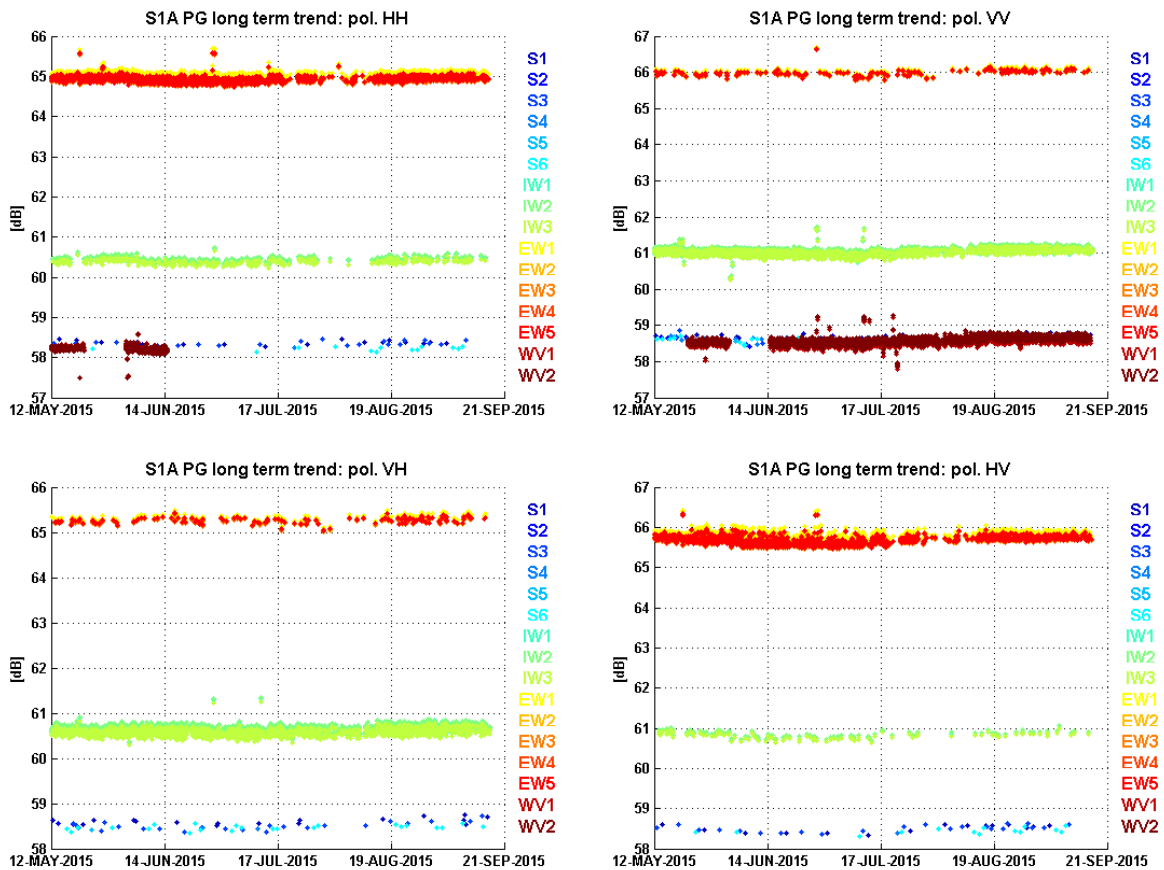


Figure 6 PG gain trend over time (closer view May-September 2015)

It is noted that the evolution of the PG is compensated within the Level 1 processor, so the radiometric quality of the data is preserved.

The source of the decay of the PG gain has been investigated in detail by analysis of the single calibration signals available (TX, RX, TA, APDN, EPDN). Following the signals routing within the

Proprietary information: no part of this document may be reproduced divulged or used in any form without prior permission from CLS.



instrument, the trends affecting the TX, the RX and the TA are compensated by the trends of the APDN and EPDN signals.

From this analysis it can be seen that the TX power shows a decay in both H and V polarizations, that is partially compensated by a positive linear trend of the power in the RX chain (except for the jump visible in September 2014 which is related to the reconfiguration of the instrument receiving gain). The TA does not show a clear increasing or decreasing trend.

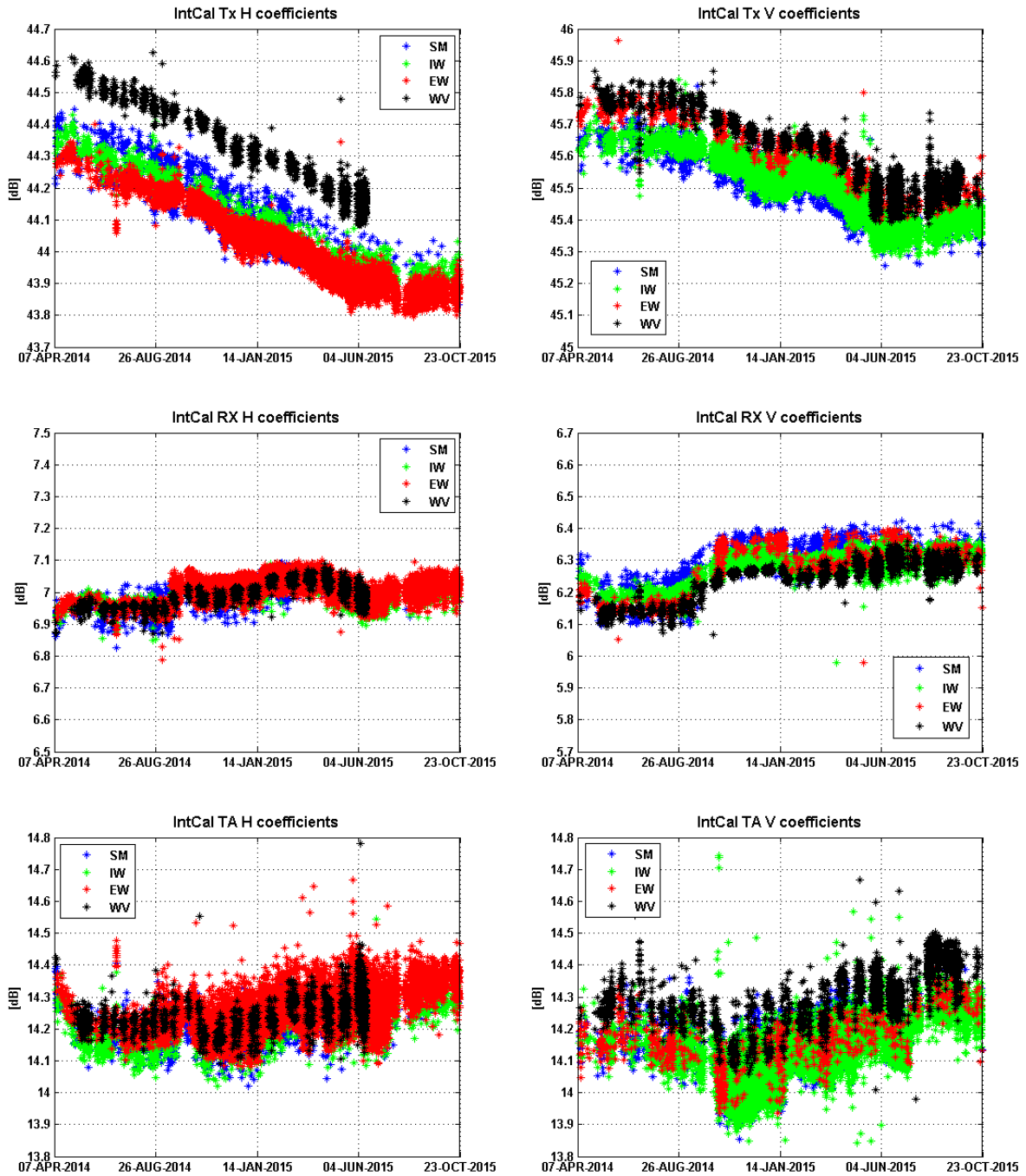


Figure 7 Analysis of the single cal pulses gain over time. *Top*: TX cal, *Mid*: RX-EPDN cal, *Bottom*: TA-APDN cal.



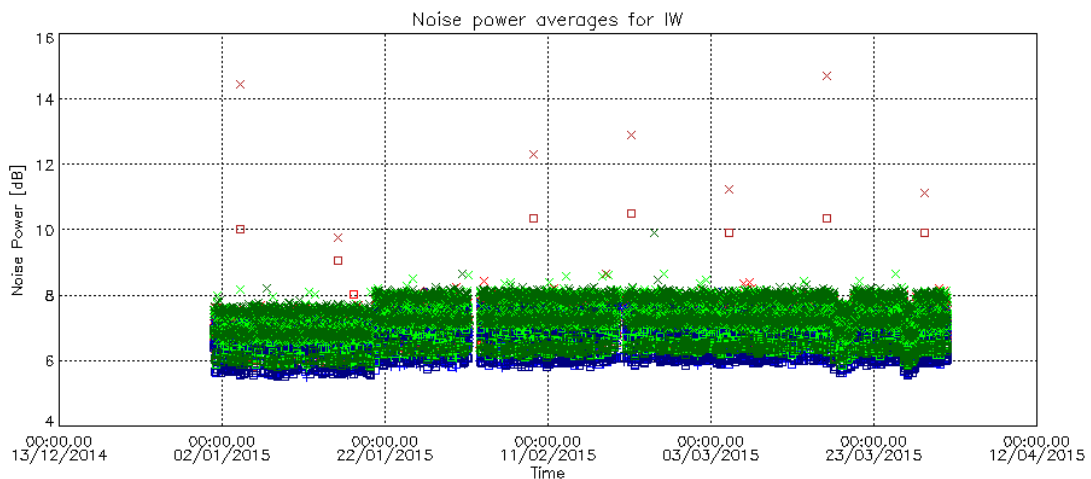
3.7.1. Noise power monitoring

The noise power is monitored through the dedicated internal calibration pulses processing embedded at the start/stop of each data-take. Figure below shows the noise power versus time in the period January-October 2015. Overall, the noise power has a good stability, with a standard deviation of approximately 1 dB in the short term (within one orbit), which can be ascribed to the temperature variation round orbit. The steps that can be observed (for example on the 20th Jan 2015 and throughout March, April and May 2015) are related to the tile #5 intermittent failure events (see section 3.1).

Table below reports the noise power stability (3σ) averaged over the full reporting period, excluding the periods with tile #5 failed. The number in the parenthesis represents the number of products considered.

Acquisition mode	Noise power stability [dB]
SM	HH: 5.0547±1.2351 (740) VV: 5.0354±0.8579 (1774) HV: 5.2224±1.1591 (738) VH: 5.0074±0.9416 (1505)
IW	HH: 6.6026±1.1354 (5277) VV: 7.3686±1.3071 (56168) HV: 7.3223±1.0982 (1515) VH: 6.7131±1.6233 (28753)
EW	HH: 5.2051±1.0725 (65535) VV: 6.1027±1.0160 (3790) HV: 6.3587±0.9133 (41790) VH: 4.9520±1.2131 (3480)
WV	HH: 5.8469±0.7073 (1344) VV: 6.1316±0.6538 (14820)

Table 5 Noise power stability (3-sigma): period JAN 2015 - DEC 2015 (co-pol)



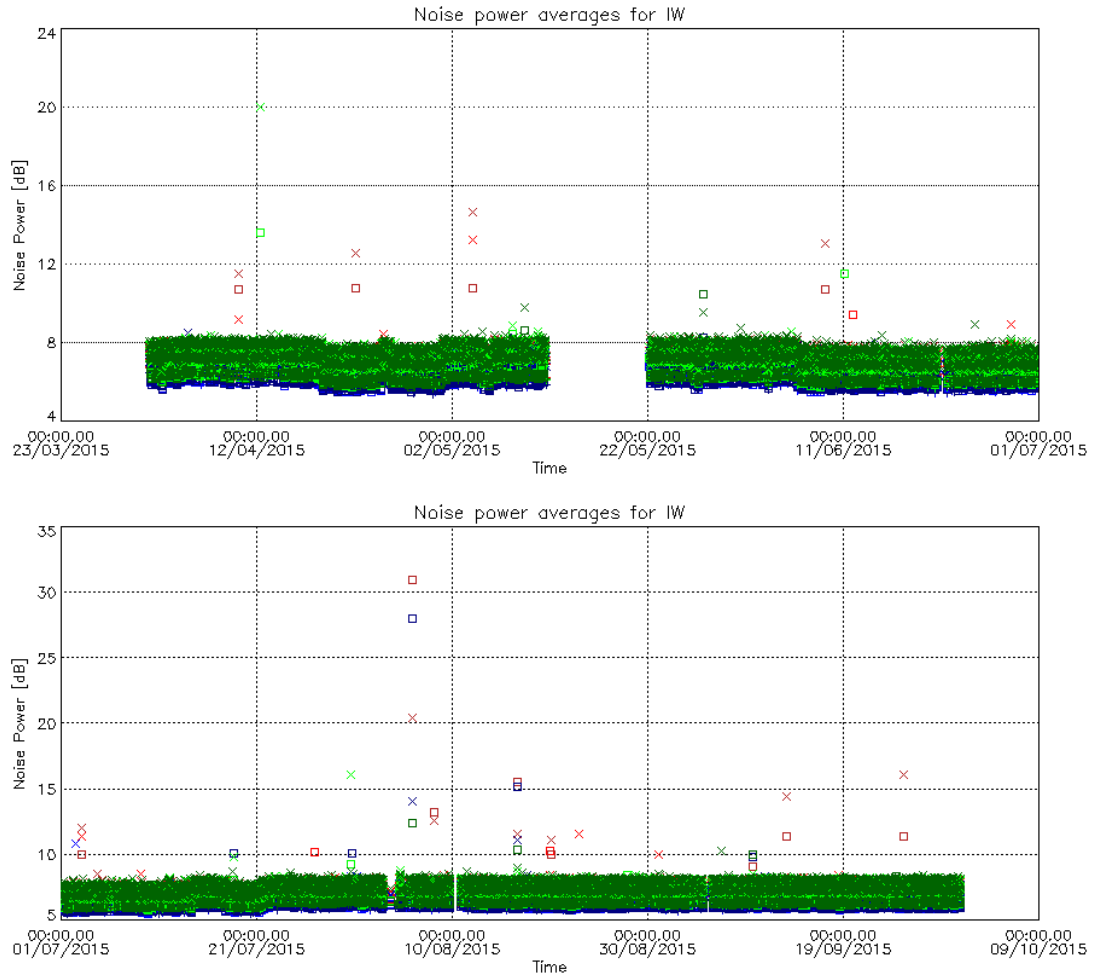


Figure 8 Noise power versus time (IW mode).



4. Products Status

4.1. Level 0 Products

4.1.1. Timeline and missing lines

The L0 quality monitoring is carried out as a routine task within the QCSS. The checks on the timeline and missing lines have not detected significant problems.

4.1.2. I/Q statistics

The analysis of I/Q bias and standard deviation allow to state that the L0 data quality is nominal. Figure shows the channel imbalance analysis for IW, showing the standard deviation that the two channels are very well aligned along the bisector of the I/Q plane.

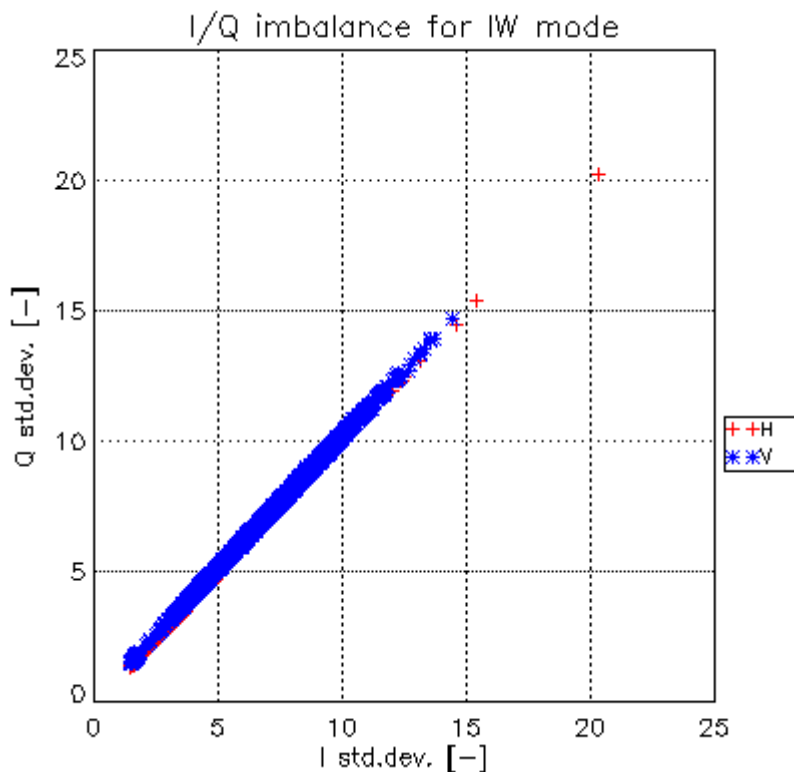


Figure 9 I/Q channel imbalance.

4.1.3. FDBAQ

The FDBAQ quantization scheme performs nominally. A detailed analysis of the FDBAQ behaviour for the first year can be found in [S1-RD-10].

The long-term statistics over the acquired data show that the average Mbit/s are reported in the following table:



Acquisition mode/swath	Average bitrate [Mbit/s]
S1	271.5
S2	213.36
S3	222.56
S4	188.58
S5	208.04
S6	178.39
IW	194.89
EW	62.32
WV1	11.8
WV2	6.7

Table 6 Average bitrate for each acquisition mode.

4.1.4. Instrument Pointing

The instrument pointing in elevation has been calibrated during the commissioning phase exploiting the availability of the elevation notch acquisitions over the Amazonian rain forest. After the commissioning, the stability has been verified with additional acquisitions (Figure 10) that confirmed the validity of the calibration carried out during the commissioning phase.

Table 7 reports the detailed measurements from the 12th October 2014 and the 24th July 2015 acquisitions. The estimated position of the notch (off-Nadir angle) is reported in the second column and is compared to the angle extracted from the quaternions (“annotated roll error”) and the expected value from the theoretical roll steering law.

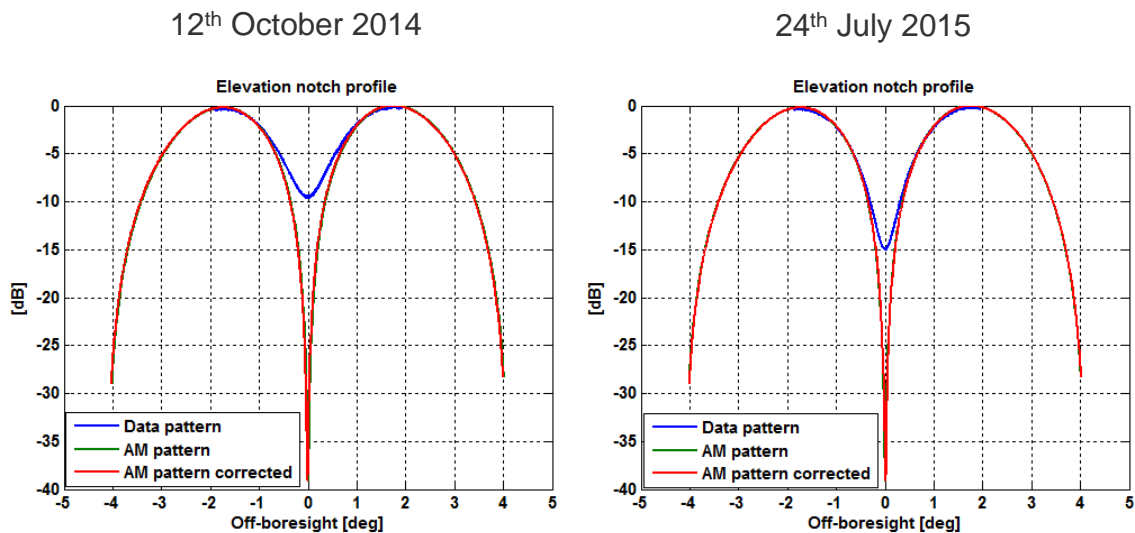


Figure 10 Elevation pointing verification with notch acquisitions over Amazon rain forest.



Data set start time	Estimated notch position [deg]	Annotated roll error [deg]	Theoretical roll error mean [deg]
24 th July 2015	-30.1026	-0.0039	-0.0011
12 th October 2014	-30.0788	0.01935	0.00937

Table 7 Elevation pointing verification.

Plots of the spacecraft attitude (yaw, pitch and roll) are shown in Appendix I.

The stability of the pointing in azimuth can be monitored through the Doppler Centroid, estimated directly from SAR data. Figure 11 shows the average Doppler Centroid on a data-take basis (dots) and on a daily basis (red line) versus time. The majority of the values are limited between +/-40 Hz, except for outliers reaching up to 80-100 Hz. The bias varies along time in correspondence of the different configurations of the star trackers (STT). Activities are on-going in order to reduce the dependency wrt the STT configuration.

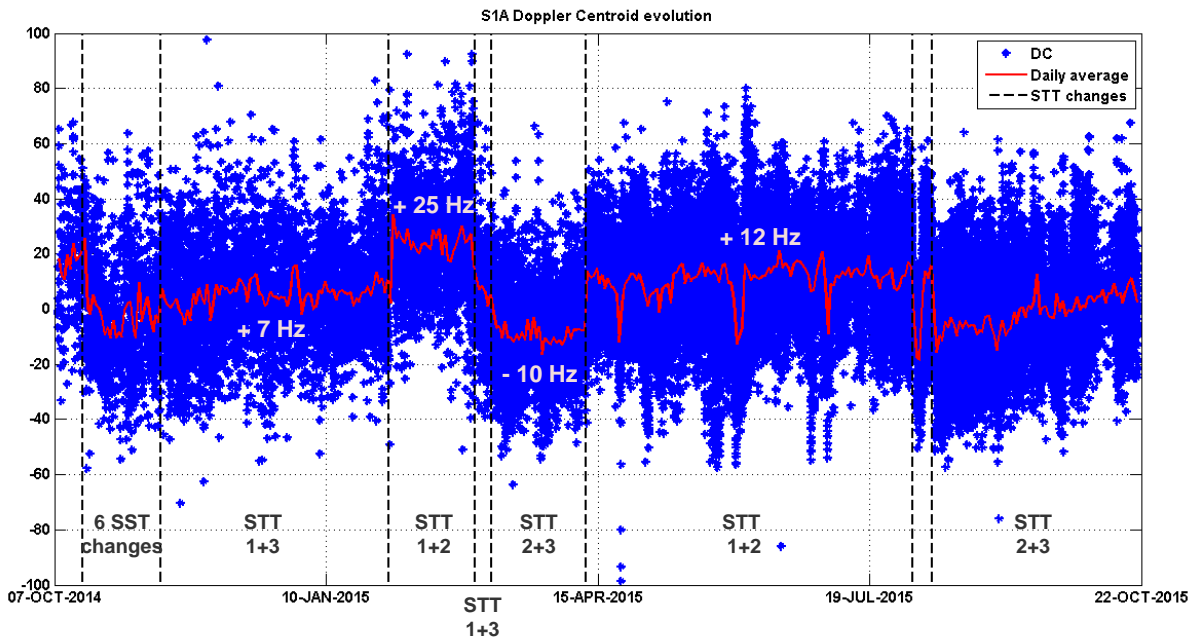


Figure 11 Doppler Centroid versus time. Average on a data-take basis (dots) and daily average (red line). The star-trackers reconfigurations events are marked by the vertical black lines.

4.2. Level 1 Products

A general summary of status of Level 1 products was presented at the 2015 CEOS SAR workshop (see [S1-RD-03]).

4.2.1. Level 1 Processor Updates

The main improvements introduced in the Level-1 Processor and impacting data quality are here below described, classified according to the release in which they have been included.

Proprietary information: no part of this document may be reproduced divulged or used in any form without prior permission from CLS.



IPF v2.4.3 (09/03/2015)

- Improved Stripmap and Topsar radiometric normalization
- Improved management of SWST and SWL variations along orbit, in order to avoid issues (gaps, ...) during merging of Topsar sub-swaths into GRD products

IPF v2.5.0 (30/06/2015)

- Support to slicing mode processing, adding the possibility to process LOS products also when the associated LOA/C/N ones are not available (e.g. in NRT scenarios)
- Improved management of orbital information contained in LOS products (better propagation accuracy), in order to support NRT processing
- Verification, improvement and calibration of de-noising step and related annotations
- Optimization of L1 SAFE products generation routine performances, in particular for the writing of measurement TIFF files

IPF v2.6.0 (09/10/2015)

- Improved orbital information annotation, reporting in the output L1 products the values really used for processing (e.g. external Restituted or Precise Orbit Files)
- Improved terrain height management during EAP correction, using one height value per sub-swath instead of only one for all the data
- Improved Quick Look scheme for dual polarization data, making it independent from the content of the acquired scene

In addition to the described L1 Processor upgrades, a summary of S1-A Auxiliary Data Files (ADFs) updates during the reporting period is provided, together with an explanation of the updates, in Appendix F. The main ones are here below summarized:

AUX_INS

- Range-variant RxGain correction coefficients refinement
- Activation of SWST bias compensation
- Internal calibration default settings (time delay, PG model and reference) refinement
- Support to Stripmap modes without interleaved calibration pulses

AUX_PP1

- Activation of range-variant RxGain correction
- Activation of internal calibration (i.e. PG) correction
- Processing gains and SAFE scaling LUT refinement

AUX_CAL

- Introduction of complex EAP
- AAP update after TRM failures
- Noise calibration factors refinement

4.2.2. Image Quality

The DLR Transponders & Corner Reflectors, the BAE Corner Reflector and the Australian Corner Reflector array have been used to assess various impulse response function parameters as described below. The products analysed were acquired in 2015 and processed with the Sentinel-1 IPF v2.36, v2.43, v2.52, v2.53 and v2.60.



4.2.2.1. Spatial Resolution

The Figures and Tables below give the azimuth and range spatial resolutions derived from SM, IW and EW SLC data. The numbers in brackets indicate the number of measurements.

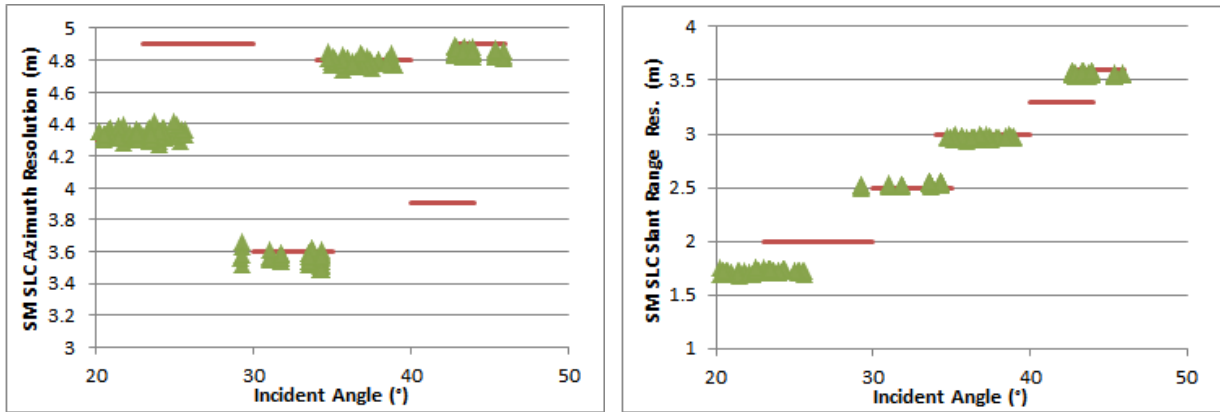


Figure 12 SM Azimuth and Slant Range Spatial Resolutions

Mode/Swath	Azimuth Spatial Resolution (m)	Slant Range Spatial Resolution (m)
S1	4.33±0.03 (112)	1.72±0.01 (112)
S3	3.56±0.04 (65)	2.54±0.02 (65)
S4	4.79±0.02 (52)	2.97±0.01 (52)
S6	4.85±0.02 (66)	3.56±0.01 (66)

Table 8 SM Azimuth and Slant Range Spatial Resolutions

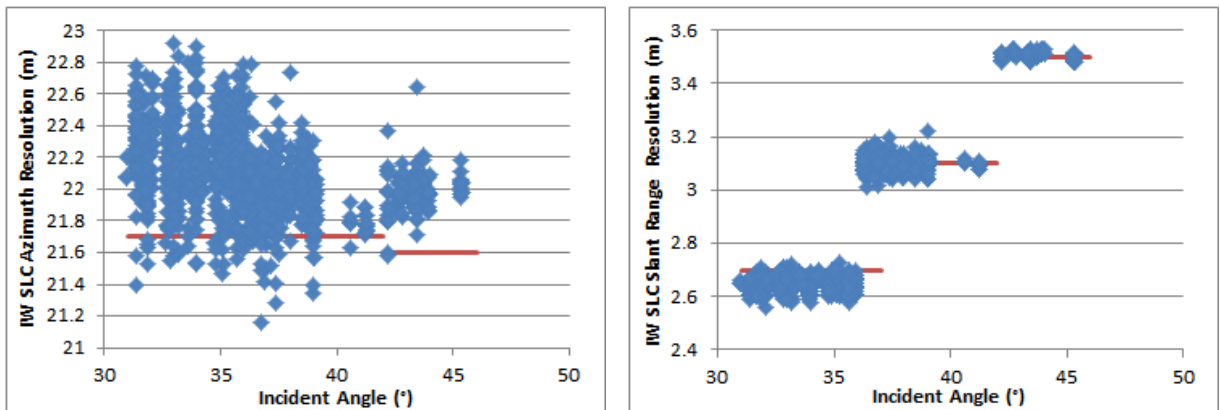


Figure 13 IW Azimuth and Slant Range Spatial Resolutions

Mode/Swath	Azimuth Spatial Resolution (m)	Slant Range Spatial Resolution (m)
IW1	22.21±0.28 (634)	2.65±0.03
IW2	21.96±0.20 (418)	3.10±0.03
IW3	21.99±0.12 (127)	3.51±0.01

Table 9 IW Azimuth and Slant Range Spatial Resolutions

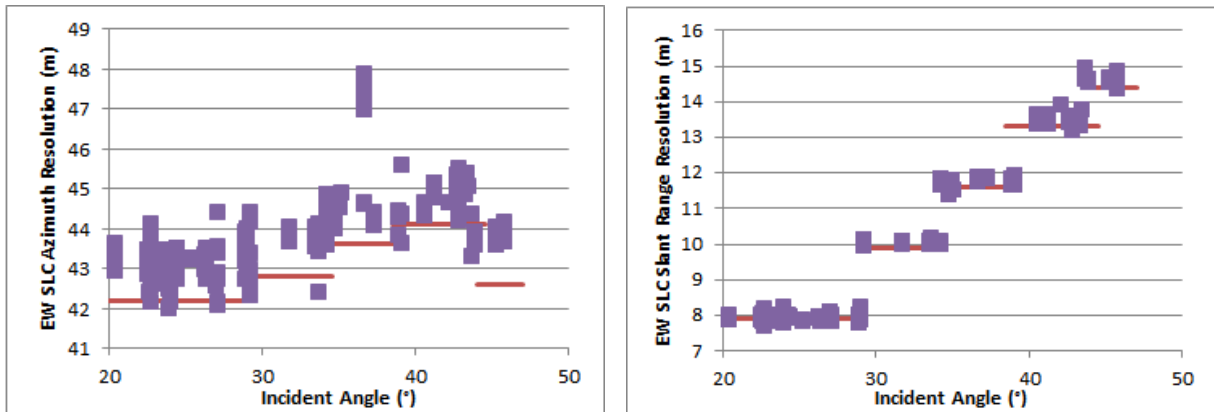


Figure 14 EW Azimuth and Slant Range Spatial Resolutions

Mode/Swath	Azimuth Spatial Resolution (m)	Slant Range Spatial Resolution (m)
EW1	43.13±0.34 (177)	7.93±0.07 (171)
EW2	43.68±0.43 (38)	10.04±0.05 (38)
EW3	44.87±1.04 (48)	11.75±0.11 (48)
EW4	45.02±0.29 (40)	13.44±0.13 (40)
EW5	43.78±0.19 (30)	14.57±0.11 (30)

Table 10 EW Azimuth and Slant Range Spatial Resolutions

With the exception of IW & EW azimuth resolutions, the measured spatial resolutions match the predicted resolutions as indicated by the red horizontal lines. The slightly higher than expected IW& EW spatial resolutions is currently being investigated but is likely to be caused by an azimuth filter length being too short (this will be increased during an IPF update planned for early 2016).

4.2.2.2. Sidelobe Ratios

The table below gives the measured impulse response function sidelobe ratios derived from SM, IW and EW SLC data - these indicate acceptable values.

Mode/Swath	Integrated Sidelobe Ratio (dB)	Peak Sidelobe Ratio (dB)	Spurious Sidelobe Ratio (dB)
SM	-12.89±1.41	-20.15±0.74	-26.49±1.65
IW	-11.48±3.82	-19.47±1.20	-22.15±2.98
EW	-13.34±3.77	-23.05±4.72	-25.39±5.42

Table 11 SM & IW Sidelobe Ratios

4.2.2.3. ENL and Radiometric Resolution

No specific Equivalent Number of Look (ENL) and Radiometric Resolution measurements were performed during 2015. Measurements below are re-produced from the S1-A Commissioning Phase Report ([S1-RD-01]):

Proprietary information: no part of this document may be reproduced divulged or used in any form without prior permission from CLS.



Large uniform distributed targets are used to measure the equivalent number of looks (ENL) and radiometric resolution (RR) in both SLC and GRD imagery as given in below. For each swath/sub-swath and product type, the first number is the ENL while the second is the RR in dB.

	SM1	SM2	SM3	SM4	SM5	SM6
SLC	0.938, 3.08	0.960, 3.05	0.981, 3.03	0.918, 3.10	0.919, 3.10	0.925, 3.09
GRDF	3.81, 1.80	3.86, 1.79	3.81, 1.80	3.76, 1.81	3.73, 1.81	3.75, 1.81

Table 12: SM ENL & RR Measurements

	IW1	IW2	IW3
SLC	0.947, 3.07	0.959, 3.06	0.921, 3.10
GRDH	4.56, 1.67	4.55, 1.67	4.56, 1.67

Table 13: IW ENL & RR Measurements

	EW1	EW2	EW3	EW4	EW5
SLC	0.940, 3.08	0.908, 3.12	0.918, 3.11	0.894, 3.13	0.894, 3.13
GRDH	2.72, 2.04	2.70, 2.06	2.74, 2.05	2.83, 2.03	2.73, 2.06

Table 14: EW ENL & RR Measurements

4.2.2.4. Ambiguity Analysis

4.2.2.4.1. Azimuth Ambiguities

No specific ambiguity measurements were performed during 2015. Measurements below are reproduced from the S1-A MPC Commissioning Phase Report [S1-RD-01]:

Azimuth ambiguities fall into two types: azimuth and range. Examples azimuth ambiguities are shown in Figure 15 to Figure 17 for SM, IW and EW modes for the ESA ESTEC transponder, which in these examples is located over dark ocean backscatter. Note that the early SM ambiguity is located at the end of the image. For these ambiguities it has been difficult to measure the ambiguity ratio as the ambiguities are contaminated by the extended azimuth sidelobe structure from the transponder mainlobe.

4.2.2.4.2. Unexpected Azimuth Ambiguities

For the IW and EW transponder IRF, additional azimuth ambiguity like features can also be seen either side of mainlobe (see Figure 16 and Figure 17) - this has been identified as being due to the length of the azimuth time unfolding and resampling filter used in the processing [AD-03]. The length of this filter is currently tuned for runtime performance. The length of this filter will be increased in a future release of IPF to reduce the impact of this additional ambiguity.

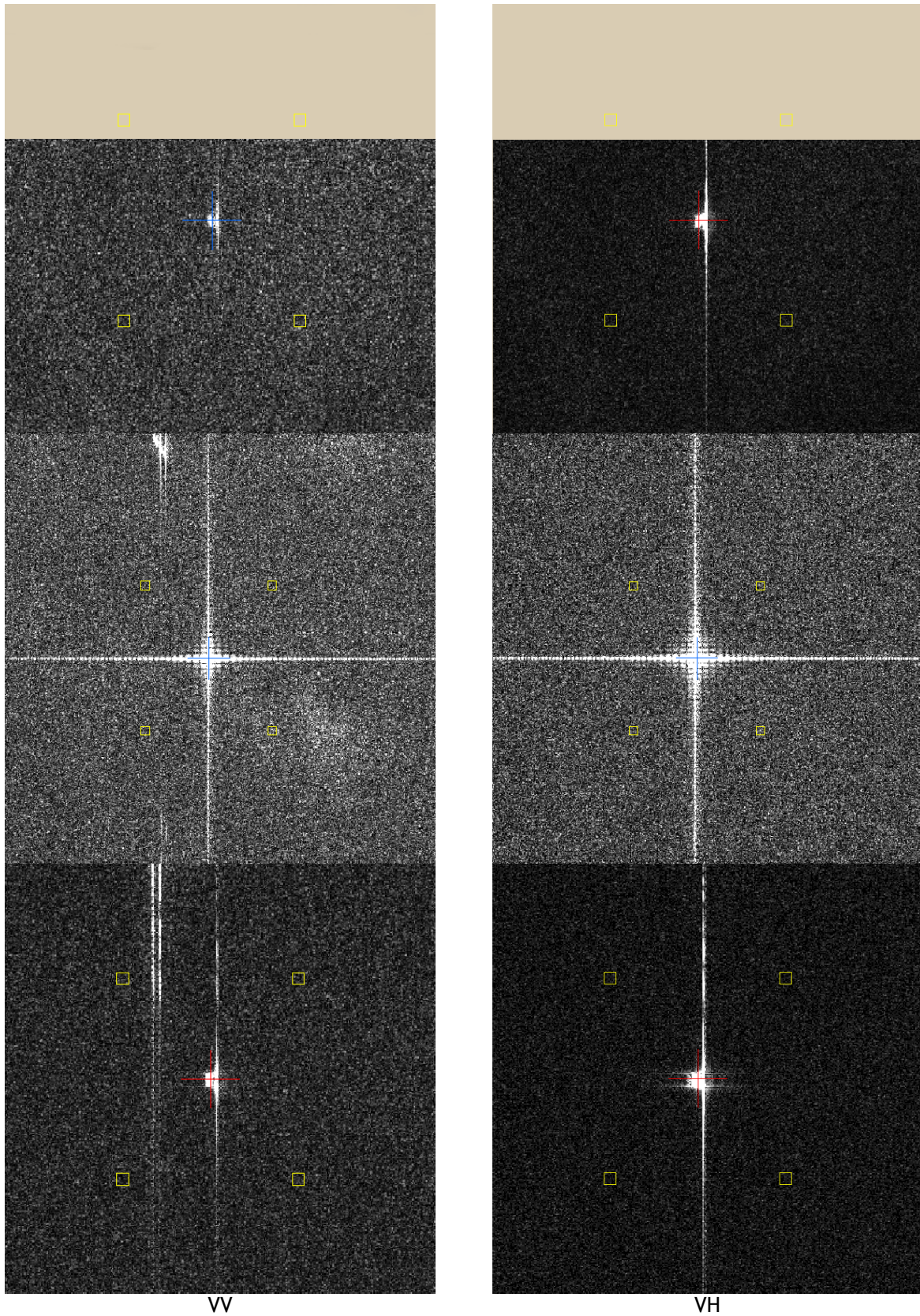


Figure 15: SM SLC Early Azimuth Ambiguity, ESTEC Transponder IRF and Late Ambiguity

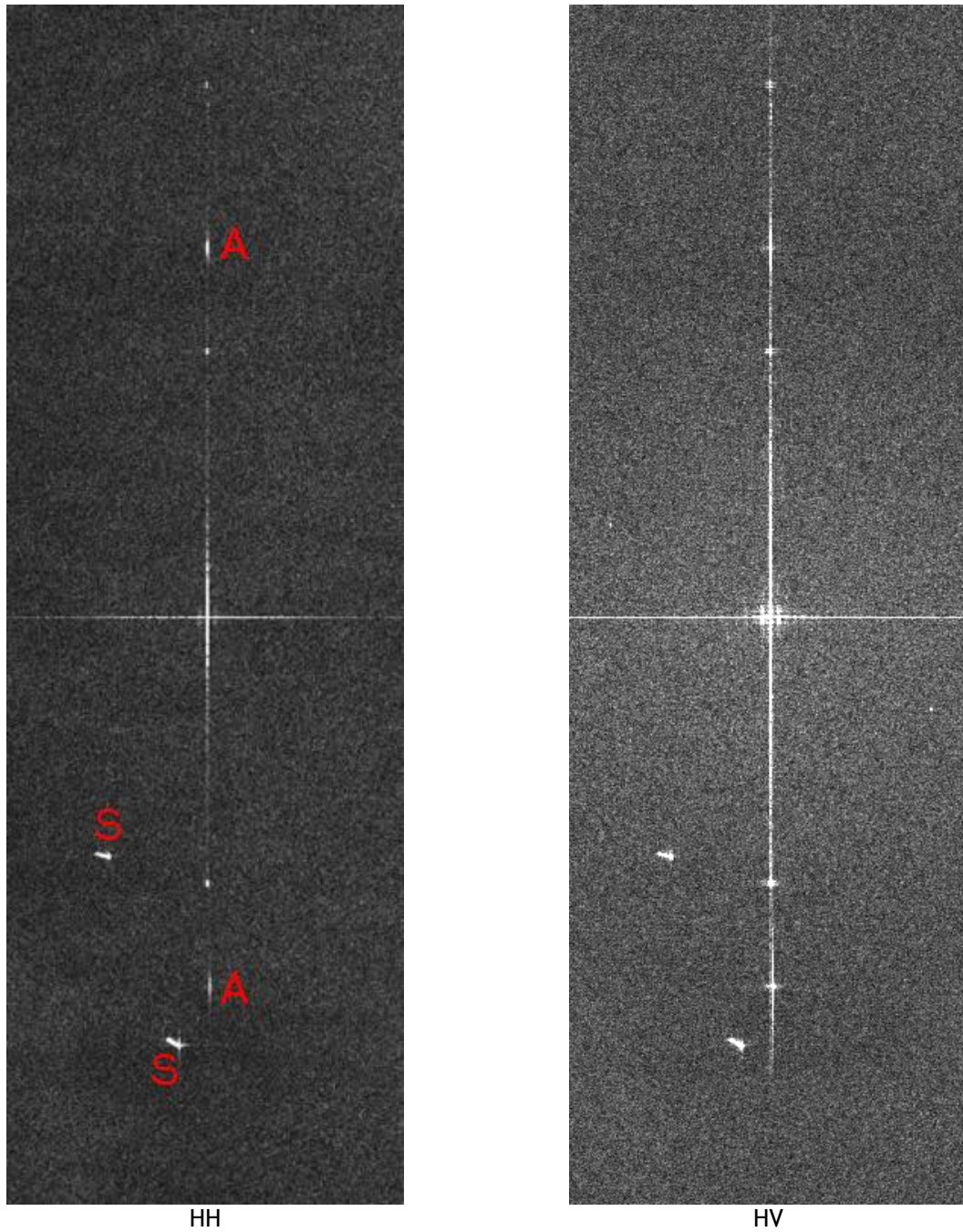


Figure 16: IW Early Azimuth Ambiguity, ESTEC Transponder IRF and Late Ambiguity (A indicates nominal ambiguity locations and S are ships - the non-nominal ambiguities are between the ambiguities and the IRF mainlobe)

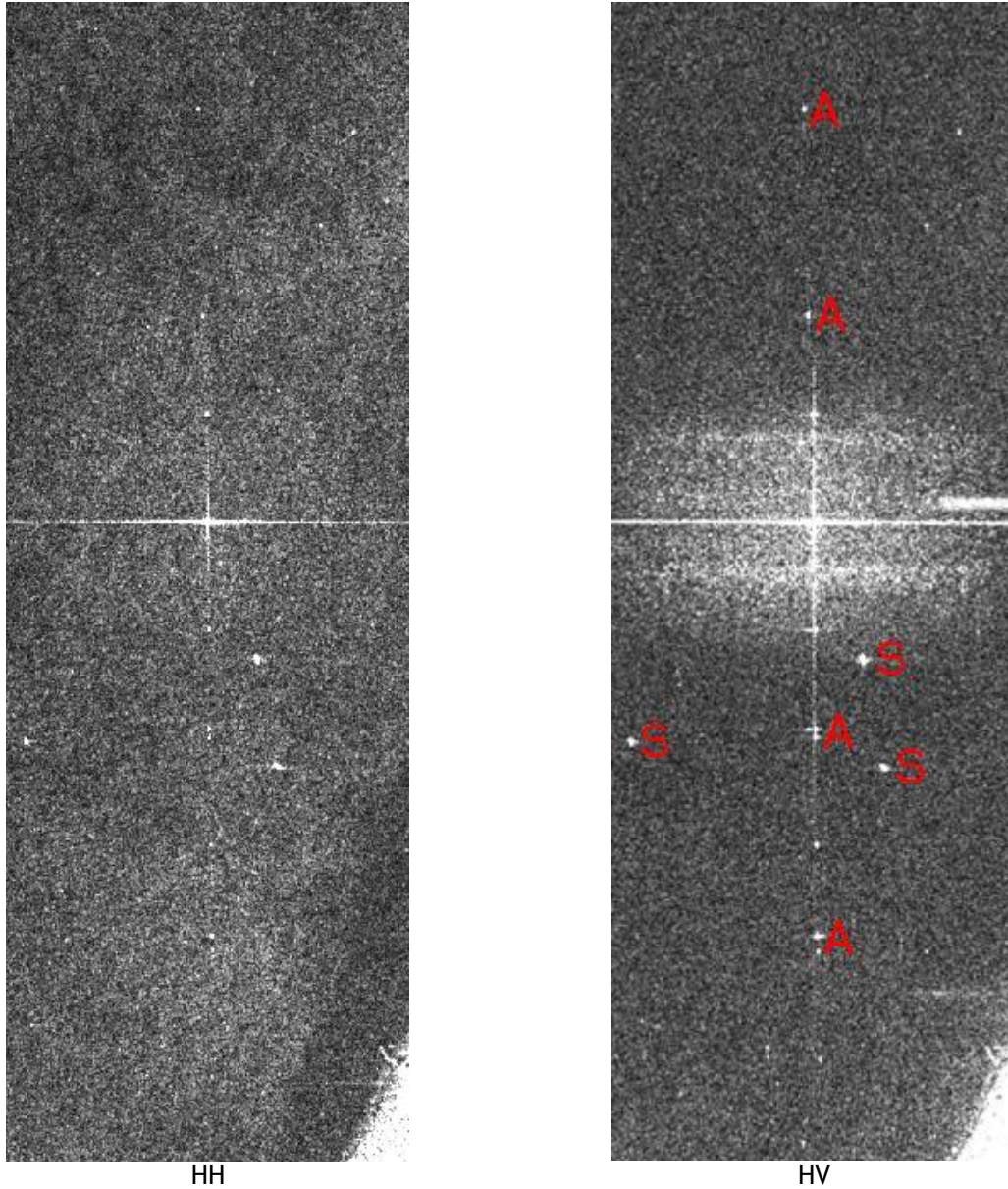


Figure 17: EW Early Azimuth Ambiguity, ESTEC Transponder IRF and Late Ambiguity (A indicates nominal ambiguity locations and S are ships - the non-nominal ambiguities are between the ambiguities and the IRF mainlobe)

The table below gives mean azimuth ambiguity ratios for DLR transponder targets for SM, IW and EW modes. Note that for EW it can be hard to detect the azimuth ambiguities and so the values given should be considered as upper limits to the ambiguity ratio.

	SM	IW	EW
Early Azimuth Ambiguity Ratio (dB)	-36.25±2.00	-30.20±2.56	-29.91±5.66
Late Azimuth Ambiguity Ratio (dB)	-32.92±3.58	-30.02±3.65	-30.36±3.15

Table 15: Azimuth Ambiguity Ratios



4.2.2.4.3. Range Ambiguities

Range ambiguities have been identified in one IW products to date. The full scene of the IW acquisition from 2nd November 2014 is shown in Figure 18 together two regions where range ambiguities are present (purple boxes). Figure 19 shows the middle ambiguity box where an extensive region of range ambiguities are seen together with non-ambiguous point targets including a wind farm. Two parts of Figure 19 are shown in Figure 20 and Figure 21 together with the source of the range ambiguities located in the city of Rotterdam, The Netherlands, some 150km away to the east. Finally, Figure 22 shows an ambiguous region in the right purple box together with the ambiguity source, which is the town of Waalwijk, The Netherlands. The source of these range ambiguities is at higher slant ranges than the ambiguities (the first far range ambiguity).

The range ambiguity ratio has been estimated for the three ambiguous regions shown in Figure 20, Figure 21 and Figure 22. The mean ambiguity ratio is -25.1 ± 4.2 dB with the individual ratios being -29.1, -20.7 and -25.4 dB respectively.

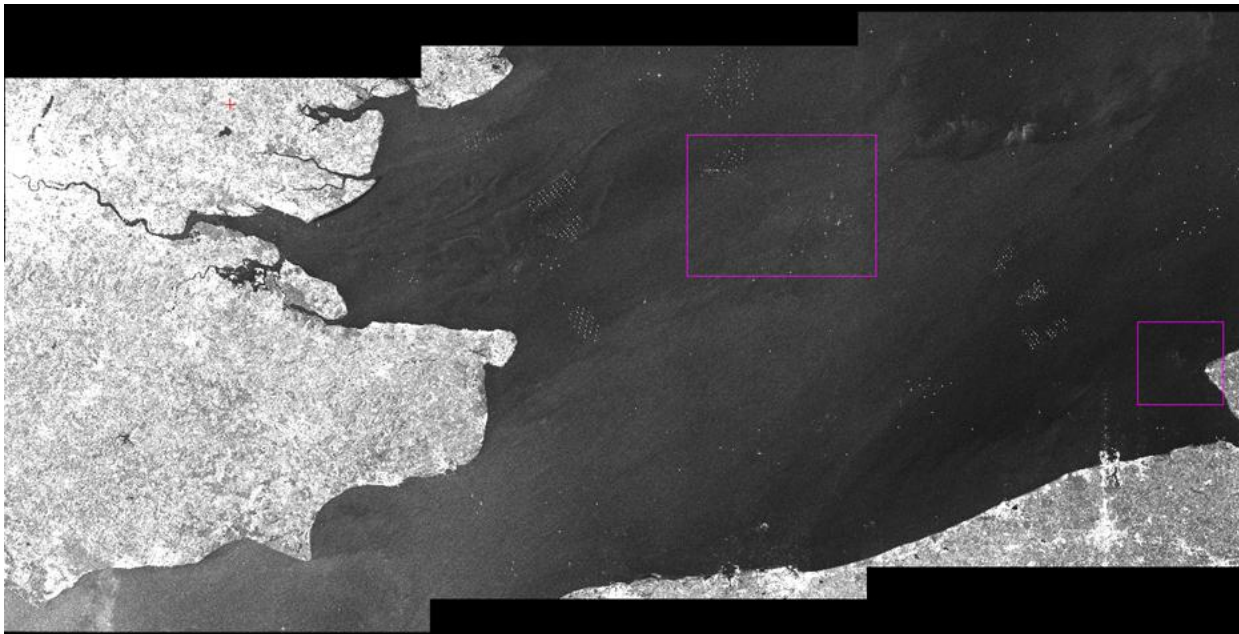


Figure 18: IW Image of SE England (showing the location of the BAE Corner Reflector) and N France with the location of two regions of range ambiguities indicated (acquisition 2nd November 2014, 17:40:53 UT).

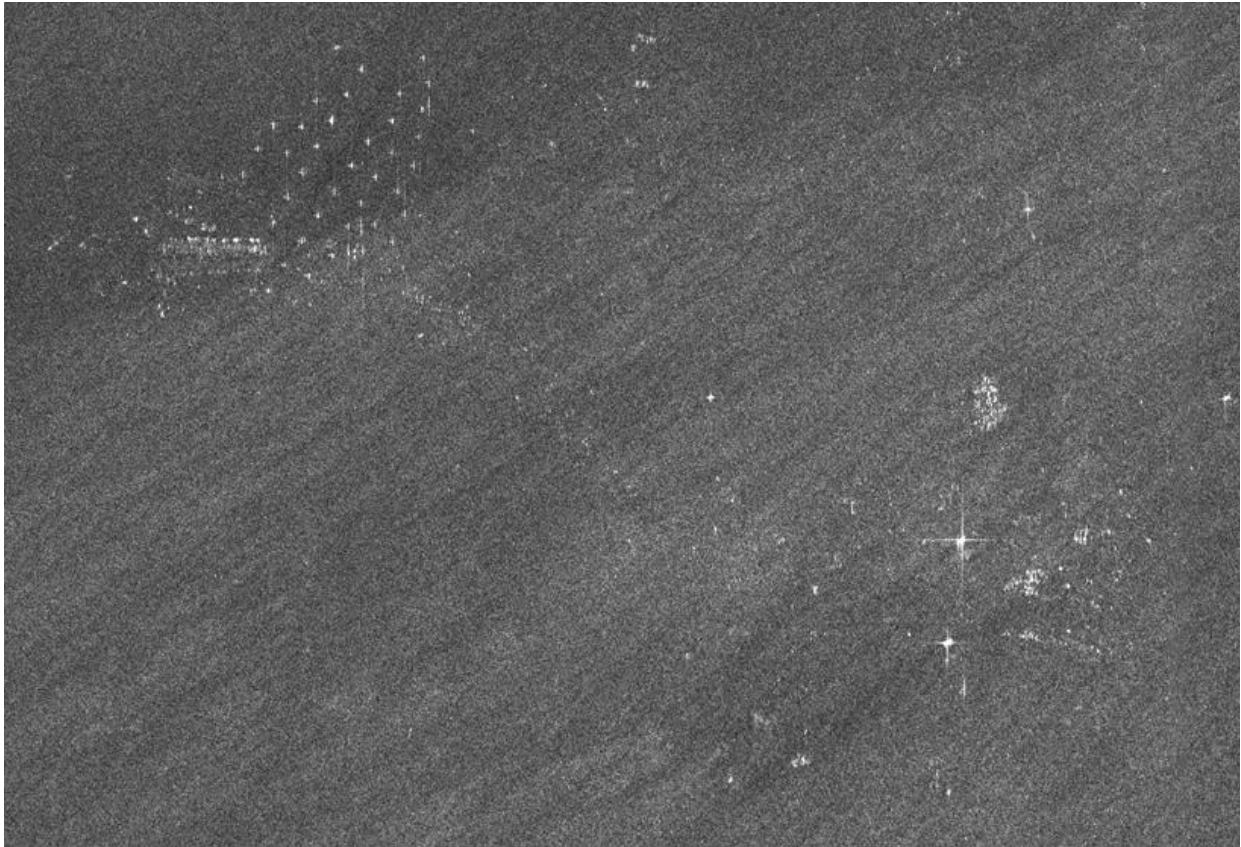


Figure 19: Extract of middle ambiguity region showing various range ambiguities plus other point targets.

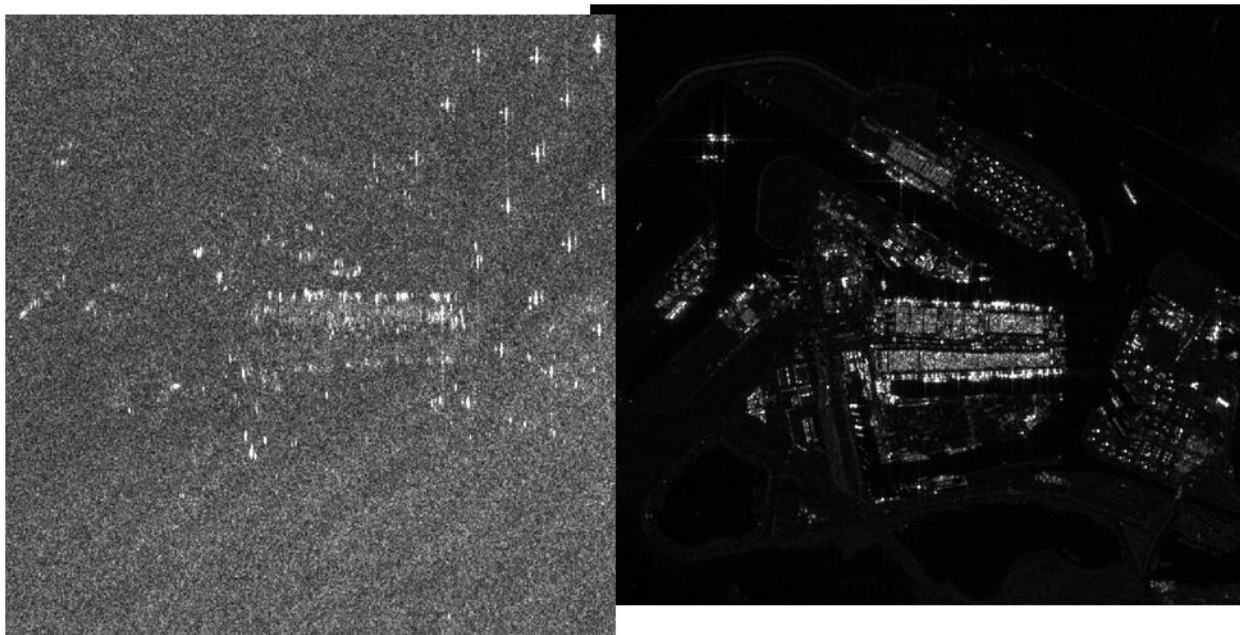


Figure 20: Detail of middle ambiguity region (left) and the source of the ambiguity in Rotterdam (right).



Figure 21: Detail of middle ambiguity region (left) and the source of the ambiguity in Rotterdam (right).

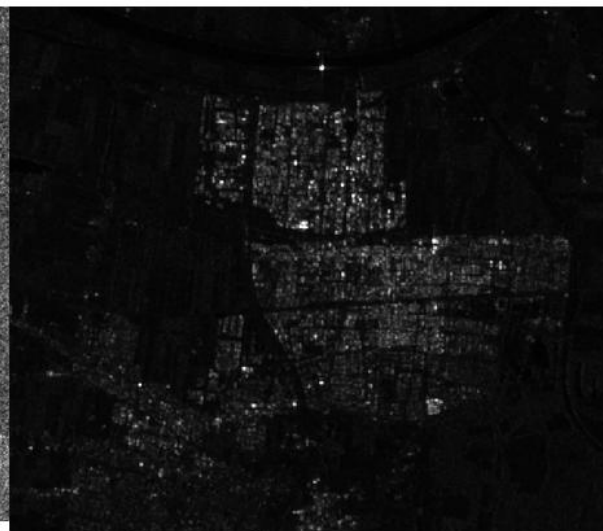
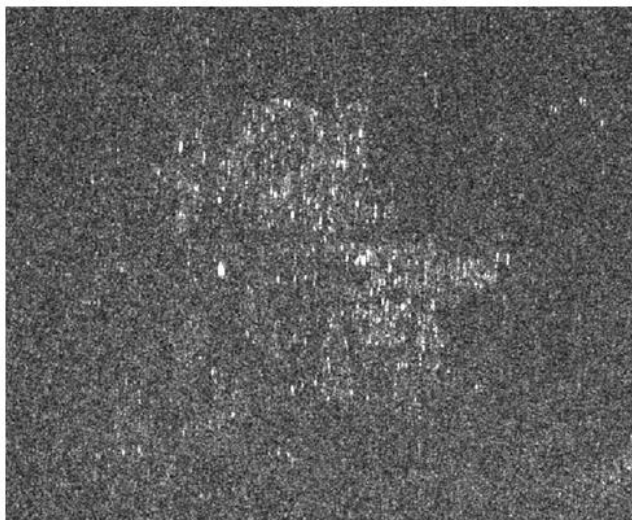


Figure 22: Detail of right ambiguity region (left) and the source of the ambiguity in Waalwijk (right).

4.2.3. Radiometric Calibration

The DLR Transponders & Corner Reflectors, the BAE Corner Reflector and the Australian Corner Reflector array have been used to measure their radar cross-section as described below. The products analysed were acquired in 2015 and processed with the Sentinel-1 IPF v2.36, v2.43, v2.52, v2.53 and v2.60. As described in Section 4.2.3.1 a major re-calibration was performed during 2015 for IW and EW mode acquisitions. All the radiometric measurements below have been corrected following this re-calibration.



An ESA User Note “Radiometric Calibration of S-1 Level-1 Products Generated by the S-1 IPF” (see Appendix C) was issued during 2015 to describe how the radar cross-section of distributed and point targets using GRD and SLC products can be calculated. Numerical examples are also included in the note (see Appendix C). For point target analysis using TOPS (IW & EW) SLC data it is necessary to remove a linear frequency modulation introduced by the electronic steering of the antenna in azimuth. This deramping step is described in another ESA User Note issued in 2015 “Definition of the TOPS SLC deramping function for products generated by the S-1 IPF”. Again a numerical example is included.

4.2.3.1. IW/EW Re-Calibration

As described in the ESA User Note “S1-A Radiometric Calibration Refinement#1” (see Appendix C) a major re-calibration was performed during the latter part of 2015 for IW and EW mode data applicable for both GRD and SLC data. This was primarily to correct the IW & EW polarimetric channel imbalance and IW absolute calibration. Further details are provided in the User Note. S1-A products processed with IPF v2.60 include the calibration refinement. All the radar cross-section measurements below include this re-calibration correction.

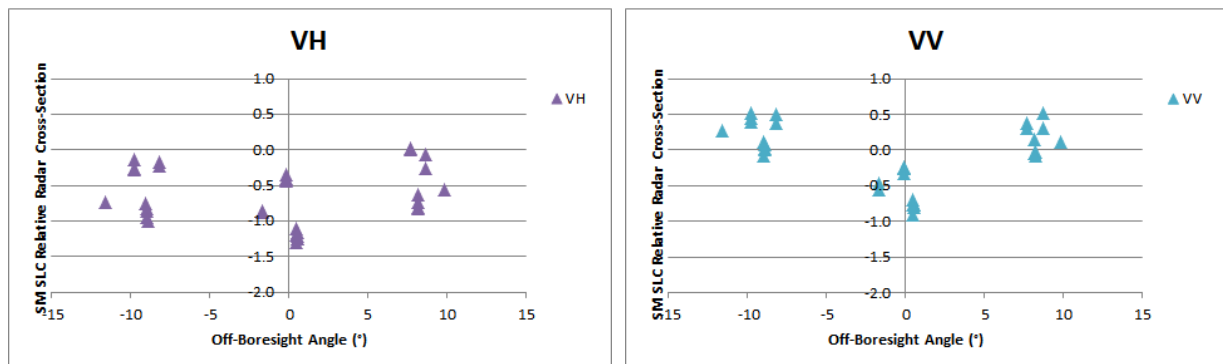
4.2.3.2. Absolute Radiometric Calibration

DLR Transponders have been used to calculate the relative radar cross-section for SM, IW and EW modes during 2015. The results per mode are shown in Table 16 where mean (radiometric accuracy) and standard deviation (radiometric stability) of the relative radar cross-section in dB are given. Note that the radiometric accuracy is close to zero while the radiometric stability is 0.5dB or better. The number of measurements is given in brackets.

SM	IW	EW
-0.14±0.50 (150)	0.00±0.33 (148)	0.07±0.43 (235)

Table 16: SLC Relative Radar Cross-Section for the DLR transponders (dB)

The following results are also for the DLR transponders but are separated by polarisation. Figure 23 and Table 17 give the results for SM mode - the relative radar cross-sections indicate a reasonable radiometric calibration but a proposed SM re-calibration would improve the measured mean relative radar cross-sections for each of the polarisations.



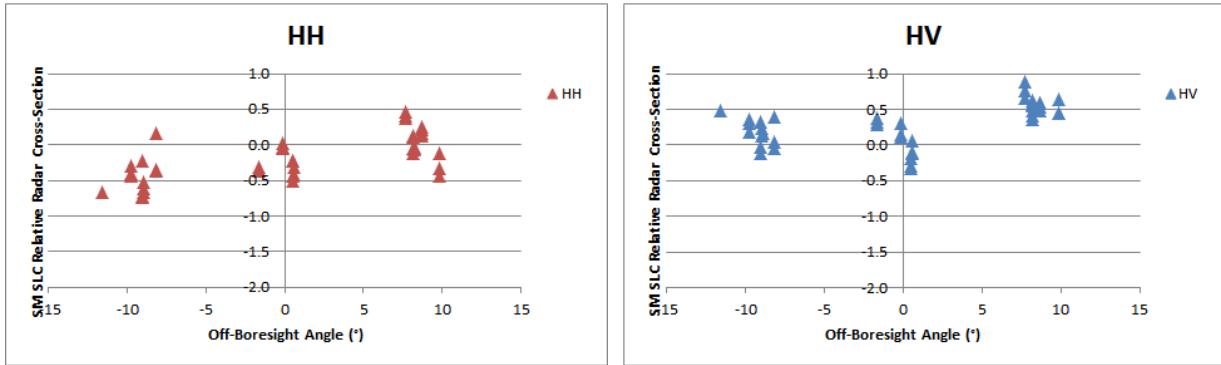


Figure 23: SM SLC Relative Radar Cross-Section for the DLR transponders

	VH	VV	HH	HV
S1	-0.56±0.35 (11)	0.24±0.22 (11)	-0.45±0.25 (13)	0.19±0.19 (13)
S3	-0.91±0.38 (13)	-0.58±0.24 (13)	-0.26±0.17 (12)	0.05±0.25 (12)
S5	-0.43±0.35 (9)	0.18±0.21 (9)	0.07±0.24 (17)	0.57±0.13 (17)

Table 17: SM SLC Relative Radar Cross-Section for the DLR transponders (dB)

The IW and EW results below indicate a good radiometric calibration with many mean relative radar cross-section values close to zero (the radiometric accuracy) and a standard deviation of typically 0.3dB (the radiometric stability). Differences between polarisations are also small (see also Section 4.2.5.1).

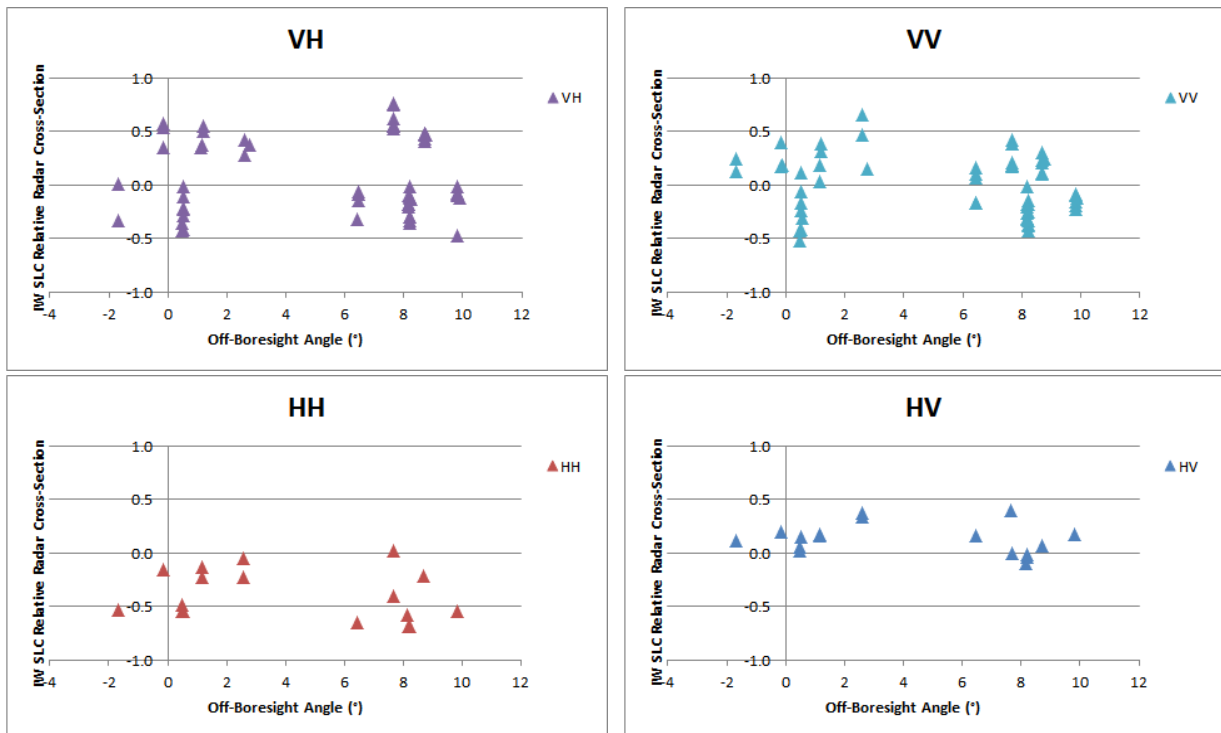


Figure 24: IW SLC Relative Radar Cross-Section for the DLR transponders

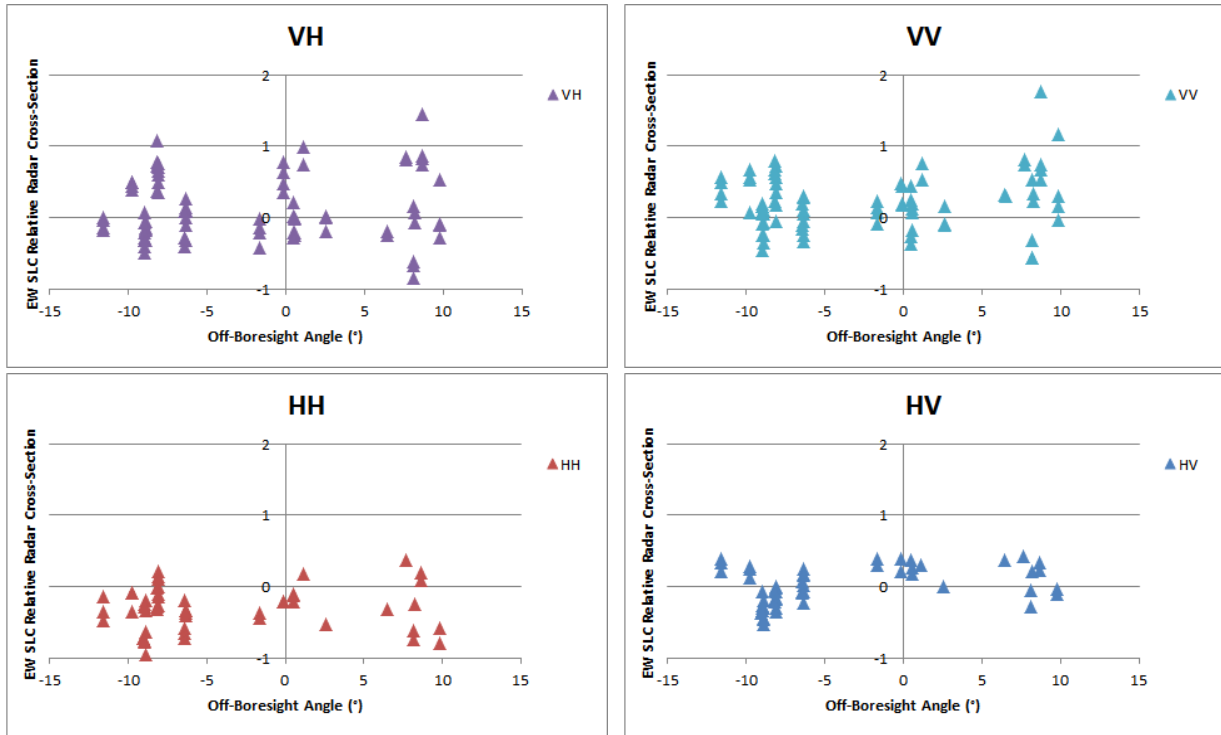


Figure 25: EW SLC Relative Radar Cross-Section for the DLR transponders

	VH	VV	HH	HV
IW	0.09±0.36 (57)	0.00±0.27 (57)	-0.39±0.23 (17)	0.13±0.14 (17)
EW	0.13±0.47 (72)	0.25±0.39 (73)	-0.31±0.30 (45)	0.05±0.25 (45)

Table 18: IW & EW SLC Relative Radar Cross-Section for the DLR transponders (dB)

	IW1	IW2	IW3
VH	0.05±0.38 (17)	0.05±0.27 (8)	0.12±0.38 (32)
VV	0.00±0.30 (17)	0.16±0.29 (8)	-0.03±0.25 (32)
HH	-0.38±0.19 (7)	-0.31±0.31 (3)	-0.44±0.26 (7)
HV	0.12±0.06 (7)	0.29±0.11 (3)	0.07±0.17 (7)

Table 19: IW SLC Relative Radar Cross-Section for the DLR transponders (dB)

	EW1	EW2	EW3	EW4	EW5
VH	0.13±0.41 (33)	0.10±0.43 (10)	0.12±0.40 (11)	-0.08±0.58 (10)	0.49±0.60 (8)
VV	0.23±0.32 (34)	0.10±0.28 (10)	0.20±0.29 (11)	0.18±0.50 (10)	0.67±0.58 (8)
HH	-0.34±0.29 (27)	-0.31±0.12 (4)	-0.16±0.25 (5)	-0.31±0.43 (5)	-0.27±0.49 (4)
HV	-0.04±0.24 (27)	0.32±0.09 (4)	0.23±0.14 (5)	0.13±0.30 (5)	0.11±0.21 (4)

Table 20: EW SLC Relative Radar Cross-Section for the DLR transponders (dB)



The radiometric calibration results using the BAE Corner Reflector and IW SLC products are shown in Figure 26 from imagery acquired since March 2015 with IPF v2.43 and later (VV polarisation only). The derived relative radar cross-section is -0.03 ± 0.12 dB.

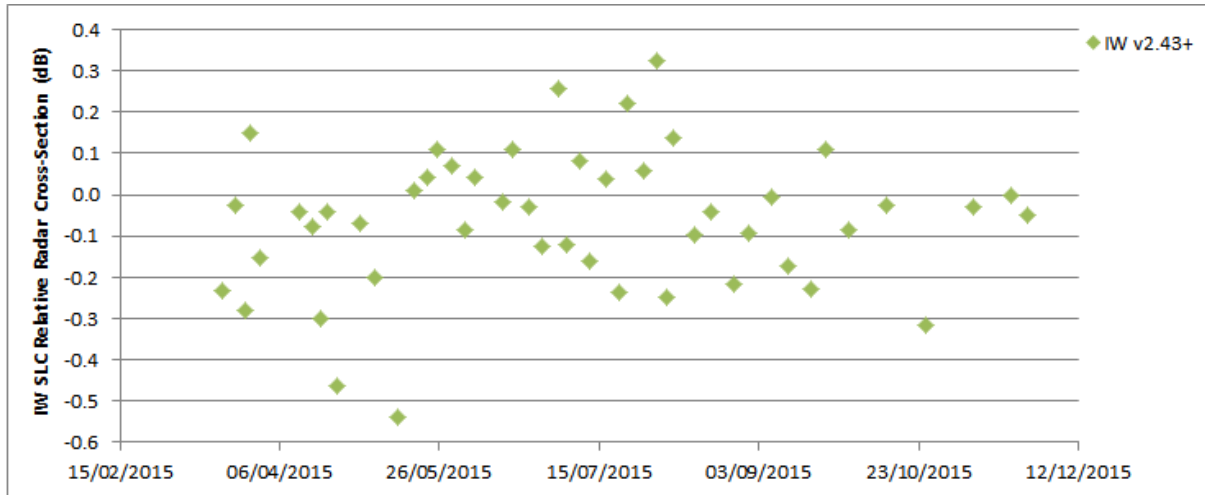


Figure 26: IW SLC Relative Radar Cross-Section for the BAE Corner Reflector

An array of 40 corner reflectors has been deployed near Brisbane, Australia as a component of the Australian Geophysical Observing System (AGOS) - see [S1-RD-04] for further details. The CRs are of size 1.5m (34), 2.0m (3) and 2.5m (3) with fixed orientations. An example corner reflector and image response in a SM image are shown in Figure 27. Given that these corner reflectors have a fixed elevation and azimuth orientation they will not be pointing directly at S1-A. Thus the measured radar cross-section will be reduced compared to the case of a perfect orientation.

Figure 28 (top and middle) shows the relative RCS from SM and IW acquisitions as a function of the difference in the actual elevation and that for a perfect orientation (the elevation offset). The red curve is the expected reduction in a trihedral corner reflector radar cross-section with elevation offset angle. The VV polarisation results show that the SM radar cross-section measurements at between -10° and -14° follow the expected radar cross-section reduction. Note that there is only a small offset in azimuth ($< 2^\circ$) which has a negligible impact on the measured radar cross-section.

Figure 28 (bottom) shows standard deviation of SM and IW standard deviation for VV and HH polarisation for each individual corner reflector. For many corner reflectors, the standard deviation (i.e. the radiometric stability) is as low as 0.1dB. The mean standard deviation for SM VV is 0.16 dB for IW VV is 0.21 dB and for IW HH is 0.24dB.

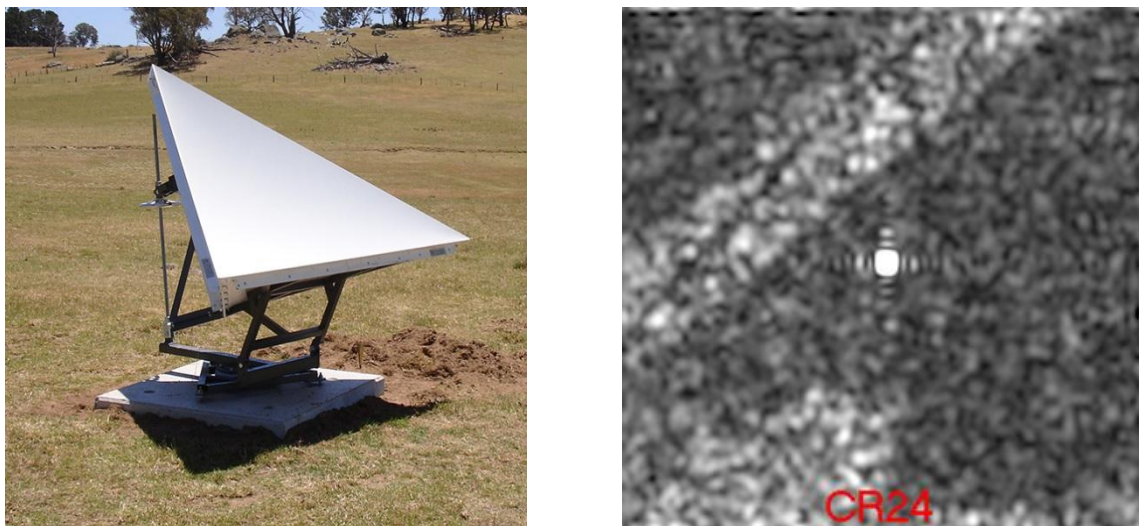


Figure 27: Example Australian Corner Reflector and Impulse Response

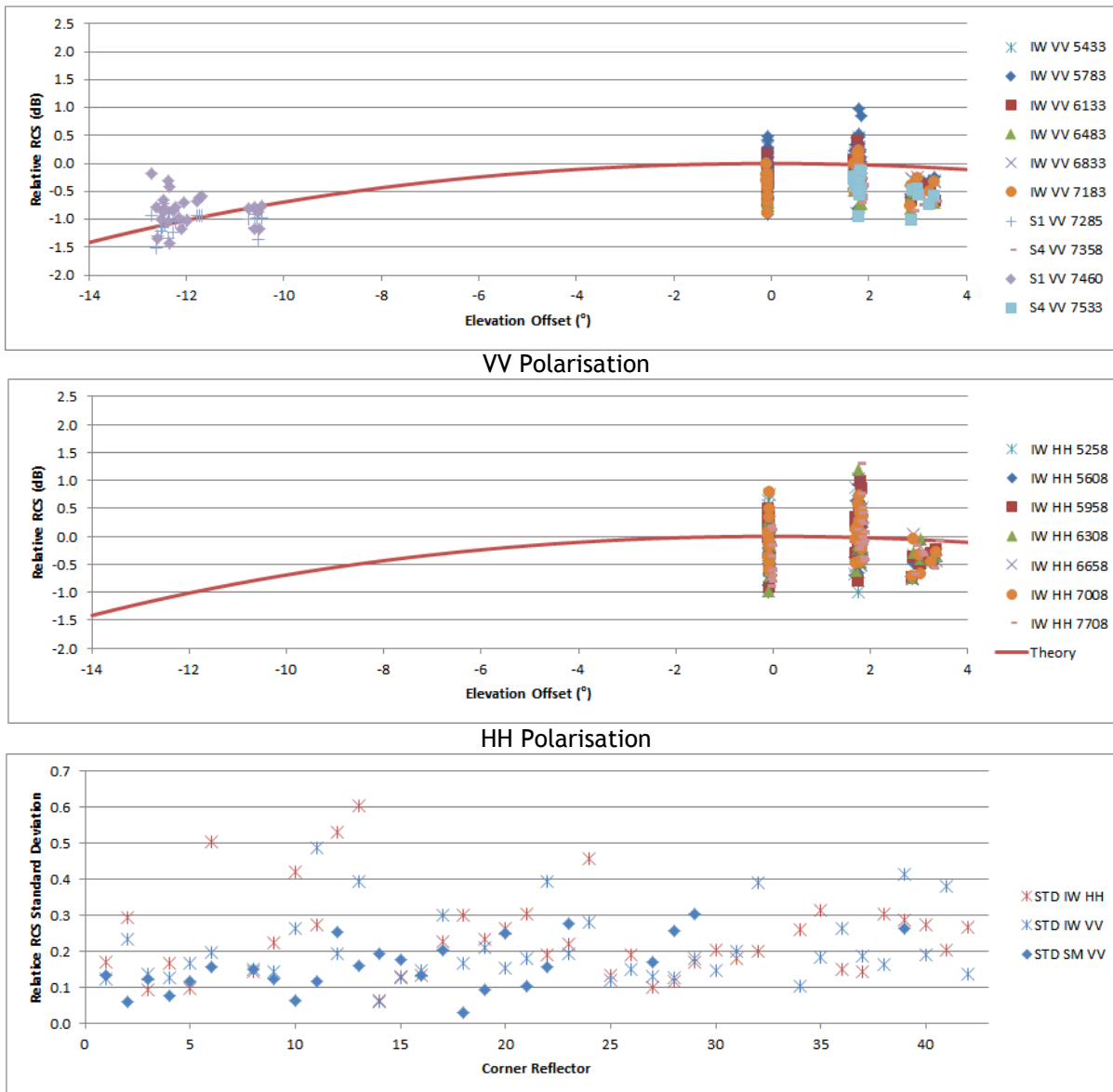


Figure 28: Australian CR relative RCS (top, middle) and RCS standard deviation (bottom).

4.2.3.3. Permanent Scatter Calibration

Figure 29 and Figure 30 show the Permanent Scatter Calibration series for a dataset of 12 Stripmap S6 products acquired over Chicago and for a dataset of 13 TopSAR IW products acquired over Milano. These indicate a good stability for the S1-A instrument and is a first demonstration of the PS-CAL processor operational readiness.

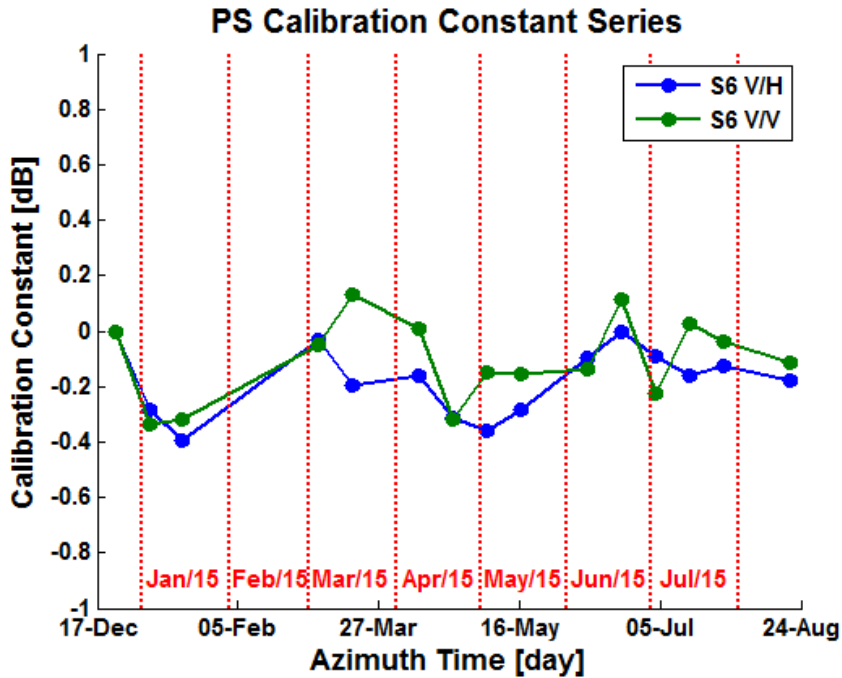


Figure 29 Permanent Scatter Calibration Time Series for Stripmap S6 over Chicago

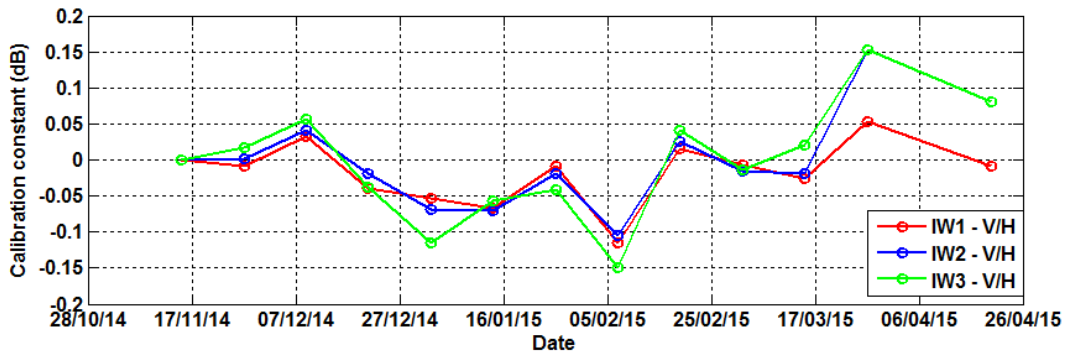
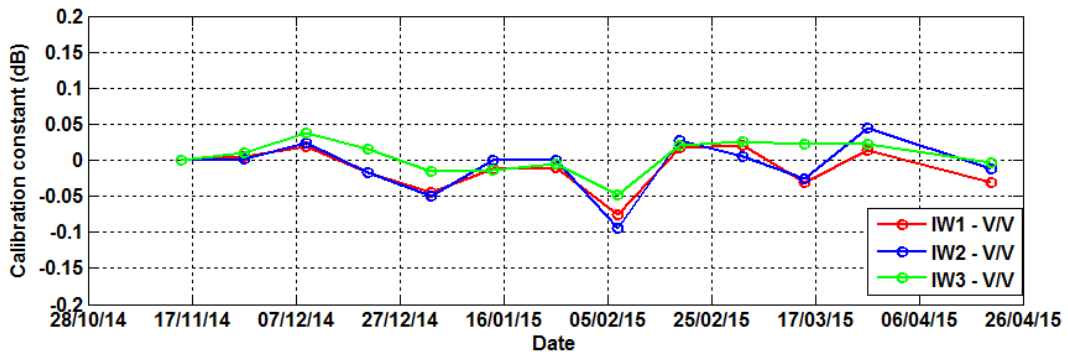


Figure 30 Permanent Scatter Calibration Time Series for TopSAR IW over Milan



4.2.4. Geometric Calibration

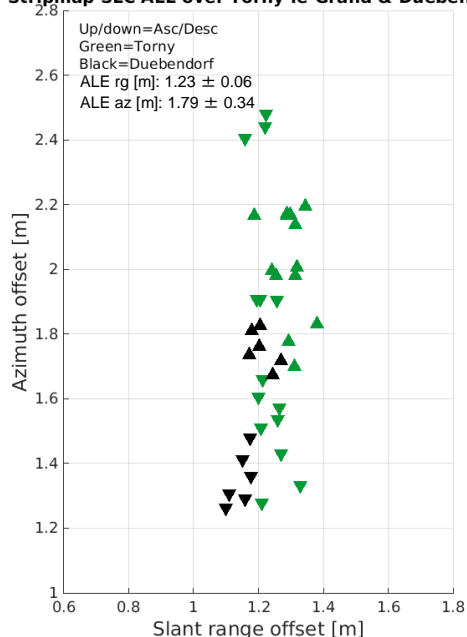
Geometric calibration of S1-A was performed by the University of Zurich (UZH) on the basis of a time series of products acquired between Aug. 2014 and Jan. 2015 over two test sites in Switzerland: *Torny-le-Grand* and *Duebendorf*. Trihedral corner reflectors (CRs) whose positions were known with cm-level accuracy were used as reference targets. For calibration purposes, we initially focussed on StripMap (SM) products, as these have the best resolution and represent the native sensor characteristics more closely than other product types. Geolocation accuracy was estimated for IW SLC products as well, also acquired over the same two test sites in 2014.

For a particular CR visible in an S1-A image product, its predicted azimuth and slant range image pixel position was calculated as follows:

- The surveyed CR position was adjusted for product-time plate **tectonic drift** and **solid Earth tide** (SET), as described in [S1-RD-06].
- The relevant timing annotations were extracted from the product annotations; these included the azimuth zero-Doppler time stamps, the orbital state vectors, the near-range fast time, and the range and azimuth sample spacings.
- Range-Doppler geolocation was performed for the CR coordinate as described e.g. in [S1-RD-08], giving a range and an azimuth time as the output.
- The resulting slant range prediction was corrected by adding the modelled **atmospheric path delay**, and the azimuth time was corrected by subtracting the **bistatic residual**. The effects and their associated correction are described in more detail in [S1-RD-06].

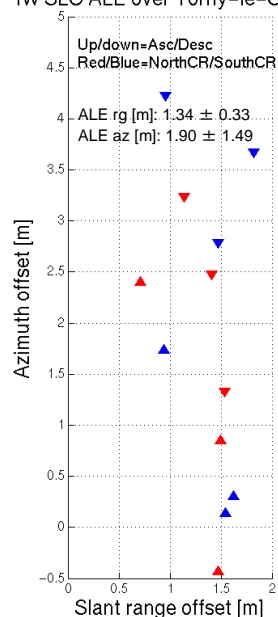
The above steps resulted in a range-azimuth *predicted* position for each target that could be compared to the position of the peak intensity in the image raster itself, i.e., the *measured* CR position. The differences between predicted and measured positions were then plotted, with the results shown for the SM and IW SLC product time series in Figure 31, at different key dates. Please refer to [S1-RD-06] and [S1-RD-07] for details on the evolution of the standard IPF processing and the geolocation methodology.

Stripmap SLC ALE over Torny-le-Grand & Duebendorf



(a) SM SLC (January 2015)

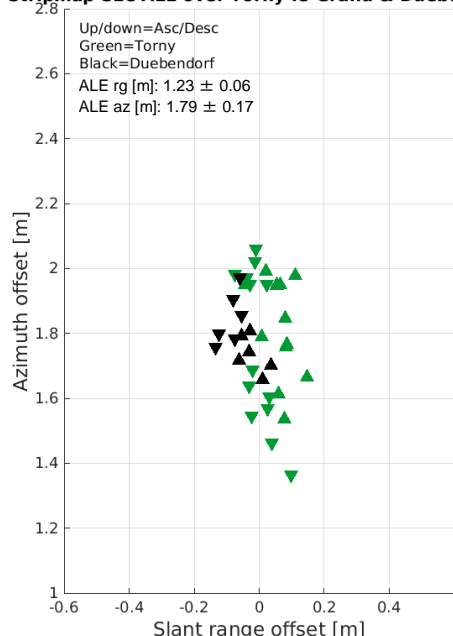
IW SLC ALE over Torny-le-Grand



(b) IW SLC (February 2015)

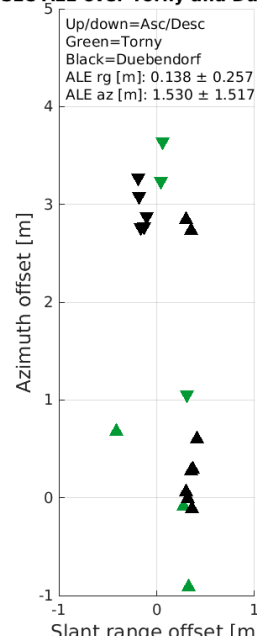


Stripmap SLC ALE over Torny-le-Grand & Duebendorf



(c) SM SLC (May 2015)

IW SLC ALE over Torny and Duebendorf



(d) IW SLC (May 2015)

Figure 31: ALE estimates for StripMap and IW SLC product time series using precise state vectors (AUX_POEORB) shortly after the calibration phase and after May 2015. In (a) and (c), each point represents a single SM SLC product over Torny-le-Grand (green) or Dübendorf (black). In (b), red and blue points represent single targets at Torny-le-Grand, while in (d) the points represent single products. Atmospheric path delay correction was applied by UZH in all cases. Bistatic residual correction was applied by UZH in (c) and (d), and the SWST (range) bias, taken from (a), was applied within the S1A processor beginning in May 2015, as can be seen in (c) and (d).

The ALE estimates were originally made using data acquired and processed during the S1-A commissioning phase. The initial geolocation results based on SM SLC products served as a basis for an update to the Sampling Window Start Time (SWST) bias annotation in the instrument auxiliary files ingested by the S1-A processor (i.e. Figure 31(a)). All products processed after May 4, 2015 used the updated SWST bias, as can be seen in Figure 31(c) and (d), where the same plots are shown as they appear since May 2015.

Figure 31(b) shows an early ALE scatterplot for several IW SLC products acquired over one of the Swiss test sites, *Torny-le-Grand*, with each point representing a single CR (two were visible in each product). The IW SLC plot shown in Figure 31(d) reflects the estimate of geolocation accuracy for this product type at the end of 2015, with each point representing a single product. The points form roughly two groups (upper and lower), which appear to be connected to a known subswath-specific relative offset (in this case, between beams IW2 and IW3) that is under continuing investigation.

The ALE plots in Figure 31(c) and (d) indicate that the localisation performance is well within the original requirements (according to sections 5.5.2.1 and 5.5.2.2 in [S1-RD-09]).



4.2.5. Polarimetric Calibration

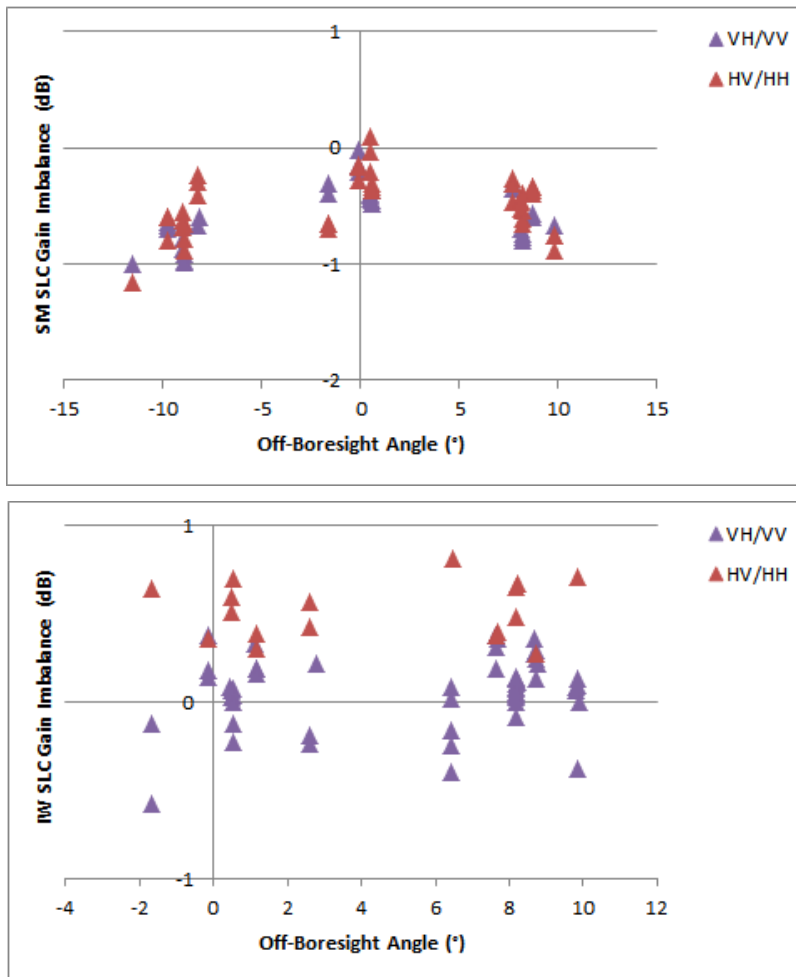
4.2.5.1. Gain Imbalance

The DLR transponders have been used to calculate the gain imbalance (the difference in radar cross-section between the two polarisations of dual polarisation products). Table 21 give a summary of the gain imbalance for the SM, IW and EW modes. As described in Section 4.2.3.1 the IW and EW re-calibration during the latter part of improved the gain imbalance for these modes.

	Gain Imbalance (dB)
SM	-0.52±0.25 (75)
IW	-0.06±0.32 (74)
EW	-0.21±0.29 (117)

Table 21: Gain Imbalance using the DLR transponders

The following results show the gain imbalance split between the two possible polarisation of VH/VV and HH/HV. Figure 32 and Table 22 give the gain imbalance for SM, IW and EW for acquisitions during 2015.



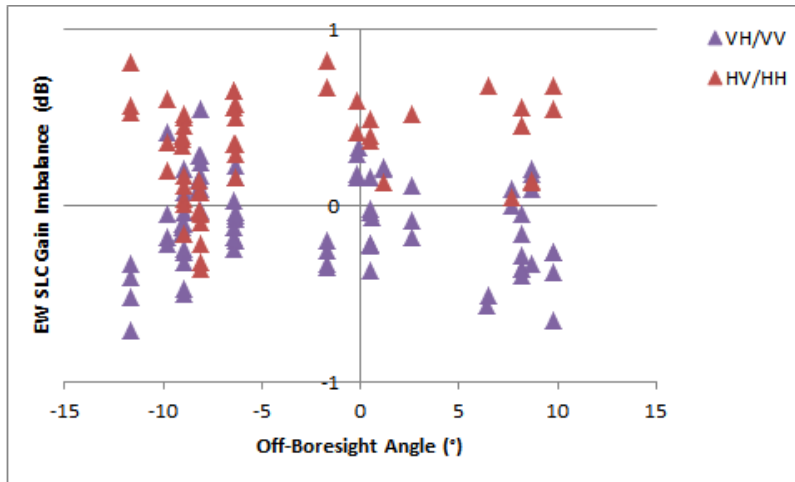


Figure 32: Gain Imbalance using the DLR transponders.

	VH/VV	HV/HH
SM	-0.56±0.26 (33)	-0.49±0.25 (42)
IW	0.08±0.21 (57)	0.52±0.16 (17)
EW	-0.12±0.25 (72)	0.36±0.28 (45)

Table 22: Gain Imbalance using the DLR transponders

4.2.5.2. Phase Imbalance

The DLR transponders have been used to calculate the phase imbalance (the difference in peak phase between the two polarisations of dual polarisation products). Figure 33 and Table 23 give the gain imbalance for SM, IW and EW for acquisitions during 2015. As expected the phase difference is close to zero.

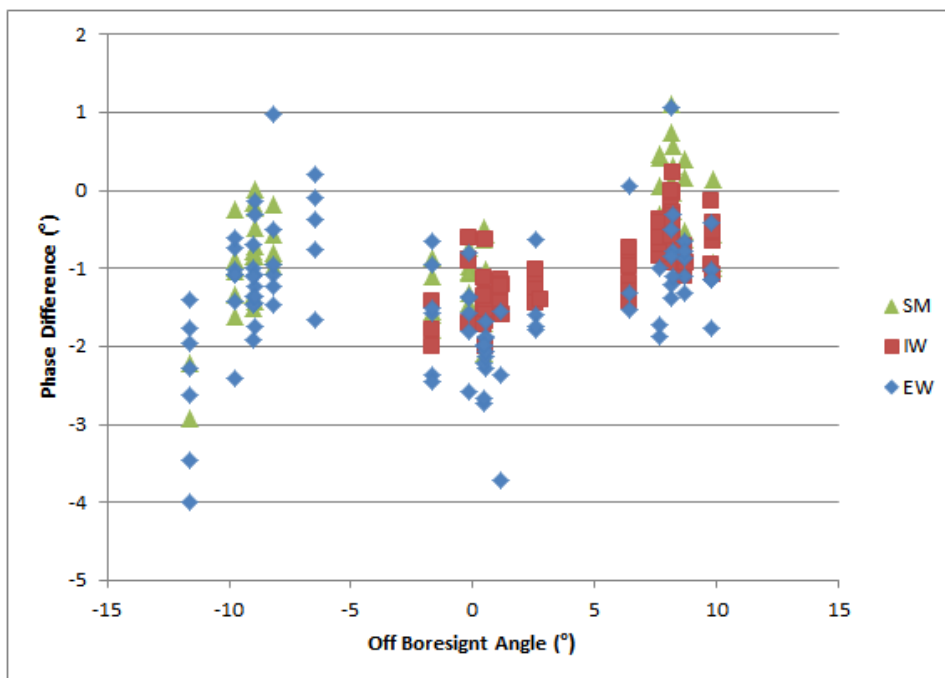


Figure 33: Phase Imbalance using the DLR transponders.

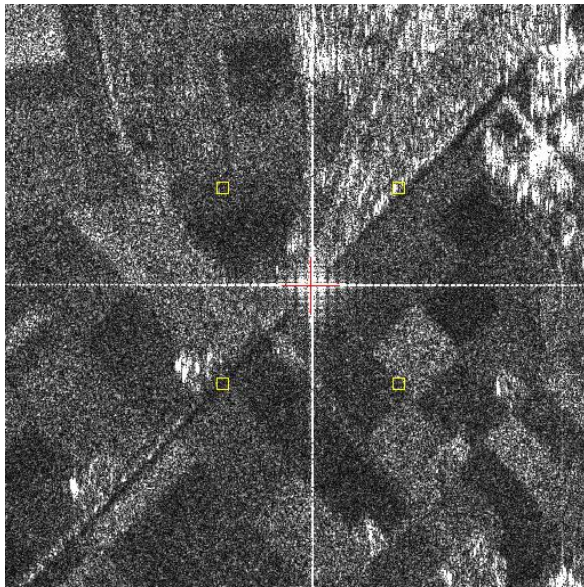


	Phase Difference (°)
SM	-0.77±0.73 (75)
IW	-0.93±0.51 (74)
EW	-1.37±0.85 (92)

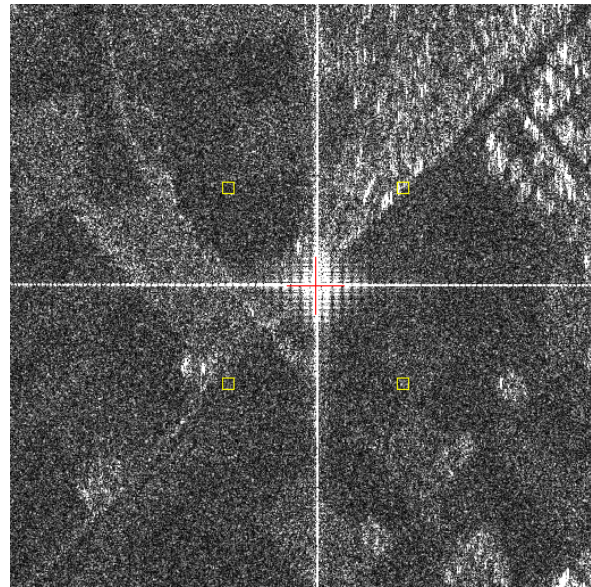
Table 23: Phase Imbalance using the DLR transponders

4.2.5.3. Coregistration

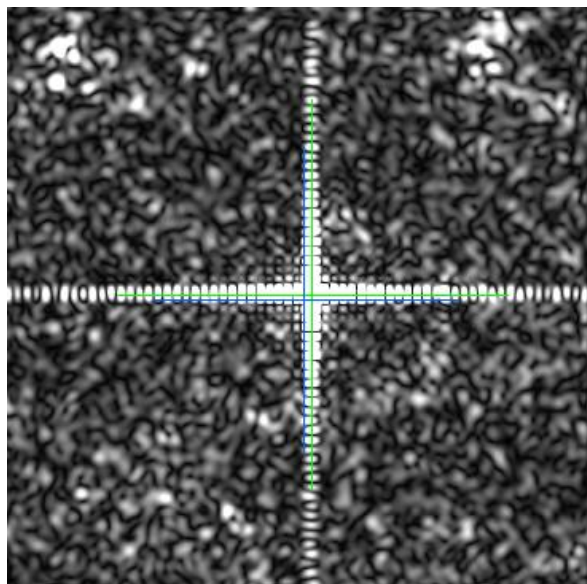
The ESA transponders deployed during the Commissioning Phase and the DLR transponders both provide an impulse response in both polarisations of dual polarisation imagery. Figure 34 shows examples of SM, IW & EW co-registration for ESA and DLR transponders (the SM acquisitions are shown at full resolution while for the IW & EW acquisitions, oversampled images are shown). In all three examples the co-registration was zero in both range and azimuth. Table 24 below shows that the average measured polarimetric co-registration derived from SLC products acquired during 2015 is very small (the IRF peak position is measured to a 1/8 of a pixel).



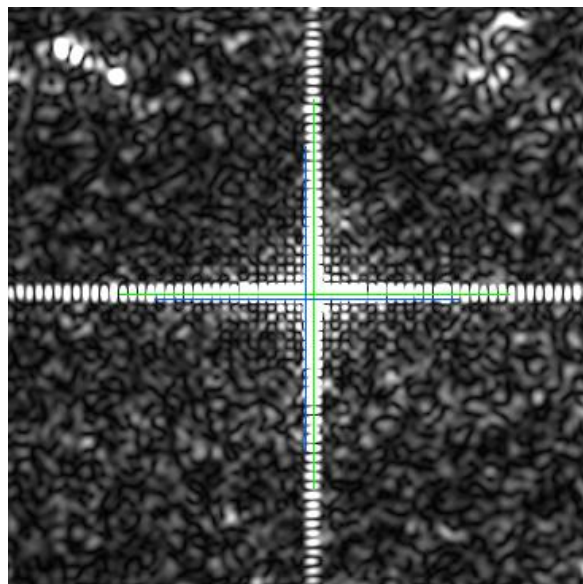
ESA NLR (S6 SLC HH)



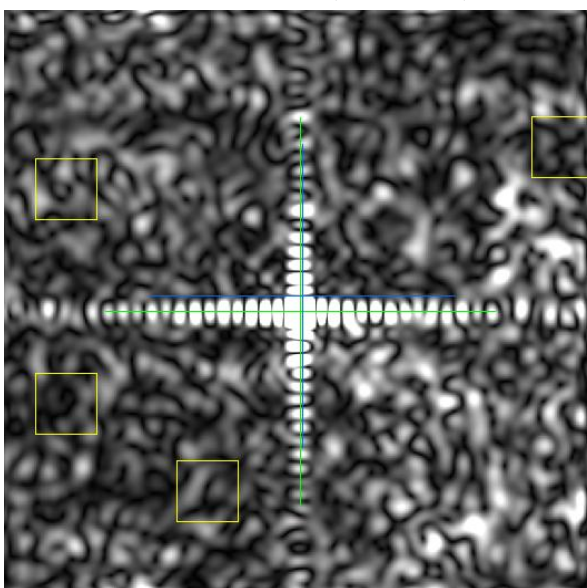
ESA NLR (S6 SLC HV)



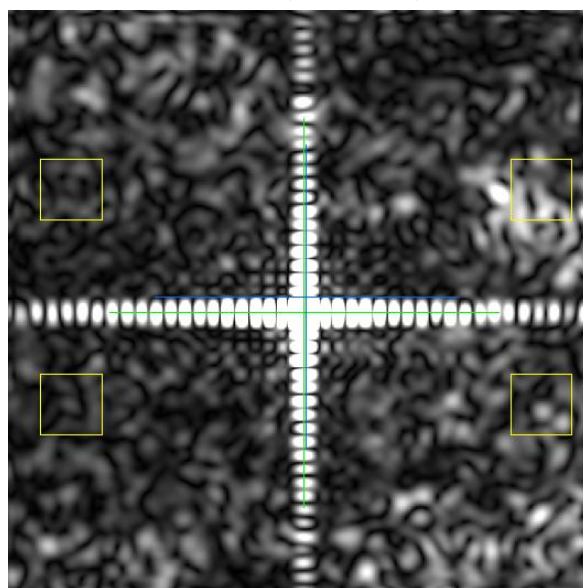
DLR D39 (IW SLC HH)



DLR D39 (IW SLC HV)



DLR D41 (EW SLC HH)



DLR D41 (EW SLC HV)

Figure 34: SLC Co-registration Examples

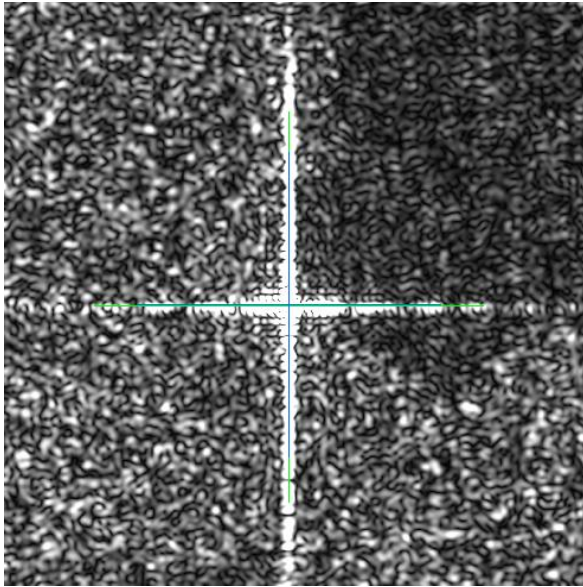
Mode/Swath	Range Co-registration Accuracy (m)	Azimuth Co-registration Accuracy (m)	Number of Measurements
SM	0.03±0.08	0.00±0.00	152
IW	0.01±0.04	0.00±0.00	561
EW	0.02±0.11	0.09±0.47	265

Table 24 Polarimetric Calibration Measurements

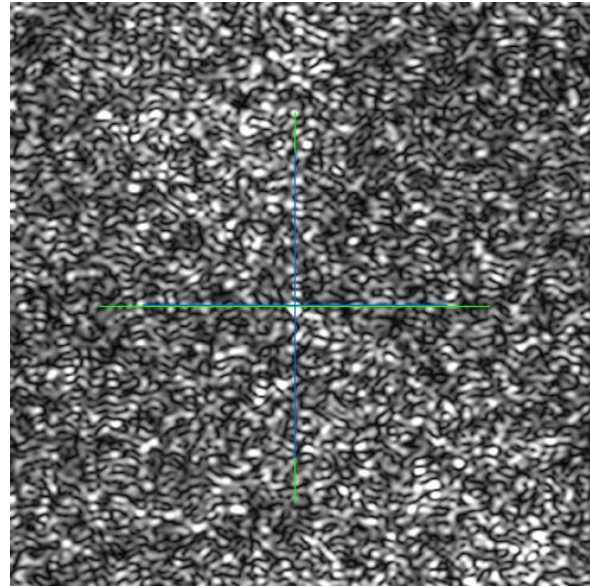


4.2.5.4. Cross-talk

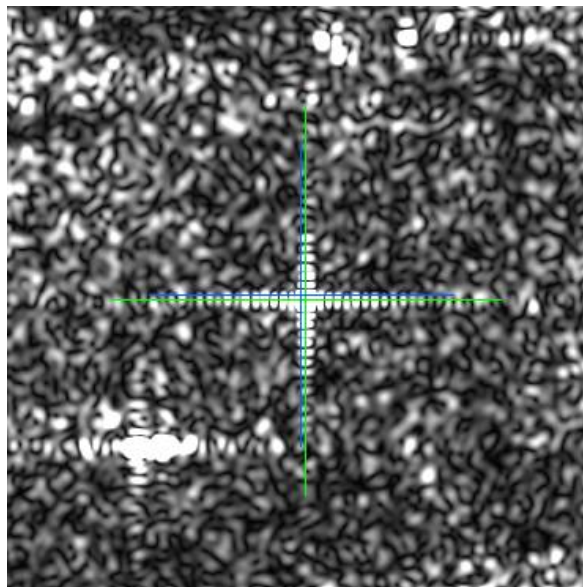
The point targets used for the cross-talk analysis are either the DLR or BAE trihedral corners reflector as they both provide an impulse response in only one polarisations (HH or VV) of dual polarisation imagery. Figure 35 shows examples of SM, IW & EW cross-talk for DLR corner reflector (the images shown are oversampled): the measured cross-talk for SM is -30.6dB, for IW is -49.20dB while for EW no cross-talk IRF could be identified. Based on results from the Commissioning Phase, Table 25 below shows that the measured cross-talk is very low. The majority of the cross-talk measurements are from SM and IW imagery but does include some EW measurements even though in many cases a response cannot be identified in the corresponding cross-polarisation image.



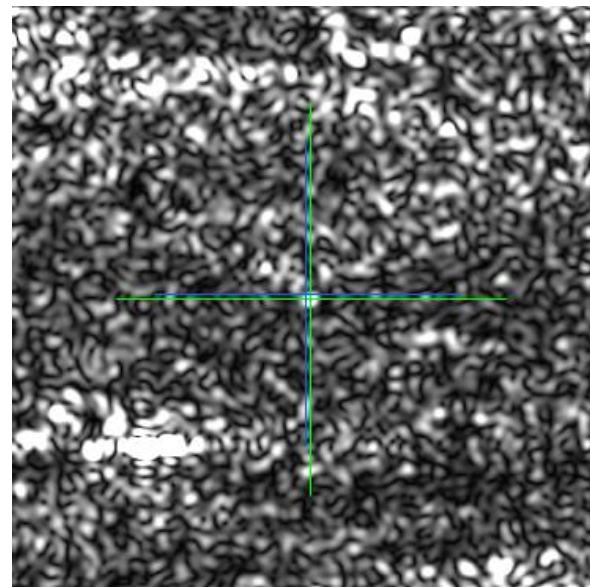
DLR CR D38 (S5 SLC VV)



DLR CR D38 (S5 SLC VH)



DLR CR D38 (IW SLC HH)



DLR CR D38 (IW SLC HV)

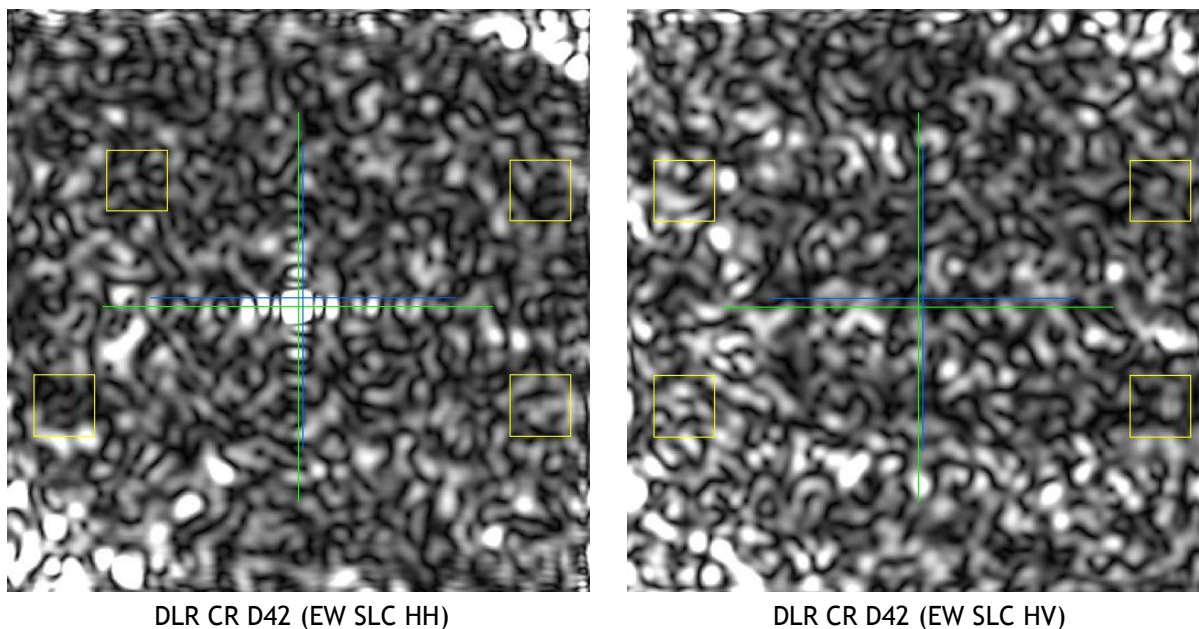


Figure 35: SLC Cross-talk Examples

Corner Reflector Cross-talk (m)	Number of Measurements
-38.7±6.9	28

Table 25: SLC Cross-talk

4.2.6. Elevation Antenna Patterns

With the IPF v2.45 update in May 2015 the elevation antenna pattern was changed to be complex but the gain of the elevation antenna patterns for all modes were not changed. These complex EAPs were included in the AUX_CAL auxiliary files generated on 4th May 2015 (see Appendix F).

As part of the IW and EW re-calibration during the latter part of the 2015, as described in the ESA User Note "S1-A Radiometric Calibration Refinement#1" (see Appendix C), the elevation antenna patterns were adjusted by applying a linear ramp. The other adjustment was refining processing gains.

4.2.7. Azimuth Antenna Patterns

During January 2015 the Azimuth Antenna Patterns (AAPs) were updated in AUX_CAL auxiliary files generated on 19th January 2015 (see Appendix F). These changes were made for all modes except WV mode to take into account the failed Tile 4 TRMs that occurred on 05-May-2014 and 09-June-2014 (see Appendix D). An example of the difference between the previous (pre-launch) and updated azimuth antenna patterns is shown in Figure 36 for SM mode, swath 6 and HH polarisation. The blue curve is the pre-launch pattern; red curve is the updated pattern with the Tile 4 TRM failures while the green curve is the difference. Similar differences are found for other modes, swaths and polarisations.

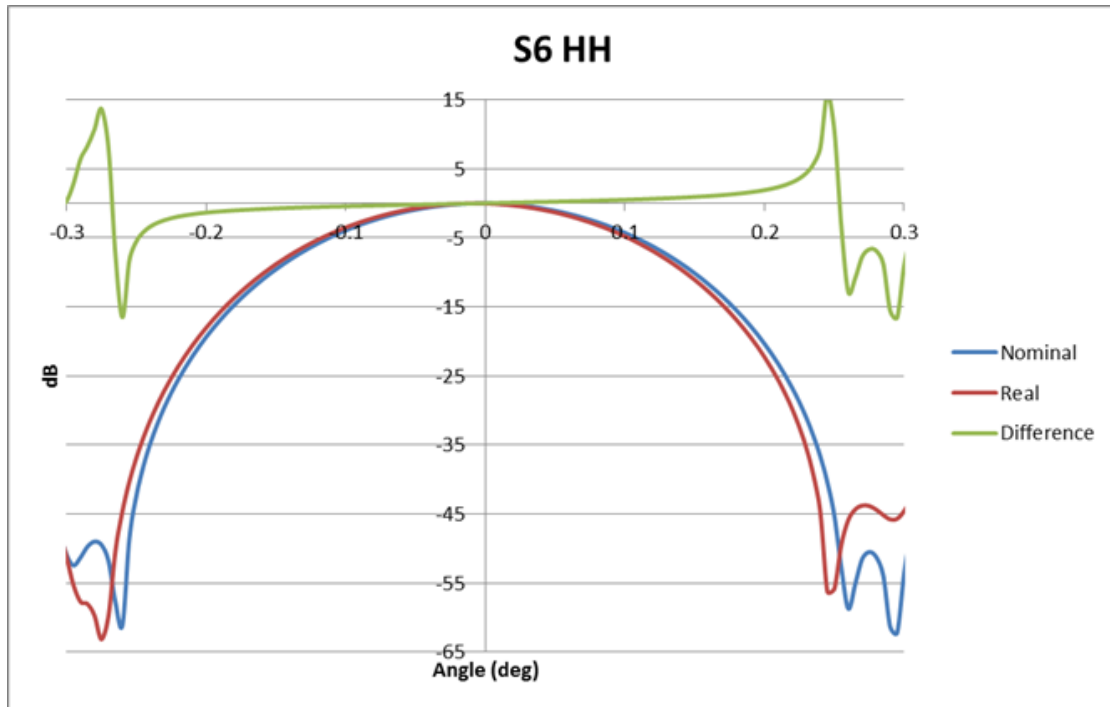


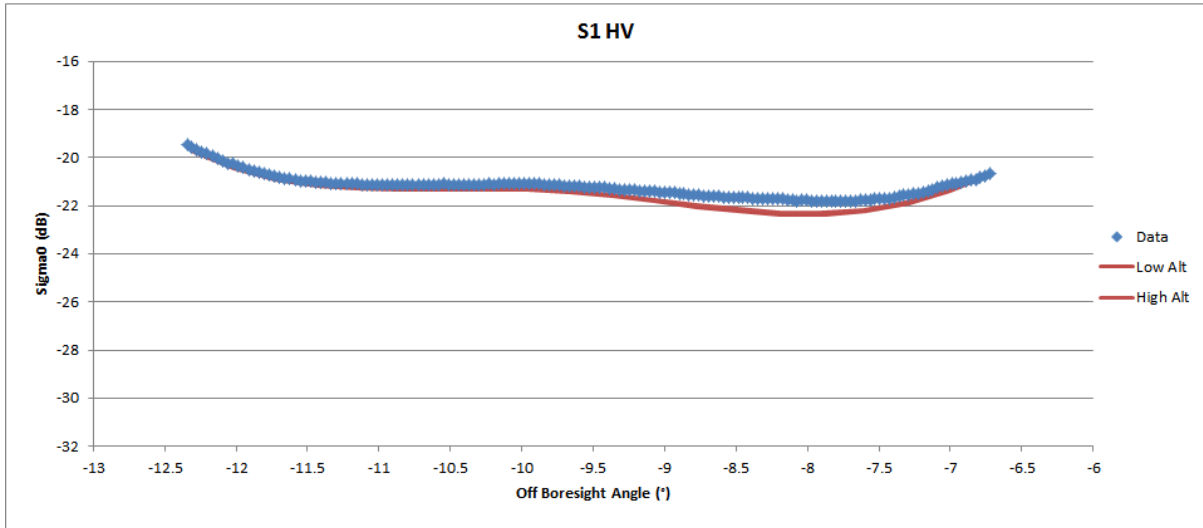
Figure 36 Example Updated Azimuth Antenna Pattern

Also with the IPF v2.45 update in May 2015 actual WV mode AAPs derived from the antenna model were included (rather than the flat patterns previously used). These were included in AUX_CAL auxiliary files generated on 4th May 2015 (see Appendix F).

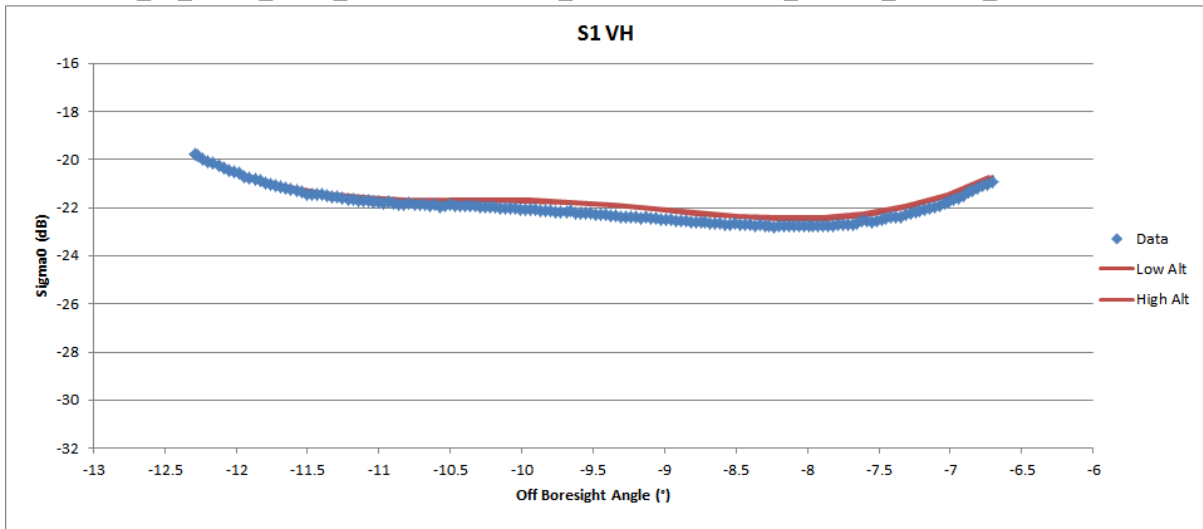
4.2.8. Noise Equivalent Radar Cross-section

Examples of S1-A imagery with low ocean backscatter have been used to estimate the Noise Equivalent Radar Cross-Section (NESZ) for all modes and swaths. These are shown in Figure 37 to Figure 40 for SM, IW, EW and WV modes respectively based on imagery acquired during 2014 and 2015. For all but WV mode, the majority of the NESZ estimates have been performed in cross-polarisation (HV or VH) as the ocean backscatter is much lower compared to co-polarisation. For WV mode where the imagerettes are only acquired in co-polarisation, suitable data has been selected by the extraction of the I and Q channel standard deviation parameters from annotation products (a low standard deviation indicates a low radar cross-section). In addition to the measured NESZ, all the plots show the predicted NESZ (at low and high orbital altitudes).

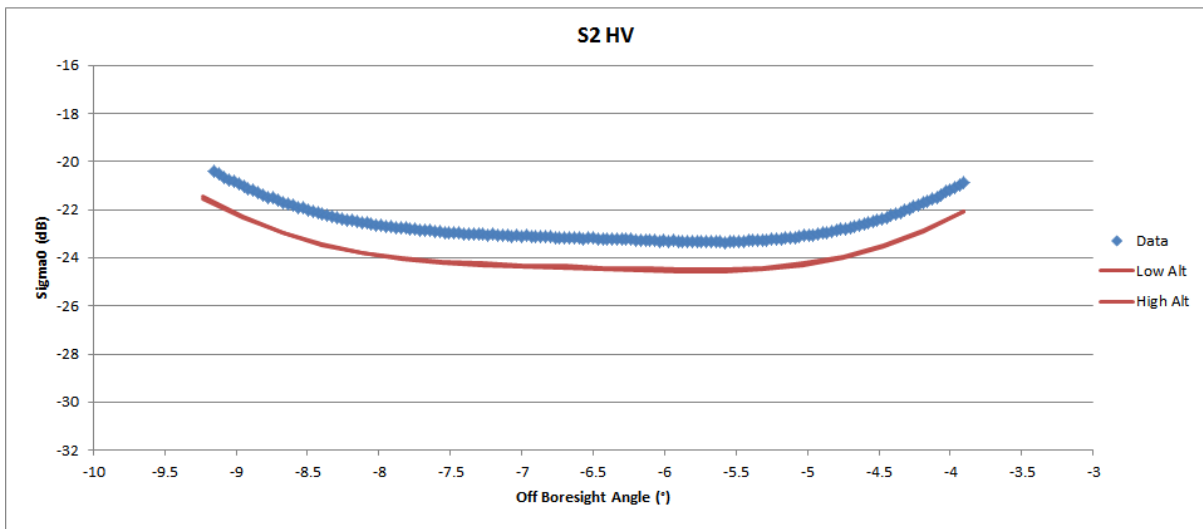
In Figure 37 for SM, the measured NESZ are close to the predicted NESZ. In addition, for many SM swaths the measured NESZ exceeds the NESZ requirements of -22 dB. The main exception is SM3 where the measured NESZ is -20dB at mid-swath. For some of the other swath, the requirement is not met at the edges of the swath.



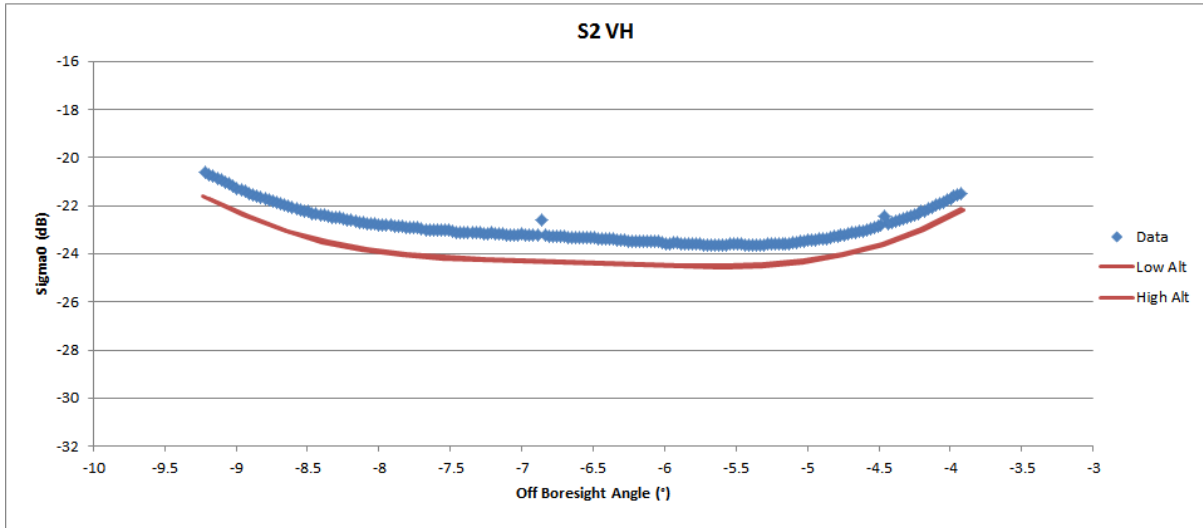
S1A_S1_GRDH_1SDH_20141226T140027_20141226T140055_003891_004AA7_BF83.SAFE



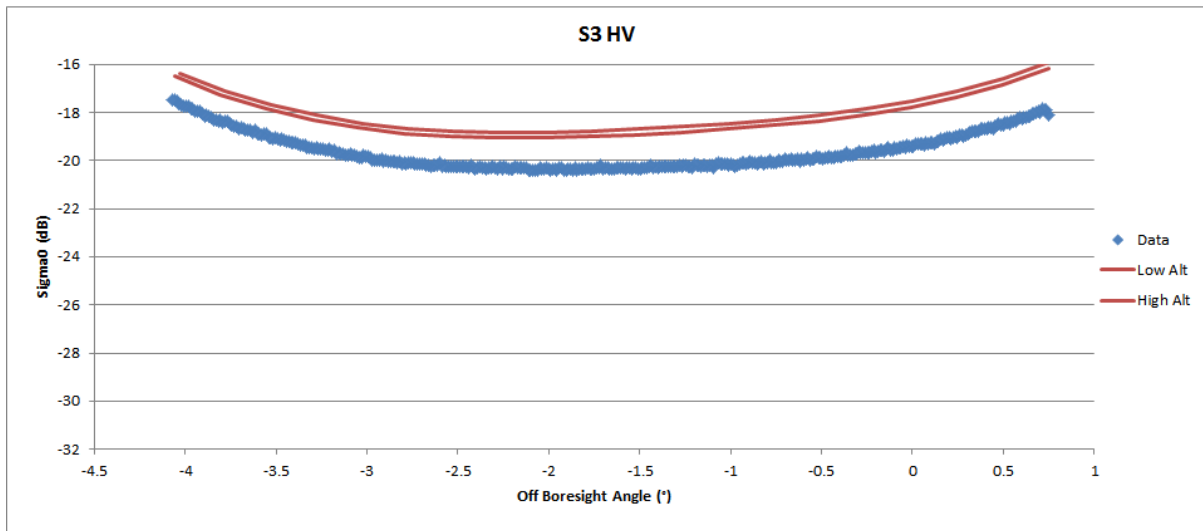
S1A_S1_GRDH_1SDV_20141230T164844_20141230T164908_003951_004C09_3702.SAFE



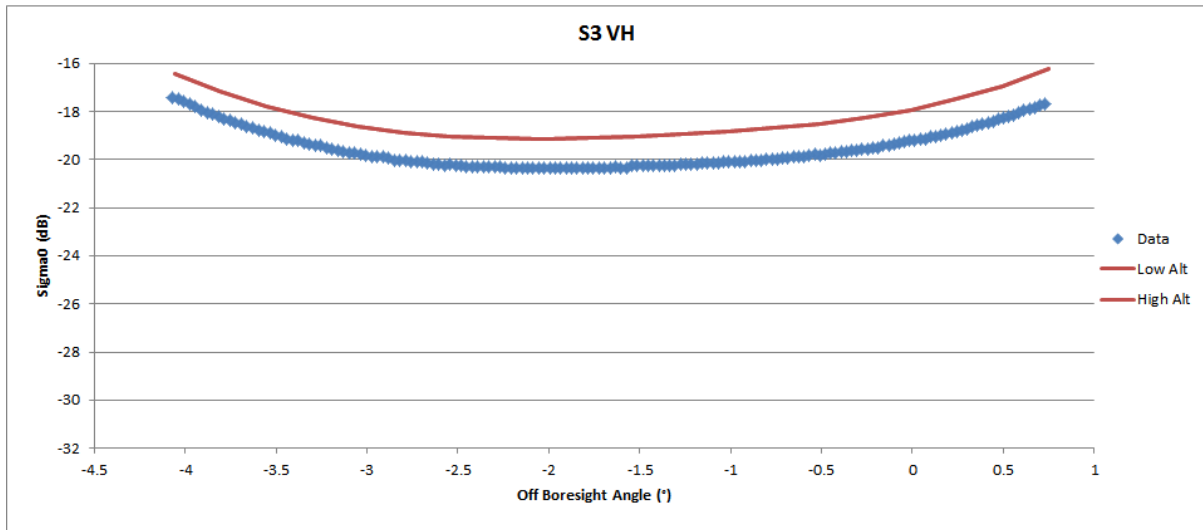
S1A_S2_GRDH_1SDH_20141225T042942_20141225T043016_003871_004A30_0213.SAFE



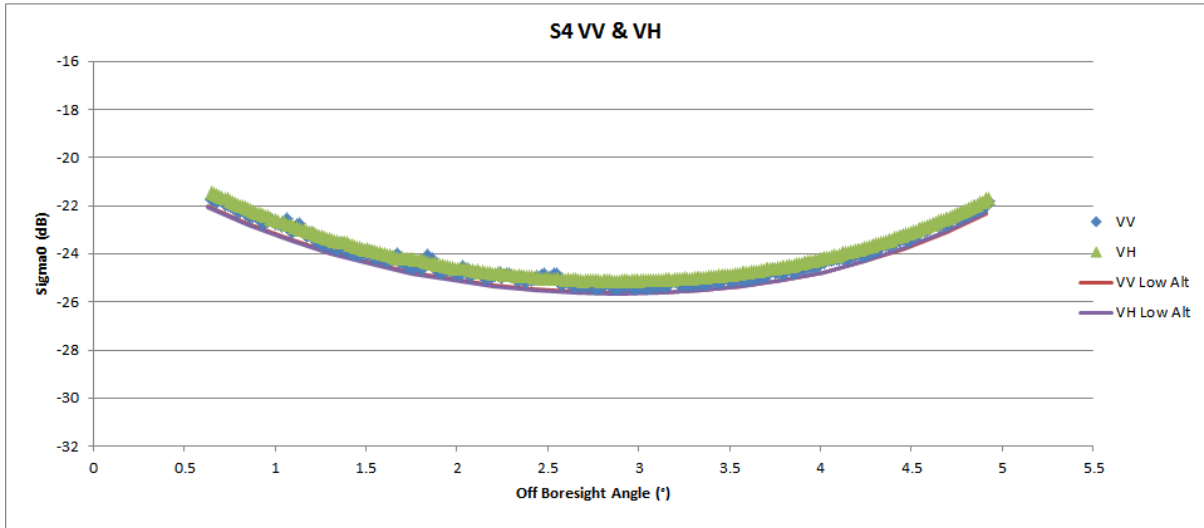
S1A_S2_GRDH_1SDV_20141215T112626_20141215T112655_003729_004706_DBAB.SAFE



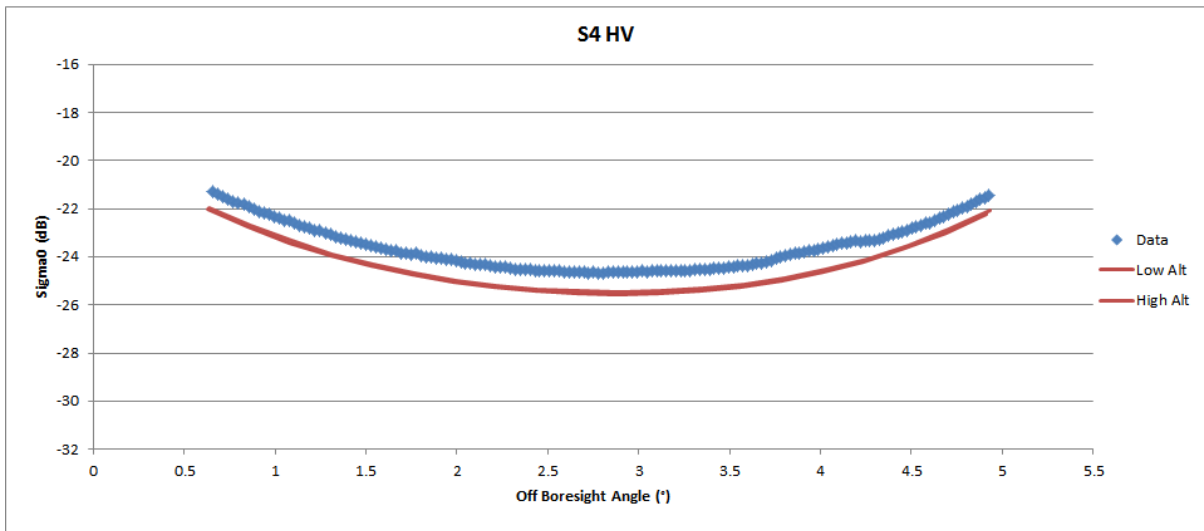
S1A_S3_GRDH_1SDH_20150126T135226_20150126T135255_004343_0054C1_ADEE.SAFE



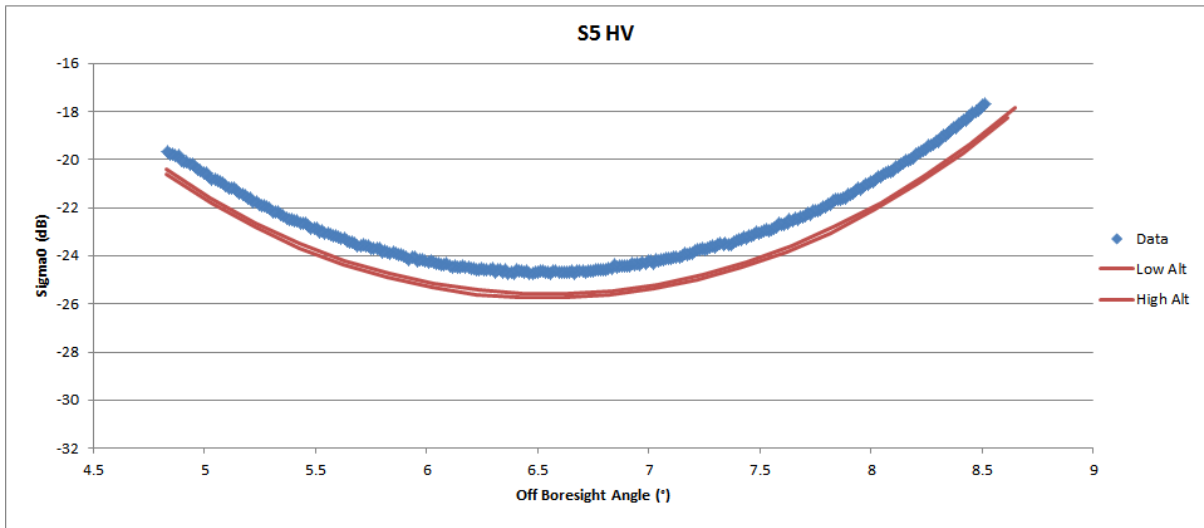
S1A_S3_GRDH_1SDV_20141214T140019_20141214T140047_003716_0046AB_447A.SAFE



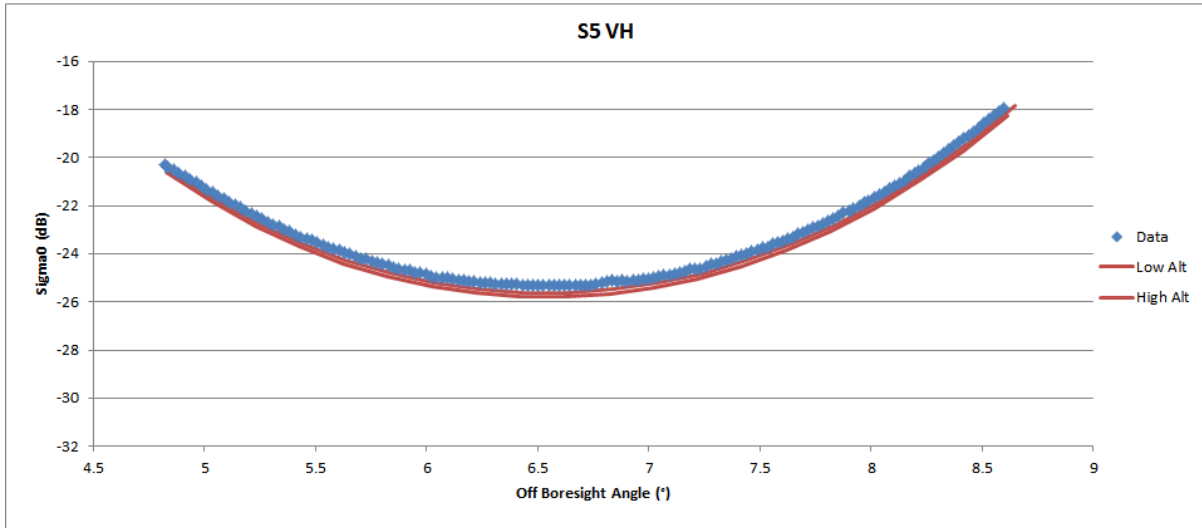
S1A_S4_GRDH_1SDV_20141208T042316_20141208T042335_003623_004494_F2EB.SAFE



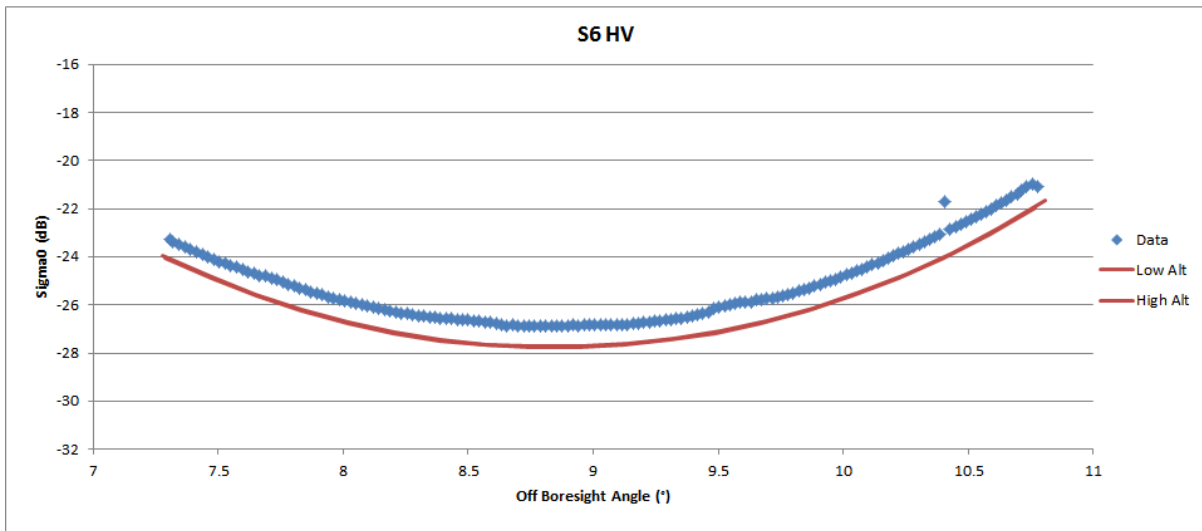
S1A_S4_GRDH_1SDH_20141217T022659_20141217T022724_003753_004794_183E.SAFE



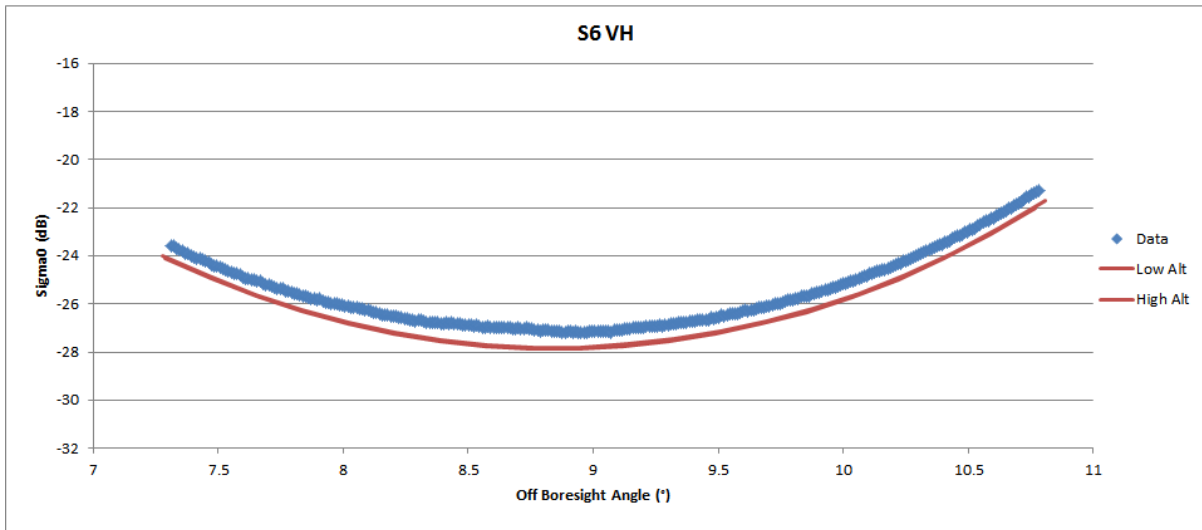
S1A_S5_GRDH_1SDH_20141126T063052_20141126T063110_003449_004087_FC6C.SAFE



S1A_S5_GRDH_1SDV_20141216T070256_20141216T070315_003741_00474D_C69B.SAFE



S1A_S6_GRDH_1SDH_20141221T103142_20141221T103210_003816_0048FC_898D.SAFE

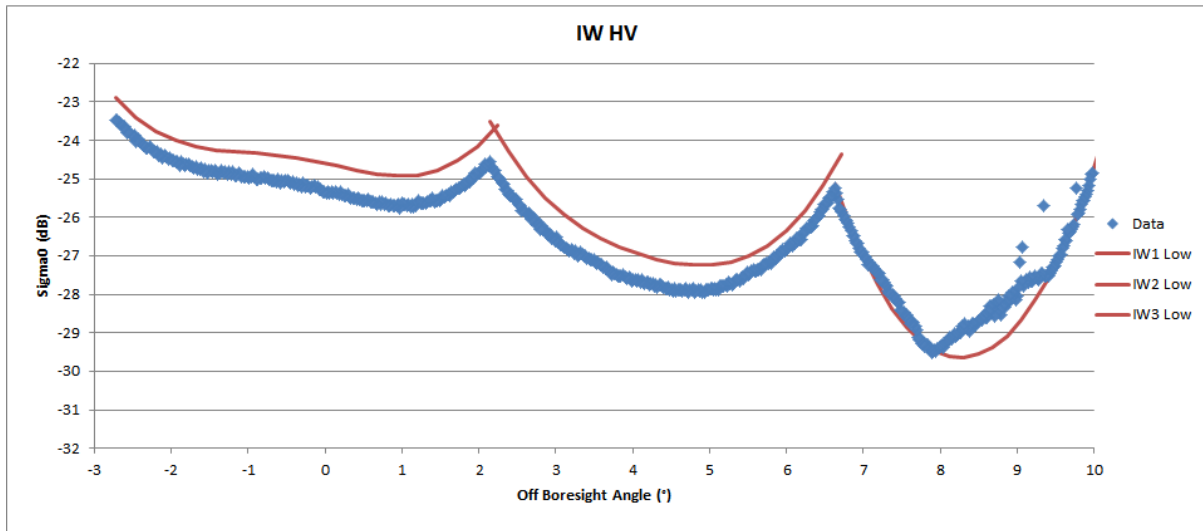


S1A_S6_GRDH_1SDV_20141208T042120_20141208T042154_003623_004493_2D18.SAFE

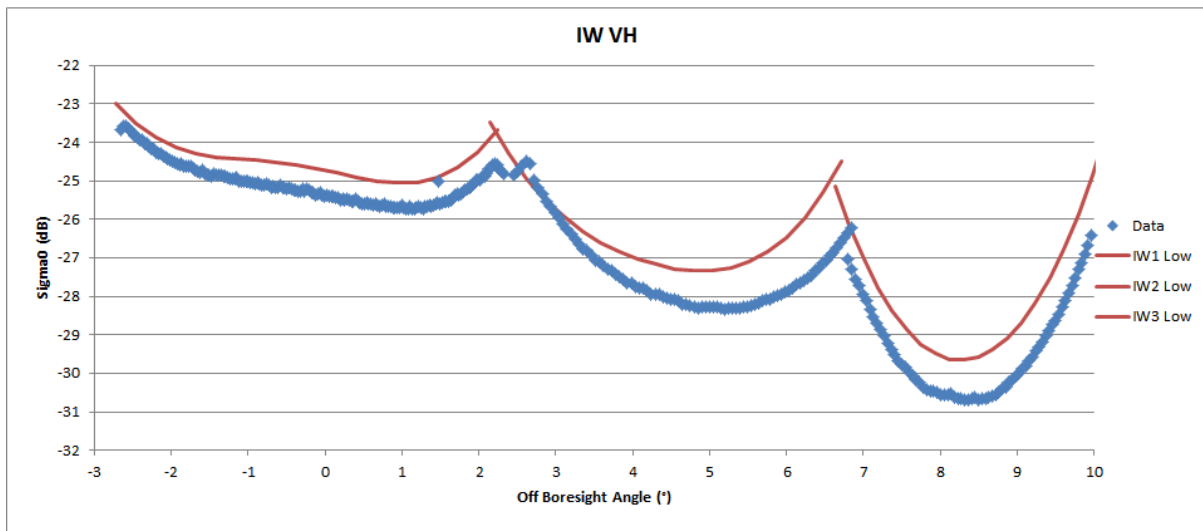
Figure 37: NESZ measures for SM. Blue is the measured NESZ and the red lines are the predicted NESZ at minimum and maximum orbital altitudes.



In Figure 38 for IW and Figure 39 for EW, the -22 dB requirement is met at all sub-swaths and all off-boresight angles. For IW the measurements are slightly better than the prediction while for EW the measurements are slightly worse than the prediction.

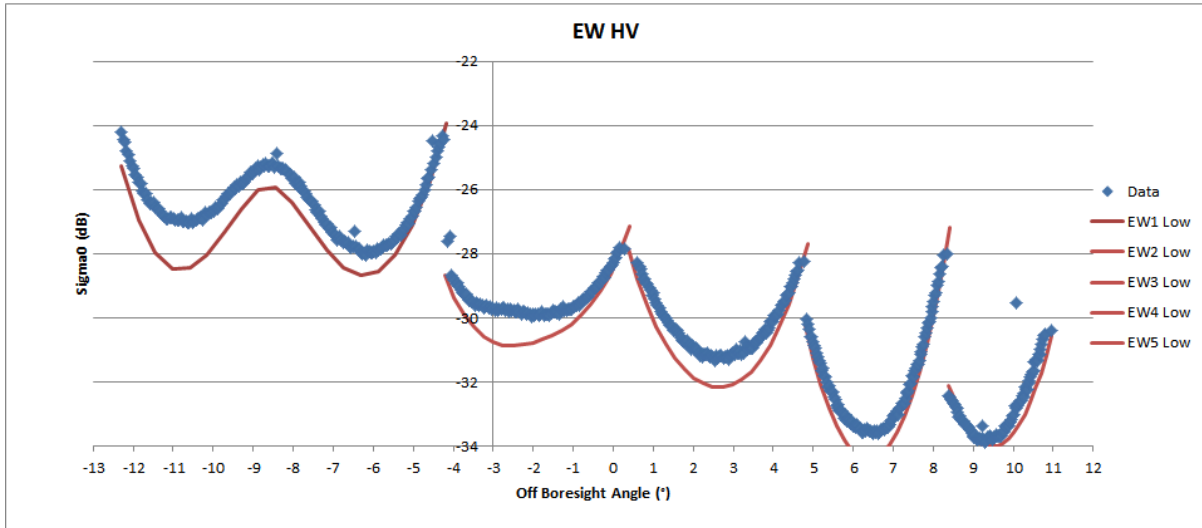


S1A_IW_GRDH_1SDH_20150127T061844_20150127T061913_004353_0054FC_3A7B.SAFE

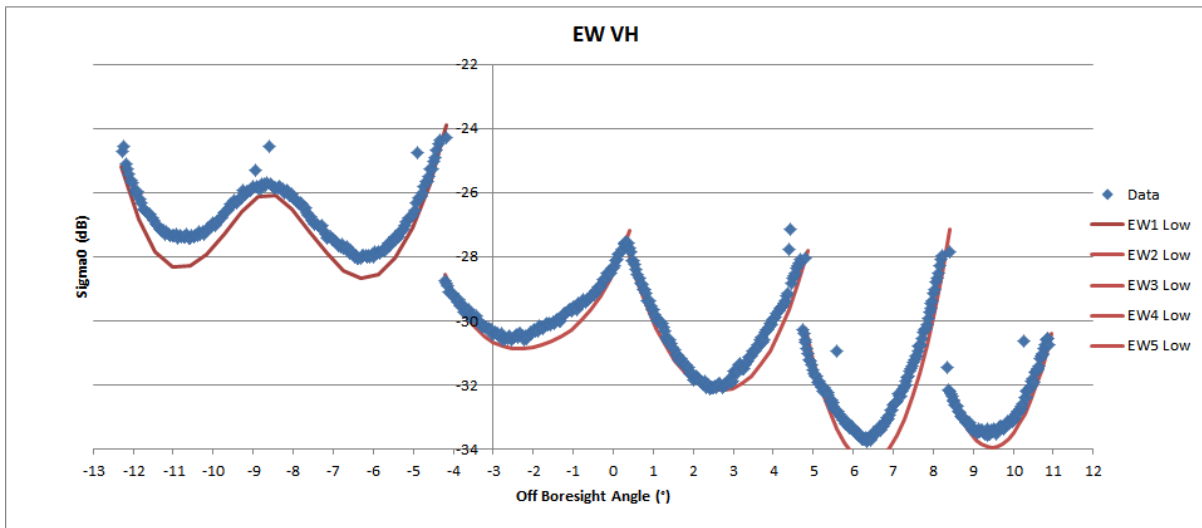


S1A_IW_GRDH_1SDV_20141126T063520_20141126T063545_003449_00408B_59BA.SAFE

Figure 38: NESZ measures for IW. Blue is the measured NESZ and the red lines are the predicted NESZ at minimum and maximum orbital altitudes.



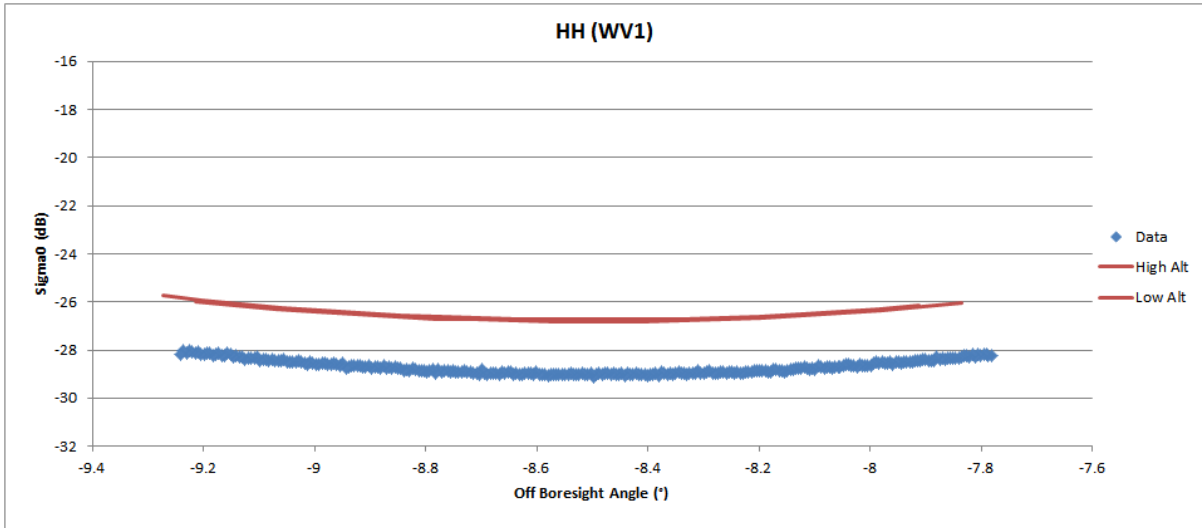
S1A_EW_GRDH_1SDH_20141126T173642_20141126T173746_003456_0040B5_8F0F.SAFE



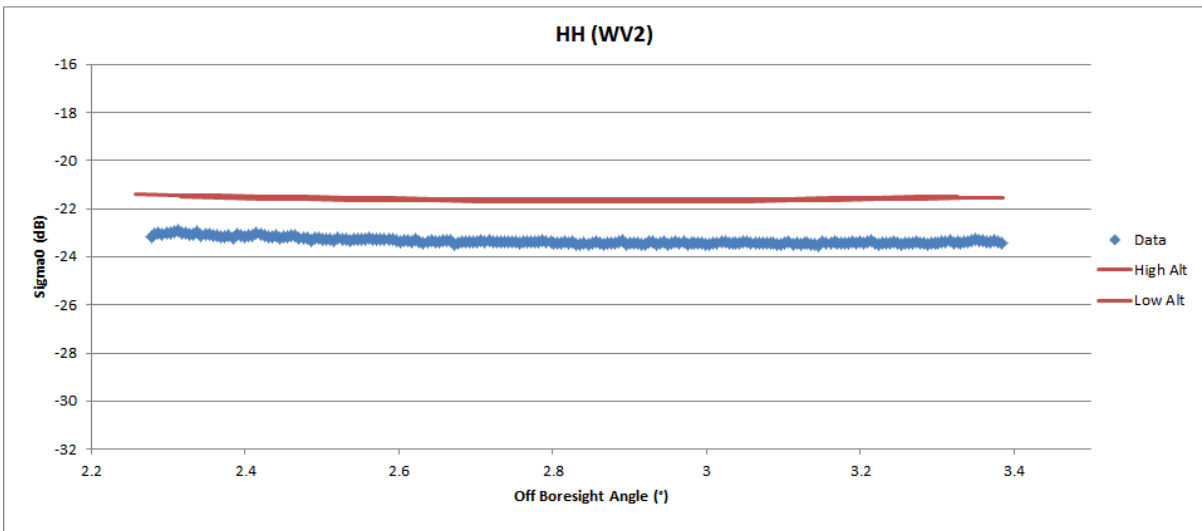
S1A_EW_GRDH_1SDV_20141208T113419_20141208T113519_003627_0044B1_385B.SAFE

Figure 39: NESZ measures for EW. Blue is the measured NESZ and the red lines are the predicted NESZ at minimum and maximum orbital altitudes.

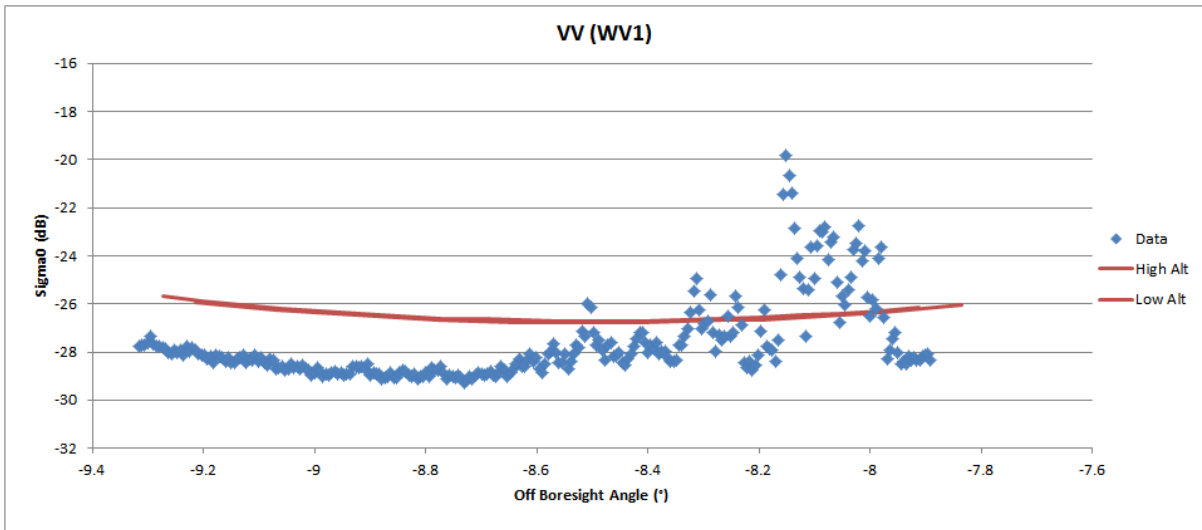
Figure 40 shows the measured NESZ for WV mode all met the -22 dB requirement and they are all slightly better than the predicted NESZ. Note the NESZ is significantly higher for imagette WV2 than for WV1. For WV1 VV there is some structure in the imagette which accounts for the structure in the NESZ measurement in the far range portion of the imagette. The number after the file name refers to the imagette number within the product.



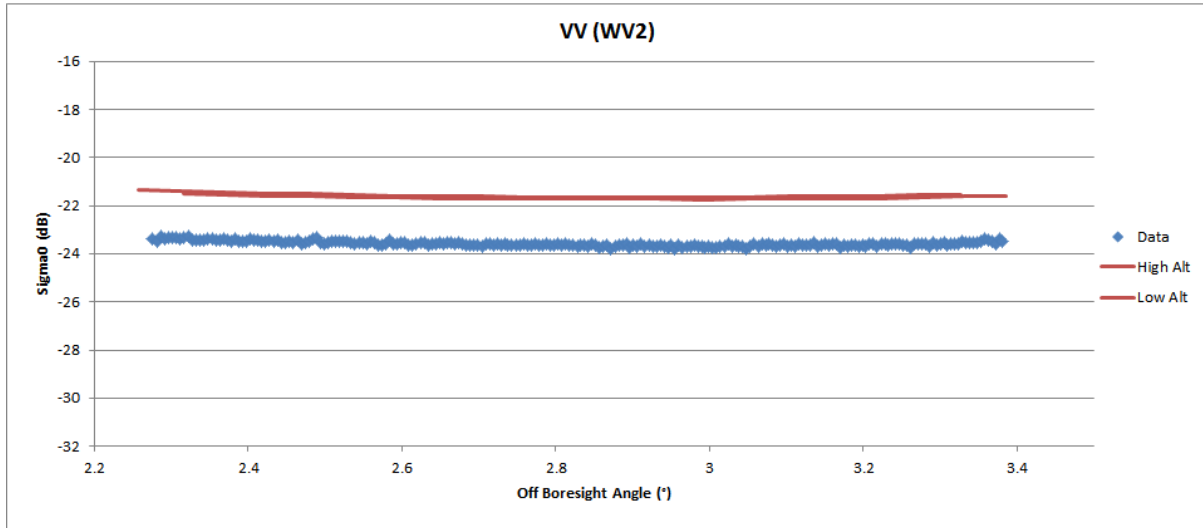
S1A_WV_SLC__1SSH_20150131T123642_20150131T124843_004415_00565A_D1D2.SAFE (009)



S1A_WV_SLC__1SSH_20150130T022919_20150130T024051_004394_0055E1_C17C.SAFE (036)



S1A_WV_SLC__1SSV_20150217T014102_20150217T020318_004656_005BF6_11FA.SAFE (025)



S1A_WV_SLC_1SSV_20150209T152948_20150209T154021_004548_005968_27D3.SAFE (020)

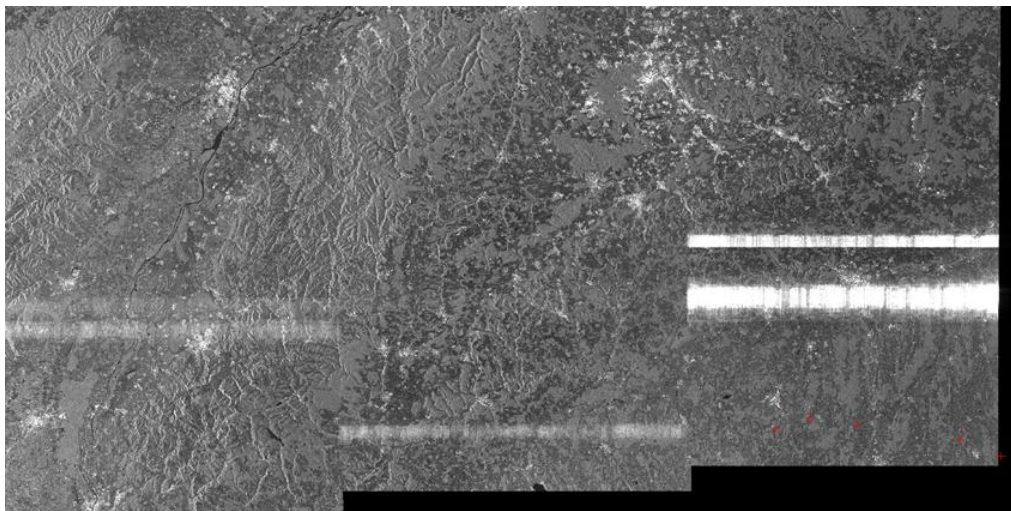
Figure 40: NESZ measures for WV. Blue is the measured NESZ and the red lines are the predicted NESZ at minimum and maximum orbital altitudes.

With the IPF v2.51 update in July 2015 the noise calibration factors were updated. These factors are used to calculate the denoising vectors included in the product annotation. The update was from default values to those corresponding to the theoretical NESZ curves shown above. The associated auxiliary file updates were made on 3rd July 2015 (see Appendix F). A further refinement was performed in September 2015 to reflect the actual NESZ profiles indicated in the above plots - the associated auxiliary file updates were made on 8th September 2015 (see Appendix F).

4.2.9. Summary of Anomalies

4.2.9.1. Radio Frequency Interference

As small percentage of Sentinel-1A imagery is affected by the presence of Radio Frequency Interference from the ground. An example is shown below over Germany (the red crosses are the location of some of the DLR corner reflectors and transponders. Usually RFI only affects a few range lines of raw data.



S1A_IW_GRDH_1SDV_20151013T171526_20151013T171555_008137_00B6BD_A92D.SAFE

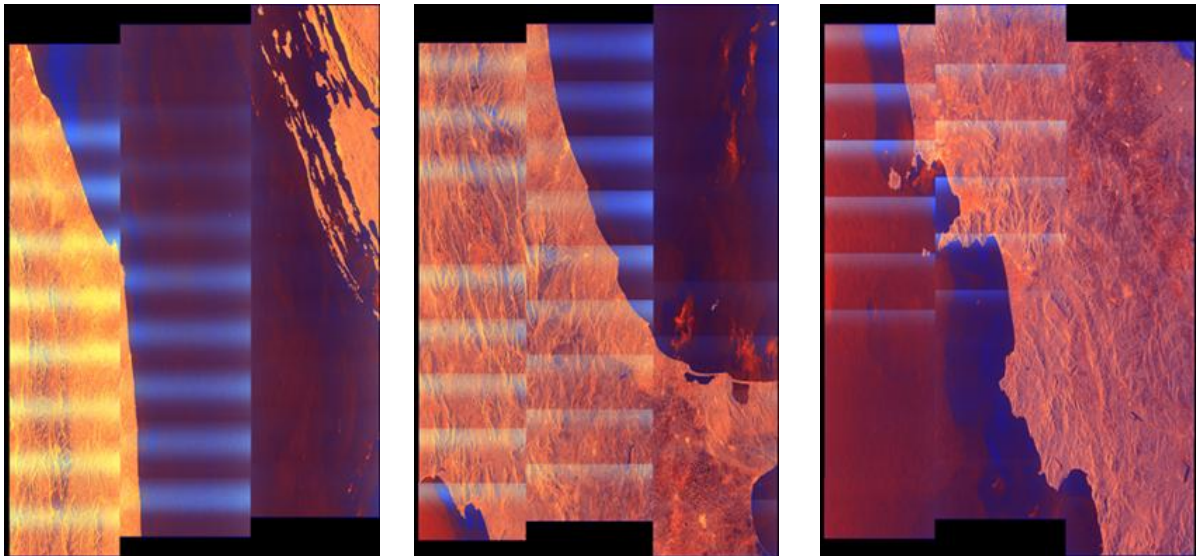
Figure 41: An example of Radio Frequency Interference



4.2.9.2. Radarsat-2/Sentinel1-A Mutual Interference

Although the orbit altitude of Radarsat-2 and Sentinel1-A are quite different (789 km and 693 km respectively) their repeat periods are a multiple of each other (24 days and 12 days respectively) and their equatorial crossing times are almost the same (~18:00 hrs at the ascending node). Another similarity is that both SARs operate at the same frequency.

The repeat period and crossing times mean that every 24 days, Radarsat-2 will be directly above Sentinel-1 and hence both may be imaging the region of the Earth's surface at the same time. If this occurs then mutual interference is detected. Figure 42 shows an example in Sentinel-1A imagery over Italy - banding can be seen in IW sub-swaths for a duration of a few minutes. Similar interference is seen in Radarsat-2 imagery. As the exact equatorial crossing time of the two satellites is slowly drifting (by a few seconds per cycle), the exact location of the mutual interference moves to a different latitude every 24 days ([S1-RD-05]).



S1A_IW_SLC__1ADV_20150816T
165644_20150816T165711_0072
91_009FF3_1C25.SAFE

S1A_IW_SLC__1ADV_20150816
T165709_20150816T165737_00
7291_009FF3_BEAC.SAFE

S1A_IW_SLC__1ADV_20150816T1
65644_20150816T165711_007291
_009FF3_1C25.SAFE

Figure 42: An example of Radarsat-2/Sentinel1-A Interference

4.2.9.3. Other Anomalies

An unusual anomaly identified by a user is shown in Figure 43 for a region near Beijing, China - the anomaly being the series of almost straight white lines. Close examination of these - see Figure 44 - concluded that they were due to trains. Any object moving with a component of its velocity in the range direction will lead to a displacement in azimuth. Figure 44 (left) shows the train and the fainter track - as the range velocity reduces so does the azimuth displacement between the track and train (as expected). Figure 44 (right) also include one of the azimuth ambiguities towards the bottom of the image.



S1A_IW_GRDH_1SSV_20141008T222018_20141008T222047_002744_003146_8417

Figure 43: An unusual user anomaly



Figure 44: Detail of an unusual user anomaly

4.2.10. Quality Disclaimers

Quality disclaimers issued during 2015 are given in Appendix H.

Proprietary information: no part of this document may be reproduced divulged or used in any form without prior permission from CLS.



4.3. Level 2 products

4.3.1. Wind measurement

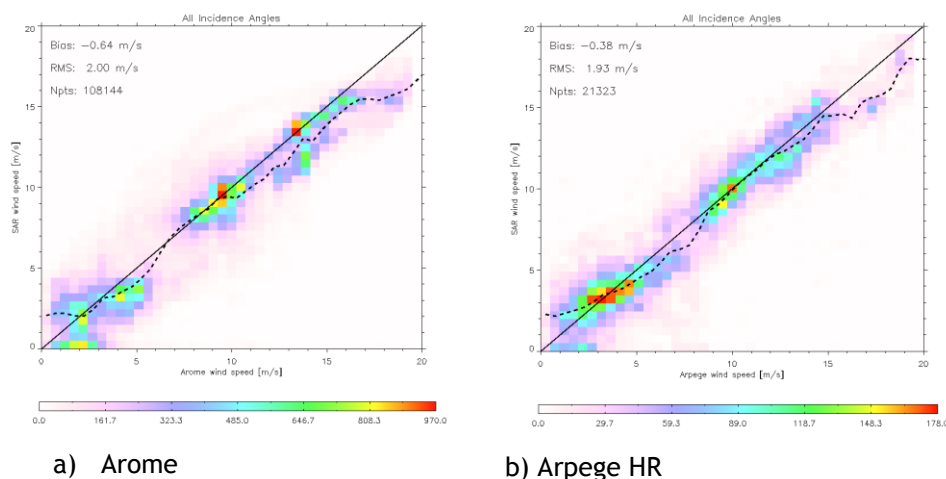
4.3.1.1. Image Mode (SM-IW-EW)

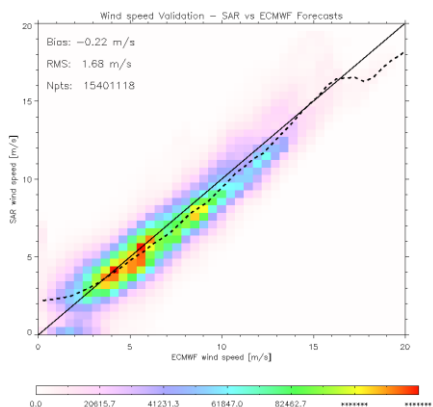
The SAR wind measurement is strongly dependant of the product calibration accuracy. Thus, its quality has improved during 2015 as far the calibration of the products has improved. It takes benefit from the efforts made on the SAR Level1 products to improve the calibration constant and align the gamma profile as the function of the elevation angle over Rain Forest. These improvements reduce the wind measurements error belong the subswath and subswath by subswath.

Statement of the wind measurements accuracy:

The strategy to assess the accuracy of the wind retrieval is to compare it with an auxiliary wind source which is used as a reference. This source could be in-situ data from buoy, other satellite data (ex: scatterometer) or atmospherical model outputs. It is important to outline the importance to multiple the types and the number of the data used as reference, due to their coverage, resolution or possible bias. In this scope, Ifremer has performed systematic collocations with such data (model: ECMWF (global), Arome, Arpege (European), hundreds of buoys, etc.) with L2 products generated by the ESA-IPF by PDGS.

Figure 45 presents the performances achieved on the month of December 2015 for IW mode in VV polarisation of the retrieved wind compared to model references (Arome, Arpege and ECMWF). It can be noticed the strong correlation of the SAR-derived wind speeds with the wind references. The bias and the RMS are less important for ECMWF re-analysis since the wind inversion is based on the ECMWF forecast as an a priori wind input. The observed bias (differences between the dotted line and the diagonal) is really close to zero when the number of observations is significant (red part on the diagram). As expected, at low wind speeds, the NESZ impacts the SAR wind measurement (sur-estimation). At high wind speeds, the SAR tends to sub estimate the wind speed; however the number of samples is low, and may not be sufficient to conclude. A typical RMS of 1.5m/s to 2m/s is observed. The quality of the wind product derived for this mode is fairly good. Same kind of performances (bias nearly equal to zero and RMS of about 2m/s) is achieved on EW HH mode. Other modes such as SM, IW in HH and EW in VV are rarely acquired or processed up to Level 2 products.





	bias	Rms
Arome	-0.64 m/s	2.00m/s
Arpege	-0.38 m/s	1.93 m/s
ECMWF	- 0.22m/s	1.68 m/s

c) ECMWF

Figure 45: SAR Wind speed compared with reference wind speed for IW mode VV polarization.

Improvement performed during 2015:

Many improvements have been performed during this year related to the way to handle the a-priori wind speed/direction -necessary for the wind inversion- and provided via the AUX_WND files (containing ECMWF forecast in GRIB format). A first improvement was performed on June 2015, by patch 2.5.1 of the IPF, allowing the correction of the reading of the zonal and meridional components of the a priori wind, which were in some cases reversed.

During July 2015, an update of the task table at the PDGS level has improved the way to handle the AUX_WND, ensuring the right choice with the closest validity date and the most recent production date. In addition since the IPF2.60 release (November 2015), the production of OWI wind product is not performed (test at the beginning of the L2 processing) in the case of invalid AUX_WND (not specified or with validity date is not in between plus/minus 1h30 compared to the product acquisition date).

Finally, it has to be outlined that during 2015, the calibration level of the L2 products has been aligned with the L1 products, as it was different due to the differences in the processing of internal IPF products. This has been performed at the end of November 2015 by an AUX_PP1 update. The remaining issues on the L2 wind product (OWI) should then be related on the SAR wind retrieval algorithm, the input parameters and/or the L1 quality.

Coming Improvements for 2016:

Some improvements of the SAR retrieved wind measurement remains in the scope of 2016.

1. Issue regarding to the look angle.

It has been recently found a minor issue on the look angle (relative angle between the input wind direction compared to the SAR geometry) used in the OWI process. This should be solved in the beginning of 2016, and will result in reducing the standard deviation and reduce bias (when a low number of occurrences) on the statistics of the SAR derived wind speed compared with the reference wind speed.

2. Issue with the Bright Target

The aim of the Pbright algorithm is to remove bright targets (such as the ships for example) on the averaging of the scattering level (normalized radar cross section) on the cell where the wind retrieval is performed to avoid their contribution. The results of the Pbright algorithm are not optimal and tend of surestimating the numbers of bright targets in the wind cell. It means that it reduce the number of points for the averaging, and then could result in a less-confident and underestimated SAR-retrieved wind speed. An update of the processing parameters will be needed via the AUX_PP2.



3. Activation of the noise removal

The activation of the noise removal will allow to reduce the impact of the NESZ on the wind measurements especially for low-to-moderate wind speed and for wind measurements performed at high incidence angle, resulting on a surestimation of the SAR derived wind speed and possible modulation of the profile of the measured wind speed by the antenna lobe.

4.3.2. Swell Measurement

4.3.2.1. Wave Mode

In 2015, there have been several updates of the LOP for waves inversion. Among them the three most important are:

- The filtering of energy at low frequency. It aims at filtering the signature of ships or rain. Coefficients have been tuned to allow a better detection of the long swell. Indeed the largest size of the imagettes allows to measure longer swells than with Envisat/ASAR.
- The computation of the image modulation spectra. Also to take advantage of the new resolution and size of Sentinel-1 and get a better resolution in the wavenumber domain, the size of the periodogram used for the spectra computation has been doubled.
- Ocean wave spectrum resolution. It has been changed to be consistent with the improved resolution of the image modulation spectra.

The performances are estimated by comparison between the significant wave height of the long waves as measured by Sentinel-1 and produced by Wave Watch 3 model (WW3). WW3 is used to produce a 2D ocean wave spectra for each Sentinel-1 acquisition. On a statistical basis, WW3 is used as the reference. For both S-1A and WW3, the significant wave height of the long waves is estimated by integration of the 2D ocean wave spectra up to the cut-off values (above this value, the inversion is not expected to work).

Figure 46 illustrates the significant wave height performances for the month of December 2015 in Wave Mode 1 and Wave Mode 2. There is a remaining bias (0.87 m) for Wave Mode 1.

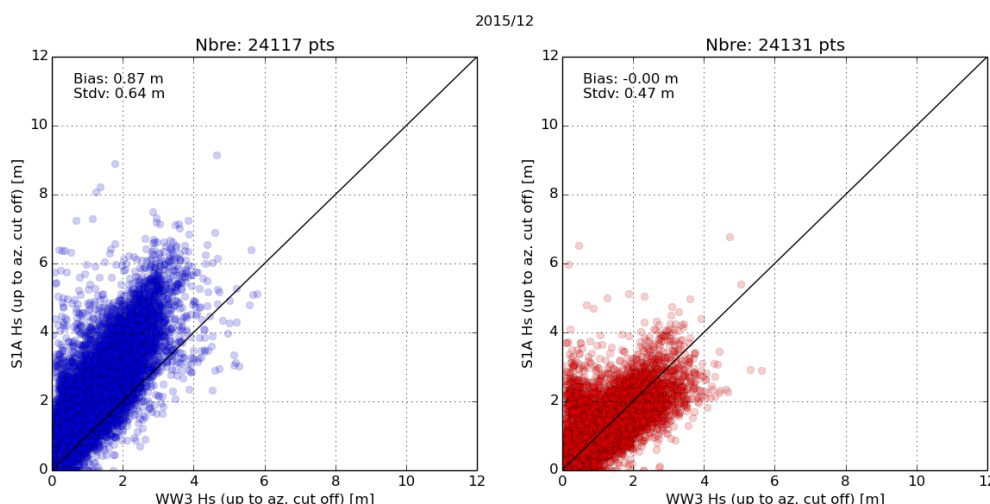


Figure 46: Significant wave height for the long waves performances for December 2015 in Wave Mode 1 (left) and Wave Mode 2 (right). The model outputs from WW3 are considered as reference here. This is only valid from a statistical point of view.

Improvement performed during 2015:

Figure 47 shows the monthly performances with respect to time in 2015. Note that no performances indicator have been estimated for April due to a lack of reference data (to be resolved soon). We

Proprietary information: no part of this document may be reproduced divulged or used in any form without prior permission from CLS.



observe a significant change after May 2015. In particular, this yields to a switch between WV1 and WV2 performances. Indeed before summer, WV1 results are good when compared to WV3 whereas significant wave heights from WV2 are underestimated. After May 2015, this is the contrary: WV2 results are good and significant wave heights from WV1 are overestimated. For the last 7 months, we observe fewer fluctuations. Indeed, the IPF is now stabilized. We observe a remaining bias for both Wave Mode 1 whereas Wave Mode 2 bias is close to zero.

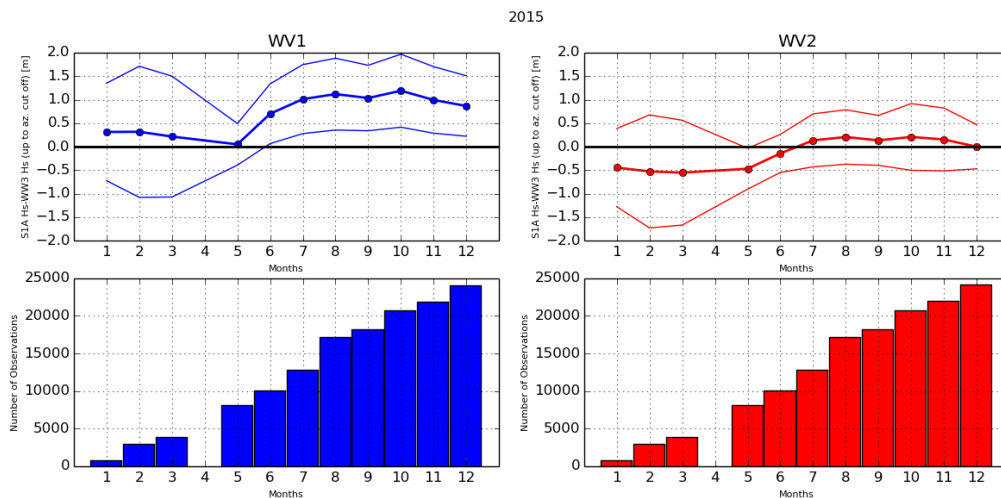


Figure 47: Monthly performances for WV1 (top-left) and WV2 (top-right) and number of acquisitions co-located to reference data for validation for WV1 (bottom-left) and WV2 (bottom-right). Thick solid lines stand for the mean difference between Sentinel-1 and WW3 model significant wave height.

Coming Improvements for 2016:

The reason of the changes in the significant wave height performances in Summer 2015 is still under investigation and is the priority for the beginning of 2016. This is a pre-requisite to stabilize the optimal version (with respect to the ATBD [S1-RD-11]) of the swell inversion algorithm before going further for fine tuning of the modulation transfer functions.

Improvements performed during Q1 2016:

During Q1 2016, several changes were put in place in order to improve these performances:

- Tuned X and Y-Hanning filters are now applied to the cross co-variance for smoothing to compensate for the large periodogram sizes.
- An adhoc RAR MTF is estimated taking into account this change, tested over the May 2015 dataset (related to AUX_SCS auxiliary files).
- An adhoc tuning of the total MTF is estimated separately for wv1 and WV2 in order to remove the different bias between the two incidence angles.
- Improvements brought to the partitioning algorithm are also expected to further improve the estimation of the integral parameters.

4.3.3. Radial Velocity Measurement

4.3.3.1. Wave Mode

The radial velocity measurement is derived from the Geophysical Doppler anomaly. In the S-1 IPF, this geophysical Doppler is estimated by:

$$F_{dc_{RVL}} = F_{dc_{SAR}} - F_{dc_{attitude}} - F_{dc_{antenna}}$$

where:

Proprietary information: no part of this document may be reproduced divulged or used in any form without prior permission from CLS.



- FdcSAR is estimated from the SAR data
- FdcOcean is the component related to the ocean radial velocities.
- FdcAttitude is estimated from the geometry knowledge (quaternion based)
- Fdcantenna is the antenna contribution related to TRM drifts, failures, misalignments, etc

At global scale, the expected relationship between the geophysical Doppler and the sea state (or ocean surface wind vector) is well known since Envisat/ASAR. The performances of the geophysical Doppler are assessed by estimating the bias between the expected Doppler given the sea state conditions (provided by ECMWF) and the geophysical Doppler as included in the Level 2 products.

Statement of the ocean surface radial velocities measurements accuracy:

Figure 48 shows the geophysical Doppler as included in the Level 2 products as a function of radial wind speed (wind speed projected in the line of sight of the radar). The colour code indicates the latitude. As observed, the Doppler and the radial wind speed are strongly correlated for both WV1 and WV2. However, the colour code indicates a clear and non-geophysical dependence to the latitude. In addition, Doppler is not 0 Hz (as it should be) when radial wind speed is 0 m/s for WV1 and WV2. This shows that the Doppler shift as processed at PDGS is not only related to ocean surface radial velocities. This prevents us for getting any quantitative geophysical signature such as ocean surface currents in the product.

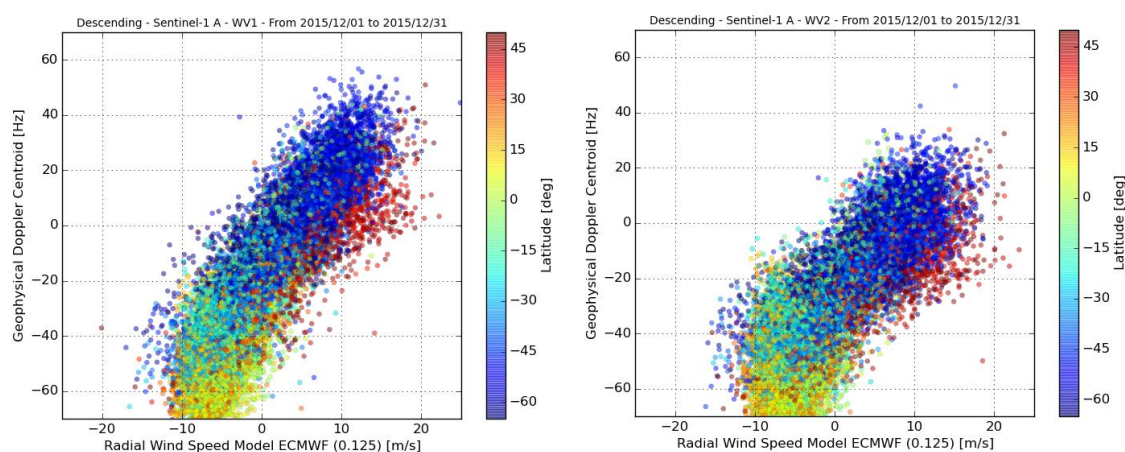


Figure 48: Geophysical Doppler as included in the Level 2 products as a function of radial wind speed (wind speed projected in the line of sight of the radar) for WV1 (left) and WV2 (right). The colour code indicates the latitude.

Improvement performed during 2015:

In 2015 the daily monitoring of this relationship allowed us to show the residual Doppler from the instrument/platform contribution (FdcAttitude and/or Fdcantenna) in geophysical Doppler. In particular, our systematic analysis revealed a contamination with respect to latitude in the geophysical Doppler. Complementary acquisition in WM over land where the geophysical Doppler is expected to be zero showed the same results. Figure 49 shows the bias as a function of latitude estimated both over ocean (blue) and land (brown). In spite of the low number of available acquisitions over land, both show Doppler variation up to 30 Hz. As observed on Figure 6, expected the geophysical signature is expected to be between -60 and 60 Hz. 30 Hz of contamination is thus far too much for ocean current applications.

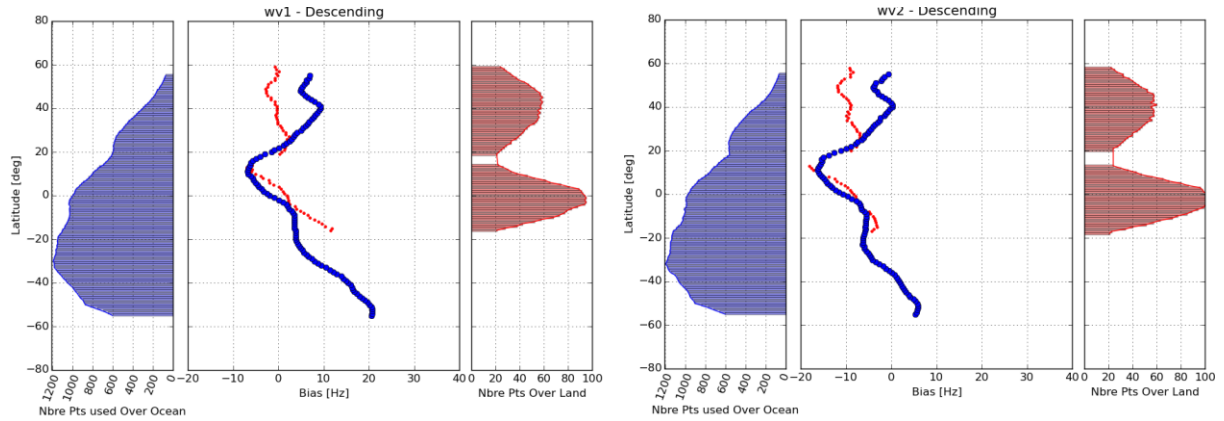


Figure 49: Doppler bias as a function of latitude estimated over ocean (blue) and land (brown).

The differences (around 10Hz) observed in the land Doppler between wv1 and wv2 can be well predicted by the recent antenna model as shown in Figure 50.

Coming Improvements for 2016:

In 2016, we will pursue the careful monitoring of the Doppler calibration using geophysical calibration. We recommend continuing acquisitions over land as there are still differences between analysis over land and ocean. Moreover a strategy to replace acquisition over land will be proposed and evaluated.

The benefit of using a new antenna model will be assessed and investigations to propose a a-posteriori calibration will be undertaken.

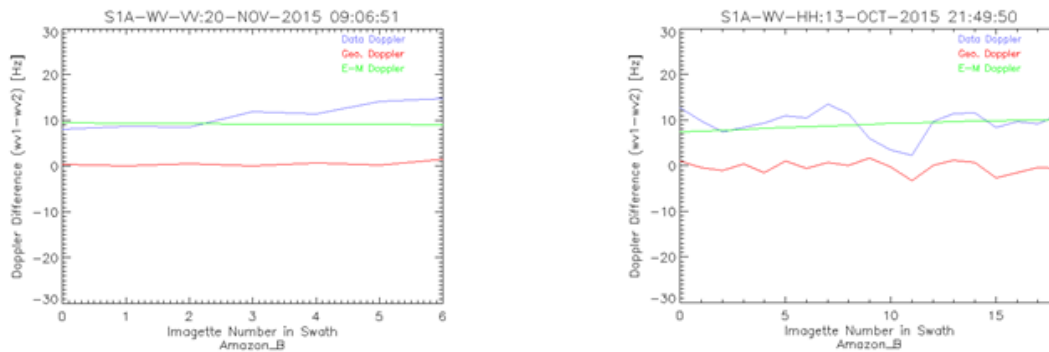


Figure 50: Geometric Doppler, data Doppler, and EM Doppler differences between wv1 and wv2 acquired over rain forest areas in VV (left) and HH (right) polarizations.

4.3.3.2. TOPS Mode

Statement of the ocean surface radial velocities measurements accuracy:

As for Wave Mode, the contamination of the geophysical Doppler by the geometry knowledge (quaternion based) and the antenna contribution prevents us for getting any quantitative geophysical signature such as ocean surface currents in the product. Nevertheless, in cases where land areas are present in the image an ad-hoc calibration has been performed, and the results shown are promising (see Figure 51).

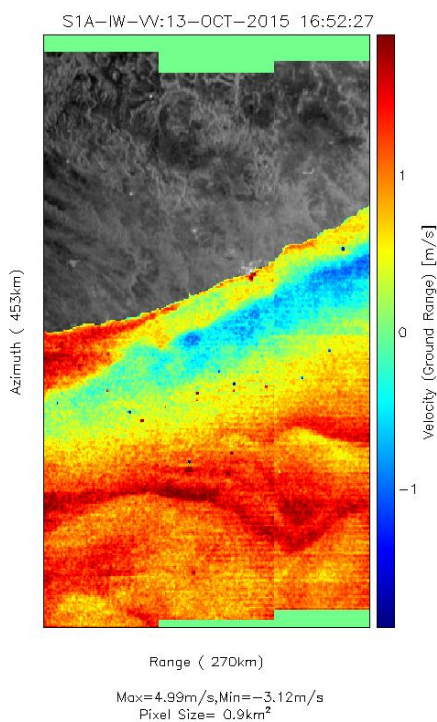
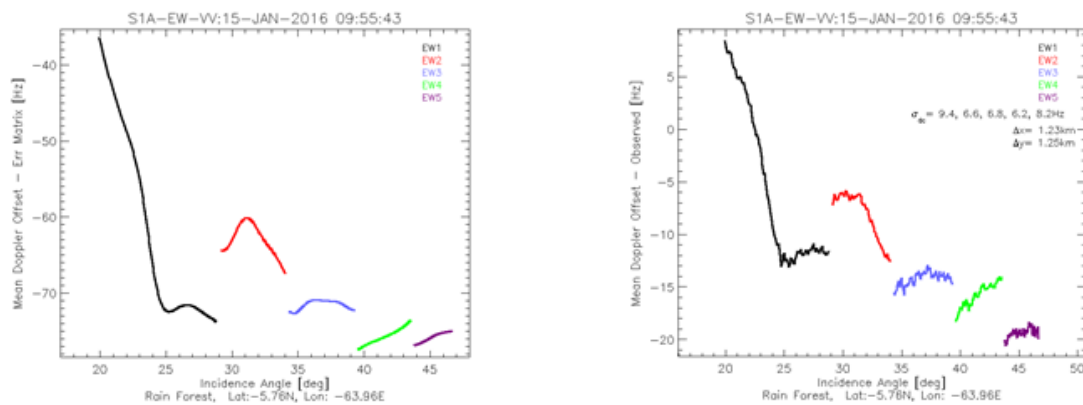


Figure 51: Radial velocity field from Sentinel 1A IW RVL product acquired over Agulhas in ascending mode. Here land areas are used to calibrate the Doppler anomaly before computing the radial velocity. A clear signature of the Agulhas current is observed as well as wind/wave induced velocity.

Improvement performed during 2015:

A main issue has been the compensation of the measured Doppler for the electromagnetic (EM) Doppler bias introduced by the skewness of the antenna elevation pattern. A refined antenna model has been implemented as part of the Level 2 processor and the EM Doppler bias over IW and EW swaths are compared with the data driven Doppler estimated over rain forest areas (see Figure 52).

Although the relative trends over swaths are predicted well, a significant Doppler bias is observed between the model and data. The jumps between swaths are also not well predicted.



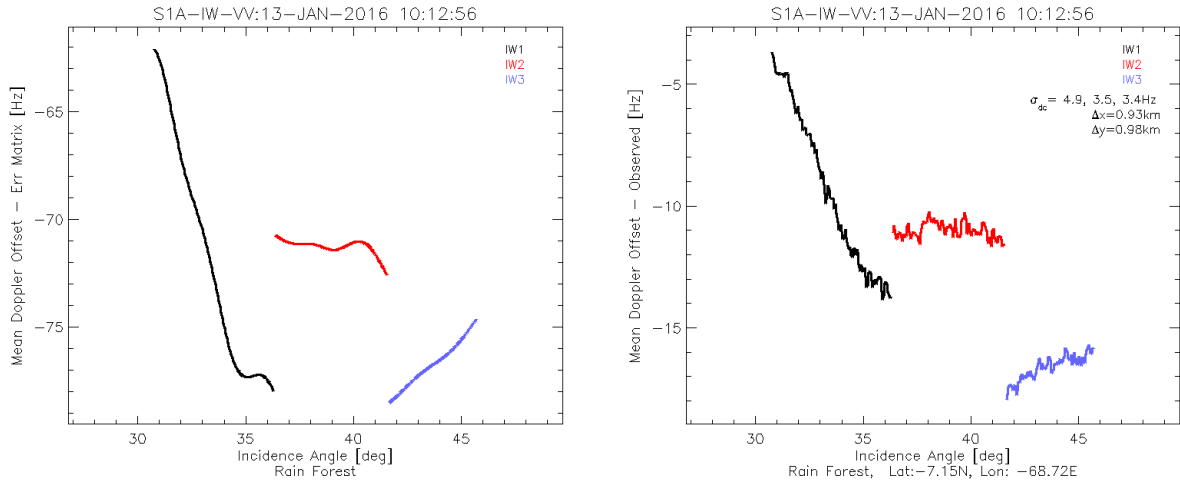


Figure 52: Left: EM doppler offset computed from antenna model with error matrix corresponding to the day of acquisition. Right: Doppler offset computed from rain forest data. Upper panel is S1A IW mode and lower panel is EW mode.

The azimuth scalloping in the RVL Doppler related to the burst overlap areas have been addressed, and a de-scalloping is implemented. This reduces the scalloping to around ± 3 Hz (see Figure 53).

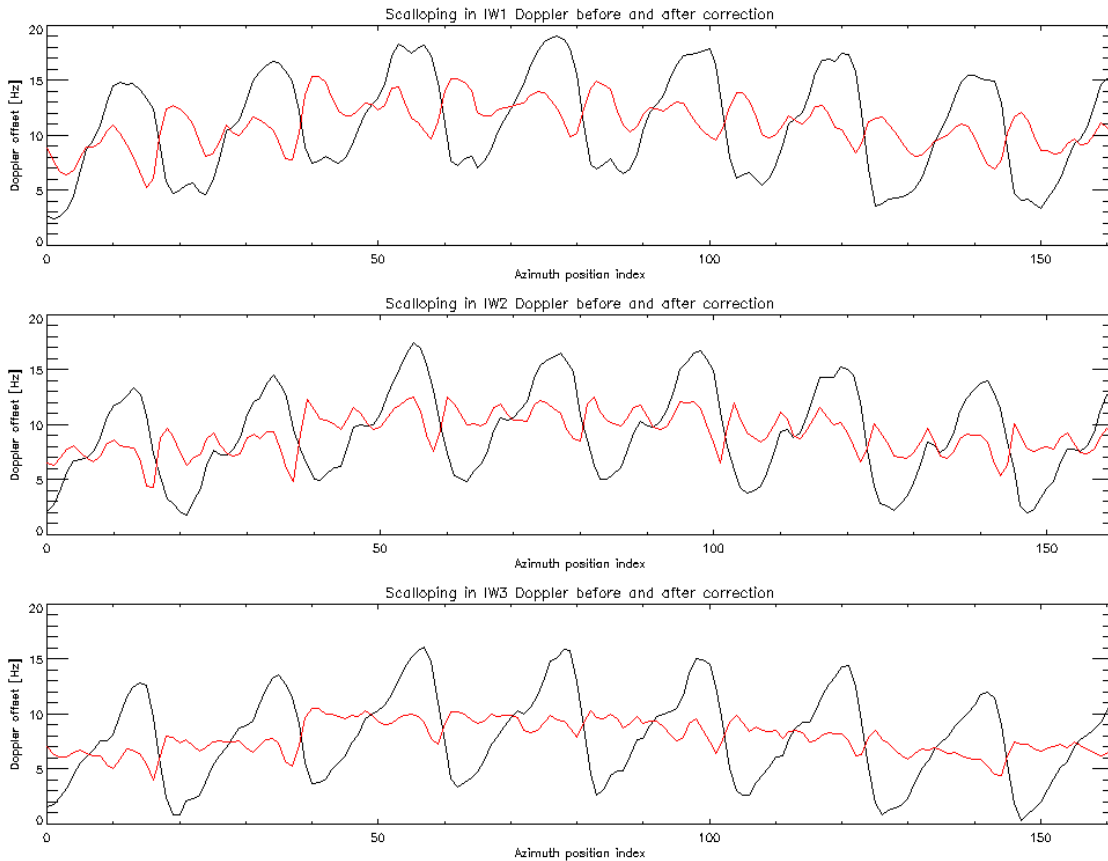


Figure 53: RVL product Doppler offset in azimuth before (black) and after (red) de-scalloping for each swath of IW mode. The data are acquired over rainforest, and the azimuth profiles area obtained by averaging in range.

Coming Improvements for 2016:

In 2016, there will be an improved antenna model for use by the Level 2 RVL processor. It is expected that this will further improve the EM Doppler offset prediction. The benefit of using a new antenna model will be assessed and investigations to propose an a-posteriori calibration will be undertaken for TOPS mode.

A further refinement of the de-scalloping will be investigated without increasing the processing time.

**Appendix A - List of Acronyms**

AD	Applicable Document
ADF	Auxiliary Data File
RD	Reference Document
TBC	To be confirmed
TBD	To be defined
TRM	Transmit Receive Module



Appendix B - S1-A Orbit Cycles and N-Cyclic Reports

The table below gives the cycle number with start and stop acquisition dates during 2015. The start of a cycle is at approximately 18:00 UT on the dates below.

Cycle	Start Date	End Date
38	09/01/2015	21/01/2015
39	21/01/2015	02/02/2015
40	02/02/2015	14/02/2015
41	14/02/2015	26/02/2015
42	26/02/2015	10/03/2015
43	10/03/2015	22/03/2015
44	22/03/2015	03/04/2015
45	03/04/2015	15/04/2015
46	15/04/2015	27/04/2015
47	27/04/2015	09/05/2015
48	09/05/2015	21/05/2015
49	21/05/2015	02/06/2015
50	02/06/2015	14/06/2015
51	14/06/2015	26/06/2015
52	26/06/2015	08/07/2015
53	08/07/2015	20/07/2015
54	20/07/2015	01/08/2015
55	01/08/2015	13/08/2015
56	13/08/2015	25/08/2015
57	25/08/2015	06/09/2015
58	06/09/2015	18/09/2015
59	18/09/2015	30/09/2015
60	30/09/2015	12/10/2015
61	12/10/2015	24/10/2015
62	24/10/2015	05/11/2015
63	05/11/2015	17/11/2015
64	17/11/2015	29/11/2015
65	29/11/2015	11/12/2015
66	11/12/2015	23/12/2015
67	23/12/2015	04/01/2016
68	04/01/2016	16/01/2016



Appendix C - ESA S1-A Technical Reports

The following ESA S1-A Technical Reports were issued during 2015:

- Nuno Miranda, “Definition of the TOPS SLC deramping function for products generated by the S-1 IPF”, [COPE-GSEG-EOPG-TN-14-0025](#), Issue 1, Revision 2, April 2015.
- Nuno Miranda, P.J. Meadows, “Radiometric Calibration of S-1 Level-1 Products Generated by the S-1 IPF”, [ESA-EOPG-CSCOP-TN-0002](#), Issue 1, Revision 0, May 2015.
- Nuno Miranda, “Sentinel-1 Instrument Processing Facility: Impact of the Elevation Antenna Pattern Phase Compensation on the Interferometric Phase Preservation”, [ESA-EOPG-CSCOP-TN-0004](#), Issue 1, Revision 0, July 2015.
- Nuno Miranda, “S-1A TOPS Radiometric Calibration Refinement#1”, [ESA-EOPG-CSCOP-TN-0012](#), Issue 1, Revision 0, November 2015.



Appendix D - S1-A Transmit Receive Module Failures

The following S1-A antenna Transmit/Receive Module (TRM) failed during 2015 (a full list since launch can be found in Appendix B of any S1-A N-Cyclic Performance Report):

TRM	Description	Date of Failure
Tile 5, all TRM failures (intermittent)	Rx, H & V	Between 18-Mar-2015, 04:09:00 UT and 20-Mar-2015, 11:46:30 UT
Tile 5, all TRM failures (intermittent)	Rx, H & V	Between 26-Mar-2015, 16:20:00 UT and 28-Mar-2015, 02:50:30 UT
Tile 12, Row 16 (intermittent)	Tx V & Rx V	Between 16-Apr-2015 and 18-Apr-2015
Tile 5, all TRM failures (intermittent)	Rx, H & V	Between 18-Apr-2015, 17:40:21 UT and 24-Apr-2015, 17:48:08 UT
Tile 12, Row 16 (intermittent)	Tx V & Rx V	Between 20-Apr-2015 and 28-Apr-2015
Tile 5, all TRM failures (intermittent)	Rx, H & V	Between 25-Apr-2015 17:37:37 UT and 30-Apr-2015, 23:01:11 UT
Tile 4, Row 11	Rx H	29-Apr-2015, 21:57:30 UT
Tile 12, Row 16 (intermittent)	Tx V & Rx V	Between 01-May-2015 and 04-May-2015
Tile 5, all TRM failures (intermittent)	Rx, H & V	Between 05-May-2015, 05:12:51 UT and 06-May-2015, 00:44:43 UT
Tile 12, Row 16	Tx V & Rx V	18-May-2015, 22:33:36 UT
Tile 5, all TRM failures	Rx, H & V	Between 26-May-2015, 19:06:00 UT and 27-May-2015, 06:07:00 UT
Tile 5, all TRM failures	Rx, H & V	Between 06-Jun-2015, 06:35:00 UT and 14-July-2015, 10:43:00 UT
Tile 5, all TRM failures	Rx, H & V	Between 17-July-2015, 19:07:00 UT and 21-July-2015, 11:58:00 UT



Appendix E - S1-A Instrument Unavailability

The S1-A instrument was unavailable during 2015 (a full list since launch can be found in Appendix C of any S1-A N-Cyclic Performance Report):

Start Date/Time	End Date/Time	MPC Reference	Summary
20/01/2015 07:30	20/01/2015 18:00	SOB-112	Sentinel-1A Unavailability - Planned maintenance
01/02/2015 07:50	02/02/2015 16:26	SOB-116	Sentinel-1A unavailability from 01/02/2015 7h50 to 02/02/2015 16h27
17/02/2015 19:56	18/02/2015 16:02	SOB-118	Sentinel-1A Unavailability - since 17/02/15 evening to 18/02/15 afternoon
19/02/2015 13:29	20/02/2015 10:15	SOB-121	Sentinel-1A unavailability from 19/02/2015 13h29 to 20/02/2015 10h15
14/04/2015 08:30	14/04/2015 17:00	SOB-147	Sentinel-1A unavailability planned on 14/04/2015 for maintenance
09/05/2015 23:19	10/05/2015 15:39	SOB-159	Sentinel-1A unavailability on 10/05/2015
19/05/2015 05:00	19/05/2015 12:00	SOB-168	Sentinel-1A planned unavailability on 19/05/2015 (RDB#4 uplink onboard)
28/05/2015 04:00	28/05/2015 14:30	SOB-170	Planned Sentinel-1A unavailability on 28/05/2015 for maintenance purpose
20/06/2015 15:30	21/06/2015 13:00	SOB-176	Sentinel-1A unavailability on 20 and 21/06/2015
22/07/2015 06:35	22/07/2015 08:21	SOB-206	Sentinel-1A Planned Unavailability (RDB#5)
03/08/2015 02:37	03/08/2015 18:33	SOB-207	Sentinel-1A Unavailability from orbit 7093 to 7101
04/08/2015 04:52	04/08/2015 13:47	SOB-208	Sentinel-1A Unavailability from orbit 7103 to 7114
04/08/2015 23:44	05/08/2015 11:20	SOB-209	Sentinel-1A Unavailability from orbit 7120 to 7128
09/08/2015 21:22	10/08/2015 16:14	SOB-210	Sentinel-1A Unavailability from orbit 7192 to 7204
04/09/2015 16:54	05/09/2015 11:08	SOB-214	Sentinel-1A Unavailability from 04/09 to 05/09/2015
23/09/2015 07:20	23/09/2015 11:56	SOB-222	Sentinel-1A Unavailability from orbit 7840 to 7842
19/10/2015 16:28	20/10/2015 07:27	SOB-226	Sentinel-1A Unavailability from 19/10 to 20/10/2015
21/10/2015 14:54	22/10/2015 07:12	SOB-227	Sentinel-1A Unavailability from 21/10 to 22/10/2015



Start Date/Time	End Date/Time	MPC Reference	Summary
05/11/2015 16:50	06/11/2015 12:20	SOB-229	Sentinel-1A Unavailability from 05/11 to 06/11/2015
2015-11-07 17:53	2015-11-08 12:10	SOB-230	Sentinel-1A Unavailability from 07/11 to 08/11/2015
2015-11-18 07:40	2015-11-18 12:28	SOB-233	Sentinel-1A Unavailability on 18/11/2015
29/11/2015 22:54	30/11/2015 11:10	SOB-251	Sentinel-1A Unavailability from 29/11 to 30/11/2015
10/12/2015 07:30	10/12/2015 13:00	SOB-252	Sentinel-1A Planned Unavailability on 10/12/2015
11/12/2015 02:30	11/12/2015 16:00	SOB-253	Sentinel-1A Unavailability on 11/12/2015



Appendix F - S1-A Auxiliary Data Files

The following S1-A Auxiliary Data Files (ADFs) were updated during 2015:

Instrument ADF (AUX_INS)

ADF	Update Reason
S1A_AUX_INS_V20140406T133000_G20150119T143434.SAFE	New AUX_INS related to RDB#1 to be used for reprocessing activities and compliant with IPF v2.36.
S1A_AUX_INS_V20140616T135500_G20150119T144502.SAFE	New AUX_INS related to RDB#2 to be used for reprocessing activities and compliant with IPF v2.36.
S1A_AUX_INS_V20140915T100000_G20150119T145343.SAFE	New AUX_INS related to RDB#3 to be used for reprocessing activities and compliant with IPF v2.36.
S1A_AUX_INS_V20140406T133000_G20150319T084951.SAFE	New AUX_INS related to RDB#1 to be used for reprocessing activities and compliant with IPF v2.43
S1A_AUX_INS_V20140616T135500_G20150319T085135.SAFE	New AUX_INS related to RDB#2 to be used for reprocessing activities and compliant with IPF v2.43
S1A_AUX_INS_V20140915T100000_G20150319T102820.SAFE	New AUX_INS related to RDB#3 to be used for reprocessing activities and compliant with IPF v2.43
S1A_AUX_INS_V20140406T133000_G20150504T145310.SAFE	New AUX_INS related to RDB#1 to be used for reprocessing activities and compliant with IPF v2.43.
S1A_AUX_INS_V20140616T135500_G20150504T151127.SAFE	New AUX_INS related to RDB#2 to be used for reprocessing activities and compliant with IPF v2.43.
S1A_AUX_INS_V20140915T100000_G20150504T152226.SAFE	New AUX_INS related to RDB#3 to be used for reprocessing activities and compliant with IPF v2.43.
S1A_AUX_INS_V20140915T100000_G20150511T155419.SAFE	Update of AUX_INS for SM without calibration pulses. Related to RDB#3.
S1A_AUX_INS_V20150722T120000_G20150720T091909.SAFE	Update related to RDB#5

Calibration ADF (AUX_CAL)

ADF	Update Reason
S1A_AUX_CAL_V20140406T133000_G20150119T143118.SAFE	New AUX_CAL related to RDB#1 to be used for reprocessing activities and compliant with IPF v2.36 + update of AAP (except for WV



	mode).
S1A_AUX_CAL_V20140616T135500_G20150119T144330.SAFE	New AUX_CAL related to RDB#2 to be used for reprocessing activities and compliant with IPF v2.36 + update of AAP (except for WV mode).
S1A_AUX_CAL_V20140915T100000_G20150119T145134.SAFE	New AUX_CAL related to RDB#3 to be used for reprocessing activities and compliant with IPF v2.36 + update of AAP (except for WV mode).
S1A_AUX_CAL_V20140915T100000_G20150319T092606.SAFE	New AUX_CAL related to RDB#3 to be used for reprocessing activities and compliant with IPF v2.43
S1A_AUX_CAL_V20140406T133000_G20150504T145757.SAFE	New AUX_CAL related to RDB#1 to be used for reprocessing activities and compliant with IPF v2.43.
S1A_AUX_CAL_V20140616T135500_G20150504T151503.SAFE	New AUX_CAL related to RDB#2 to be used for reprocessing activities and compliant with IPF v2.43.
S1A_AUX_CAL_V20140915T100000_G20150504T152619.SAFE	New AUX_CAL related to RDB#3 to be used for reprocessing activities and compliant with IPF v2.43.
S1A_AUX_CAL_V20140406T133000_G20150703T090000.SAFE	Update of noiseCalibrationFactors. Related to RDB#1.
S1A_AUX_CAL_V20140616T135500_G20150703T091031.SAFE	Update of noiseCalibrationFactors. Related to RDB#2.
S1A_AUX_CAL_V20140915T100000_G20150703T091411.SAFE	Update of noiseCalibrationFactors. Related to RDB#3.
S1A_AUX_CAL_V20150519T120000_G20150703T091533.SAFE	Update of noiseCalibrationFactors. Related to RDB#4.
S1A_AUX_CAL_V20150722T120000_G20150720T091726.SAFE	Update related to RDB#5
S1A_AUX_CAL_V20140406T133000_G20150908T074704.SAFE	Revised Noise Calibration Factor values. Related to RDB#1.
S1A_AUX_CAL_V20140616T135500_G20150908T074804.SAFE	Revised Noise Calibration Factor values. Related to RDB#2.
S1A_AUX_CAL_V20140915T100000_G20150908T074836.SAFE	Revised Noise Calibration Factor values. Related to RDB#3.
S1A_AUX_CAL_V20150519T120000_G20150908T074910.SAFE	Revised Noise Calibration Factor values. Related to RDB#4.
S1A_AUX_CAL_V20150722T120000_G20150908T074943.SAFE	Revised Noise Calibration Factor values. Related to RDB#5.
S1A_AUX_CAL_V20140406T133000_G20151125T103600.SAFE	TOPS first recalibration (revised EAP for IW and EW). Related to RDB#1.
S1A_AUX_CAL_V20140616T133500_G20151125T103748.SAFE	TOPS first recalibration (revised EAP for IW and EW). Related to



	RDB#2.
S1A_AUX_CAL_V20140915T100000_G20151125T103928.SAFE	TOPS first recalibration (revised EAP for IW and EW). Related to RDB#3.
S1A_AUX_CAL_V20150519T120000_G20151125T104142.SAFE	TOPS first recalibration (revised EAP for IW and EW). Related to RDB#4.
S1A_AUX_CAL_V20150722T120000_G20151125T104733.SAFE	TOPS first recalibration (revised EAP for IW and EW). Related to RDB#5.

L1 Processor Parameters ADF (AUX_PP1)

ADF	Update Reason
S1A_AUX_PP1_V20140406T133000_G20150119T143703.SAFE	New AUX_PP1 related to RDB#1 to be used for reprocessing activities and compliant with IPF v2.36.
S1A_AUX_PP1_V20140616T135500_G20150119T144631.SAFE	New AUX_PP1 related to RDB#2 to be used for reprocessing activities and compliant with IPF v2.36.
S1A_AUX_PP1_V20140915T100000_G20150119T145501.SAFE	New AUX_PP1 related to RDB#3 to be used for reprocessing activities and compliant with IPF v2.36.
S1A_AUX_PP1_V20140406T133000_G20150319T085539.SAFE	New AUX_PP1 related to RDB#1 to be used for reprocessing activities and compliant with IPF v2.43
S1A_AUX_PP1_V20140616T135500_G20150319T085656.SAFE	New AUX_PP1 related to RDB#2 to be used for reprocessing activities and compliant with IPF v2.43
S1A_AUX_PP1_V20140915T100000_G20150319T103002.SAFE	New AUX_PP1 related to RDB#3 to be used for reprocessing activities and compliant with IPF v2.43
S1A_AUX_PP1_V20140406T133000_G20150504T145602.SAFE	New AUX_PP1 related to RDB#1 to be used for reprocessing activities and compliant with IPF v2.43.
S1A_AUX_PP1_V20140616T135500_G20150504T151343.SAFE	New AUX_PP1 related to RDB#2 to be used for reprocessing activities and compliant with IPF v2.43.
S1A_AUX_PP1_V20140915T100000_G20150504T152401.SAFE	New AUX_PP1 related to RDB#3 to be used for reprocessing activities and compliant with IPF v2.43.
S1A_AUX_PP1_V20140915T100000_G20150504T152401.SAFE	The Doppler Centroid estimation root mean squared error threshold (dcRmsErrorThreshold) has been reduced to 20 in order to reduce IPF failures related to high DC acquisitions. Related to RDB#3.
S1A_AUX_PP1_V20140406T133000_G20150703T092038.SAFE	Activate internalCal for Wave Mode. Related to RDB#1.



S1A_AUX_PP1_V20150519T120000_G20150703T092554.SAFE	Activate internalCal for Wave Mode. Related to RDB#2.
S1A_AUX_PP1_V20140616T135500_G20150703T092216.SAFE	Activate internalCal for Wave Mode. Related to RDB#3.
S1A_AUX_PP1_V20140915T100000_G20150703T092417.SAFE	Activate internalCal for Wave Mode. Related to RDB#4.
S1A_AUX_PP1_V20150722T120000_G20150720T092048.SAFE	Update related to RDB#5.
S1A_AUX_PP1_V20140406T133000_G20151125T102226.SAFE	TOPS first recalibration (new EW and IW gains). Related to RDB#1.
S1A_AUX_PP1_V20140616T135500_G20151125T102437.SAFE	TOPS first recalibration (new EW and IW gains). Related to RDB#2.
S1A_AUX_PP1_V20140915T100000_G20151125T102627.SAFE	TOPS first recalibration (new EW and IW gains). Related to RDB#3.
S1A_AUX_PP1_V20150519T120000_G20151125T102820.SAFE	TOPS first recalibration (new EW and IW gains). Related to RDB#4.
S1A_AUX_PP1_V20150722T120000_G20151125T104803.SAFE	TOPS first recalibration (new EW and IW gains). Related to RDB#5.

L2 Processor Parameters ADF (AUX_PP2)

ADF	Update Reason
S1A_AUX_PP2_V20140406T133000_G20150119T143838.SAFE	New AUX_PP2 related to RDB#1 to be used for reprocessing activities and compliant with IPF v2.36.
S1A_AUX_PP2_V20140616T135500_G20150119T144800.SAFE	New AUX_PP2 related to RDB#2 to be used for reprocessing activities and compliant with IPF v2.36.
S1A_AUX_PP2_V20140915T100000_G20150119T145621.SAFE	New AUX_PP2 related to RDB#3 to be used for reprocessing activities and compliant with IPF v2.36.
S1A_AUX_PP2_V20140406T133000_G20150703T092947.SAFE	Optimisation of LOP parameters in order to capture long swell + update of rangeLookFilterWidth. Related to RDB#1.
S1A_AUX_PP2_V20140616T135500_G20150703T093156.SAFE	Optimisation of LOP parameters in order to capture long swell + update of rangeLookFilterWidth. Related to RDB#2.
S1A_AUX_PP2_V20140915T100000_G20150703T093301.SAFE	Optimisation of LOP parameters in order to capture long swell + update of rangeLookFilterWidth. Related to RDB#3.
S1A_AUX_PP2_V20150519T120000_G20150703T093420.SAFE	Optimisation of LOP parameters in order to capture long swell + update of rangeLookFilterWidth. Related to RDB#4.
S1A_AUX_PP2_V20150722T120000_G20150720T092233.SAFE	Update related to RDB#5.



Appendix G - S1-A Orbit Manoeuvres

The S1-A orbit manoeuvres during 2015 were:

Start Date	Start Time	Stop Date	Stop Time
14/01/2015	23:46:39.692	14/01/2015	23:47:05.817
16/01/2015	12:30:16.912	16/01/2015	12:30:44.287
16/01/2015	14:09:01.512	16/01/2015	14:09:28.887
16/01/2015	15:47:44.900	16/01/2015	15:48:14.900
16/01/2015	17:26:29.500	16/01/2015	17:26:59.500
21/01/2015	21:15:52.190	21/01/2015	21:19:02.940
22/01/2015	00:29:29.776	22/01/2015	00:29:35.276
29/01/2015	01:08:33.913	29/01/2015	01:08:54.538
01/02/2015	06:13:38.790	01/02/2015	06:14:08.915
02/02/2015	23:05:06.821	02/02/2015	23:05:35.196
03/02/2015	00:43:51.441	03/02/2015	00:44:19.816
05/02/2015	00:45:32.808	05/02/2015	00:45:53.433
05/02/2015	01:35:25.984	05/02/2015	01:35:46.609
05/02/2015	02:25:08.958	05/02/2015	02:25:29.583
12/02/2015	00:18:53.830	12/02/2015	00:19:11.955
12/02/2015	01:08:30.526	12/02/2015	01:08:46.401
19/02/2015	00:22:25.643	19/02/2015	00:22:30.768
19/02/2015	01:11:52.073	19/02/2015	01:11:57.448
26/02/2015	00:14:40.517	26/02/2015	00:14:45.767
26/02/2015	01:04:07.012	26/02/2015	01:04:29.887
05/03/2015	00:27:27.017	05/03/2015	00:27:33.142
05/03/2015	01:16:59.510	05/03/2015	01:17:13.635
12/03/2015	02:00:24.537	12/03/2015	02:00:31.287
12/03/2015	02:49:57.910	12/03/2015	02:50:13.285
19/03/2015	02:42:28.208	19/03/2015	02:42:46.583
26/03/2015	02:35:36.221	26/03/2015	02:36:02.721
02/04/2015	02:20:52.984	02/04/2015	02:21:15.984
09/04/2015	02:17:40.555	09/04/2015	02:18:06.930
15/04/2015	22:05:31.119	15/04/2015	22:07:58.619
15/04/2015	23:44:15.669	15/04/2015	23:46:43.294
16/04/2015	00:37:09.300	16/04/2015	00:37:35.175
16/04/2015	02:16:19.629	16/04/2015	02:16:46.129
22/04/2015	22:50:41.630	22/04/2015	22:51:01.505
23/04/2015	00:29:46.074	23/04/2015	00:30:05.949
30/04/2015	00:21:13.312	30/04/2015	00:21:35.687
30/04/2015	01:10:53.519	30/04/2015	01:11:07.519
06/05/2015	23:23:33.049	06/05/2015	23:23:46.799



07/05/2015	00:13:13.337	07/05/2015	00:13:43.337
13/05/2015	21:32:37.334	13/05/2015	21:35:04.709
13/05/2015	23:11:21.905	13/05/2015	23:13:49.405
14/05/2015	00:04:45.805	14/05/2015	00:05:08.930
14/05/2015	01:43:53.381	14/05/2015	01:44:16.756
14/05/2015	03:23:01.176	14/05/2015	03:23:24.926
20/05/2015	23:56:32.811	20/05/2015	23:56:46.561
24/05/2015	15:17:21.730	24/05/2015	15:17:51.855
24/05/2015	16:56:36.234	24/05/2015	16:57:03.234
27/05/2015	22:58:53.042	27/05/2015	22:59:13.042
27/05/2015	23:48:39.586	27/05/2015	23:49:07.461
03/06/2015	22:01:21.633	03/06/2015	22:01:50.508
03/06/2015	22:51:08.287	03/06/2015	22:51:24.037
11/06/2015	01:10:37.541	11/06/2015	01:11:07.666
11/06/2015	02:00:25.457	11/06/2015	02:00:36.957
18/06/2015	01:18:56.964	18/06/2015	01:19:27.089
18/06/2015	02:08:47.948	18/06/2015	02:09:00.323
24/06/2015	23:09:57.273	24/06/2015	23:10:26.148
24/06/2015	23:59:15.281	24/06/2015	23:59:31.906
09/07/2015	00:34:58.485	09/07/2015	00:35:23.860
15/07/2015	22:46:47.993	15/07/2015	22:49:13.993
16/07/2015	00:26:45.489	16/07/2015	00:27:19.614
16/07/2015	01:16:37.140	16/07/2015	01:17:11.765
23/07/2015	00:18:32.522	23/07/2015	00:18:53.397
23/07/2015	01:08:11.165	23/07/2015	01:08:26.915
29/07/2015	22:30:21.053	29/07/2015	22:32:46.303
30/07/2015	00:59:37.163	30/07/2015	00:59:39.163
06/08/2015	07:07:42.931	06/08/2015	07:08:06.806
06/08/2015	08:46:51.175	06/08/2015	08:47:15.050
06/08/2015	10:25:59.440	06/08/2015	10:26:29.315
06/08/2015	12:05:13.798	06/08/2015	12:05:43.673
12/08/2015	22:14:23.418	12/08/2015	22:15:53.168
19/08/2015	22:04:50.322	19/08/2015	22:08:59.822
20/08/2015	01:18:55.220	20/08/2015	01:19:04.720
20/08/2015	02:08:22.689	20/08/2015	02:08:44.439
27/08/2015	01:58:28.564	27/08/2015	01:58:35.564
03/09/2015	01:30:44.630	03/09/2015	01:30:48.505
03/09/2015	02:20:10.409	03/09/2015	02:20:17.284
10/09/2015	02:18:19.571	10/09/2015	02:18:23.446
16/09/2015	23:11:49.596	16/09/2015	23:13:43.221
24/09/2015	01:48:24.015	24/09/2015	01:48:30.640
01/10/2015	01:33:41.045	01/10/2015	01:33:51.045
08/10/2015	01:18:30.330	08/10/2015	01:18:37.955



15/10/2015	01:07:31.834	15/10/2015	01:07:36.834
22/10/2015	00:53:48.720	22/10/2015	00:54:06.220
29/10/2015	01:14:33.469	29/10/2015	01:14:43.719
04/11/2015	23:02:36.981	04/11/2015	23:06:22.481
05/11/2015	00:44:05.468	05/11/2015	00:44:36.843
10/11/2015	23:33:51.910	10/11/2015	23:34:09.410
19/11/2015	01:48:37.314	19/11/2015	01:48:48.064
26/11/2015	01:38:14.345	26/11/2015	01:38:26.095
03/12/2015	01:29:35.939	03/12/2015	01:29:46.314
10/12/2015	00:01:10.813	10/12/2015	00:03:00.063
10/12/2015	01:37:53.733	10/12/2015	01:38:09.858
17/12/2015	01:25:41.963	17/12/2015	01:25:59.963
24/12/2015	01:12:36.906	24/12/2015	01:12:50.656
31/12/2015	00:59:27.754	31/12/2015	00:59:33.879



Appendix H - S1-A Quality Disclaimers

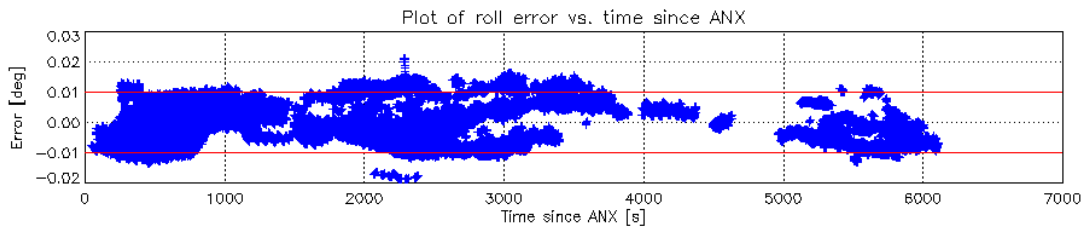
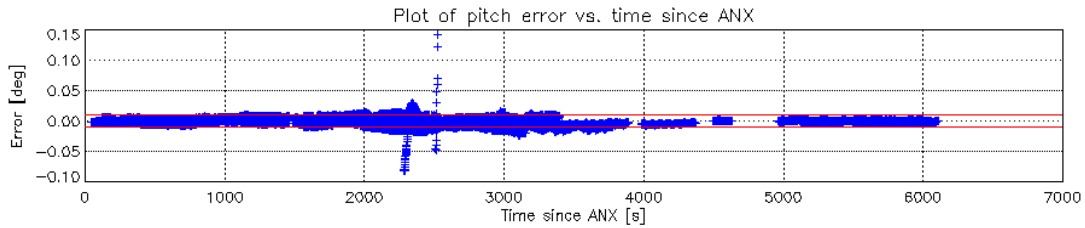
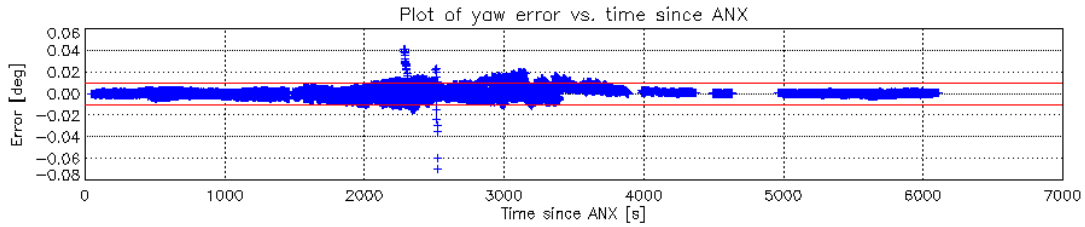
S1-A quality disclaimers were issued during 2015:

Number	Description	Start Validity Date	End Validity Date	Issue Status
1	S1A_WV_SLC_1S products filled with zero (black products)	2014-09-30 15:17:26 UT	2014-10-03 03:34:01 UT	Issued
2	Failure on tile amplifier #5 of the receiving antenna	2014-10-18 15:29:30 UT	2015-01-20 19:04:54 UT	Issued
3	Level 1 products processed with incorrect gains	2014-09-30 15:17:26 UT	2014-10-03 04:07:54 UT	Issued
4	Incorrect Cycle Number and Relative orbit number in products processed in PAC2/DPA	2014-12-09 11:45:25 UT	2015-01-21 03:53:00 UT	Issued
5	Failure on Tile amplifier #5 of the receiving antenna from 18/03/2015 and 20/03/2015	2015-03-18 04:09:00 UT	2015-03-20 11:46:30 UT	Issued
6	Failure on Tile amplifier #5 of the receiving antenna from 26/03/2015 to 28/03/2015	2015-03-26 16:20:00 UT	2015-03-28 02:50:30 UT	Issued
7	Failure on Tile amplifier #5 of the receiving antenna from 18/04/2015 to 24/04/2015	2015-04-18 17:40:21 UT	2015-04-24 17:48:08 UT	Issued
8	Failure on Tile amplifier #5 of the receiving antenna from 25/04/2015 to 30/04/2015	2015-04-25 17:37:37 UT	2015-04-30 23:01:11 UT	Issued
9	Failure on Tile amplifier #5 of the receiving antenna from 05/05/2015 to 06/05/2015	2015-05-05 05:12:51 UT	2015-05-06 00:44:43 UT	Issued
10	Denoising vectors not qualified	2014-10-03 00:00:00 UT	2015-07-03 06:33:15 UT	Issued
11	S-1 L2 OCN product preliminary qualified	2015-07-02 00:31:03 UT	2030-01-01 00:00:00 UT	Issued
12	Failure of TRM #5 between 2015-05-26 and 2015-05-27.	2015-05-26 21:10:28 UT	2015-05-27 05:53:00 UT	Issued
13	Failure of TRM #5 between 2015-06-06 and 2015-07-14	2015-06-06 06:44:28 UT	2015-07-14 07:50:55 UT	Issued
14	Invalid radiometric calibration of WV L1 and L2 products	2015-03-19 02:29:22 UT	2015-07-03 08:09:02 UT	Issued
15	Failure of TRM #5 from 2015-07-17 to 2015-07-21	2015-07-17 18:58:56 UT	2015-07-21 12:04:57 UT	Issued
16	Invalid Orbit Number at UPA - before 2014-10-10	2014-10-03 00:00:00 UT	2014-10-10 06:28:50 UT	Issued

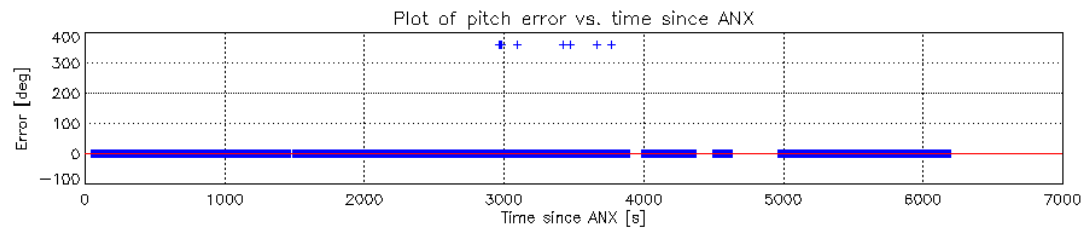
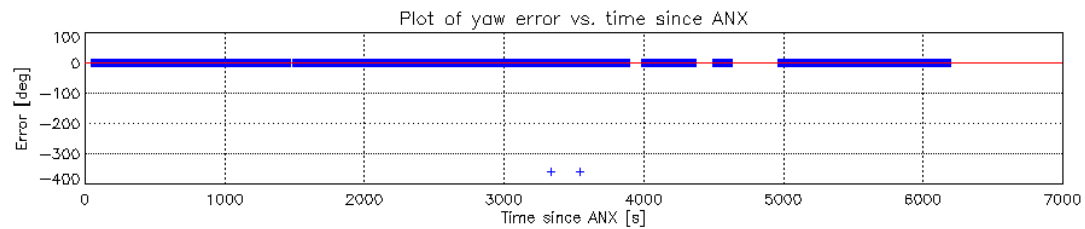


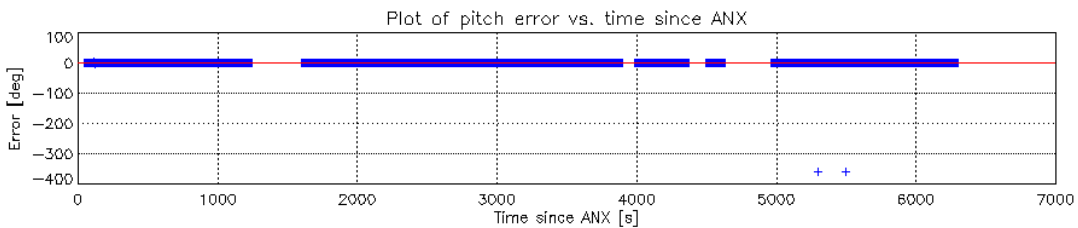
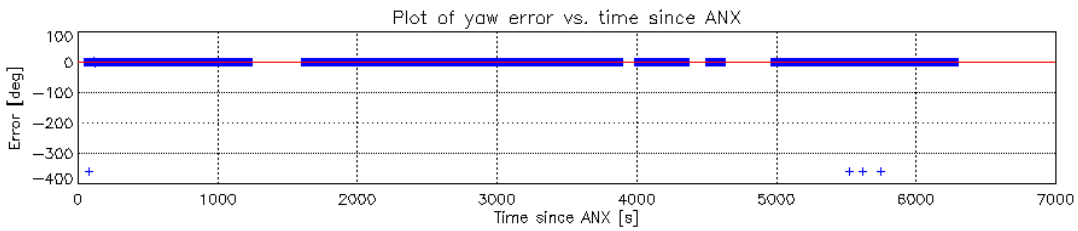
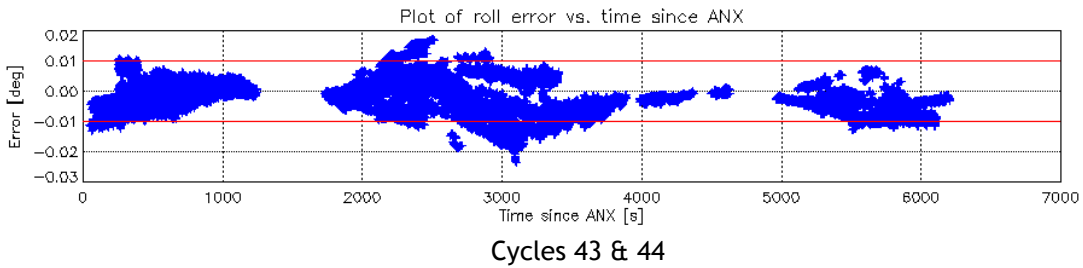
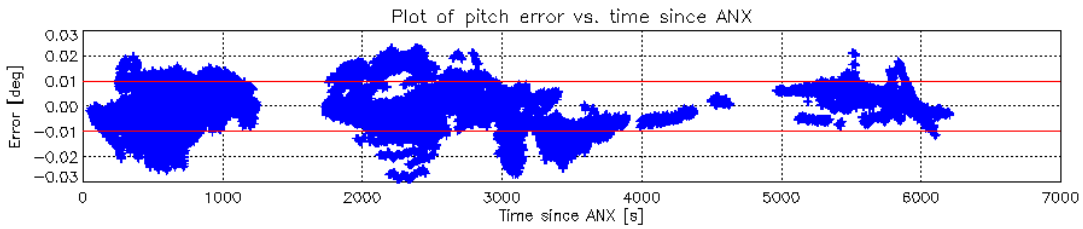
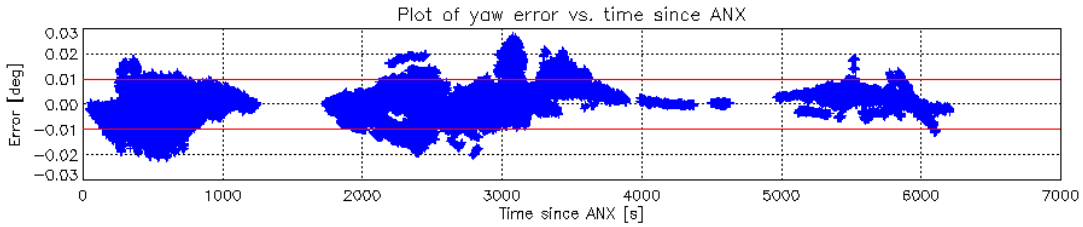
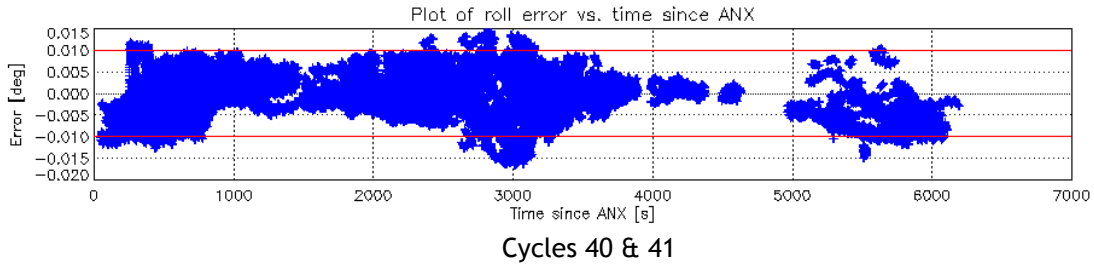
Appendix I - S1-A Antenna Pointing

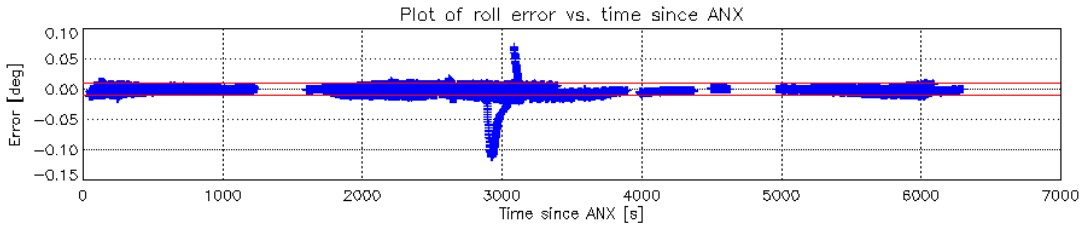
The following plots show trends for yaw, pitch and roll errors calculated for the reporting period against ascending node crossing time (ANX). The red horizontal lines show the nominal $\pm 0.01^\circ$ bounds for these attitude errors. The short duration changes in yaw are due to orbit manoeuvres. The increase in calculated yaw around ANX of 3000 is not an issue with Sentinel1-A itself but with how the yaw is calculated on-ground and consequently there is no impact of the quality of products.



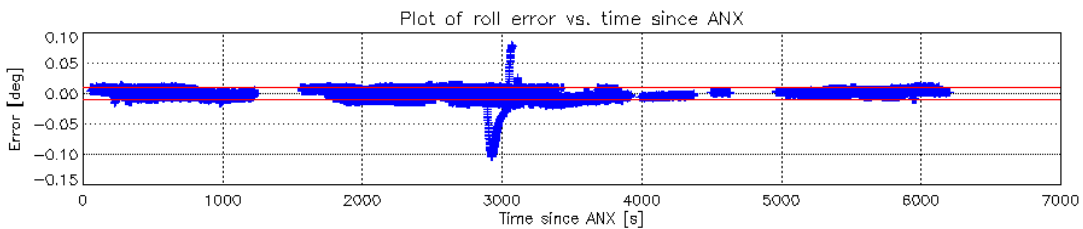
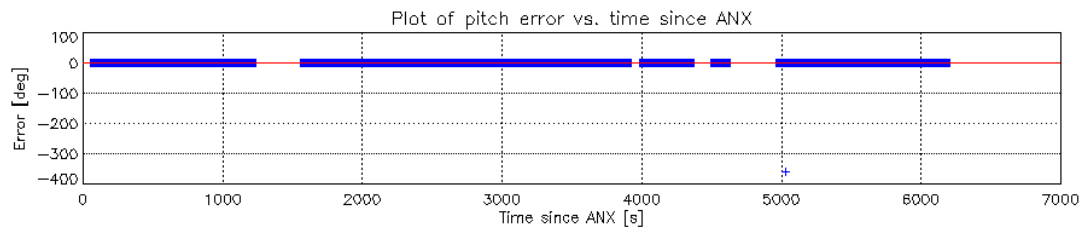
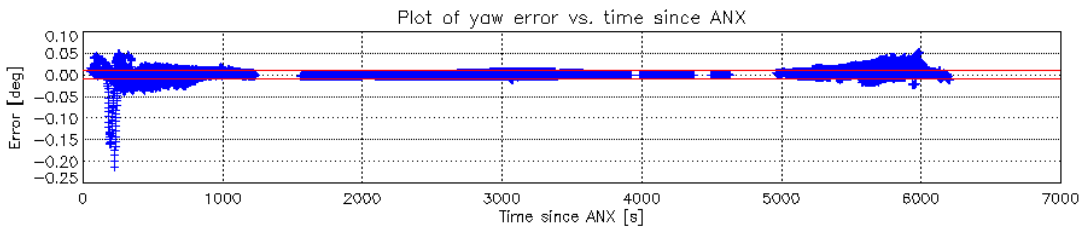
Cycles 38 & 39



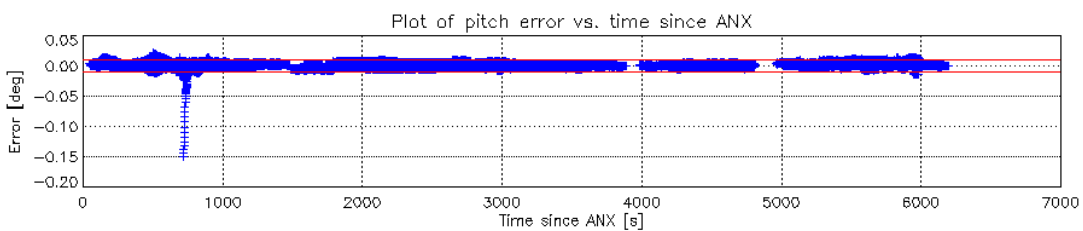
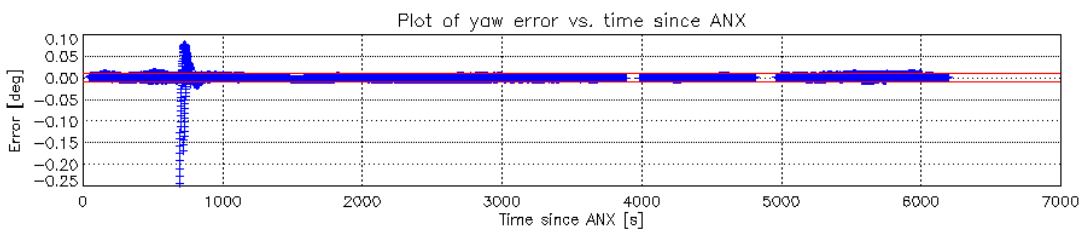


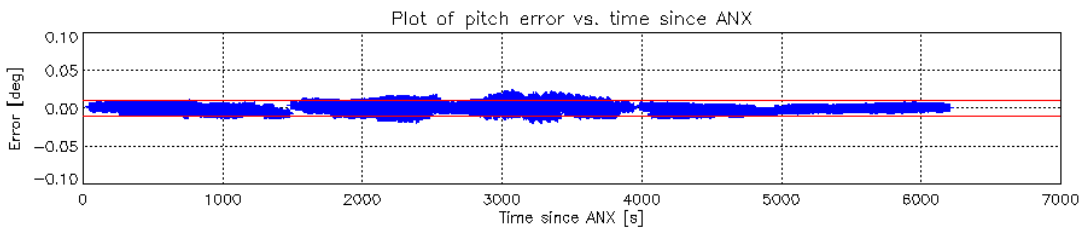
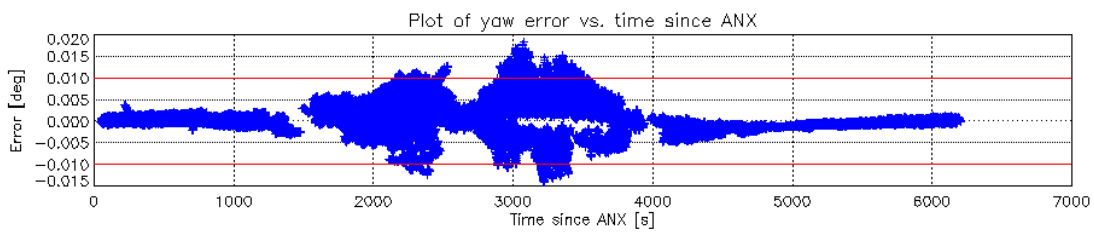
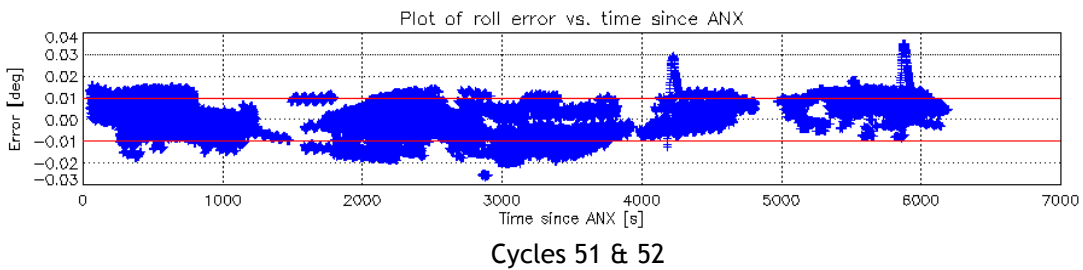
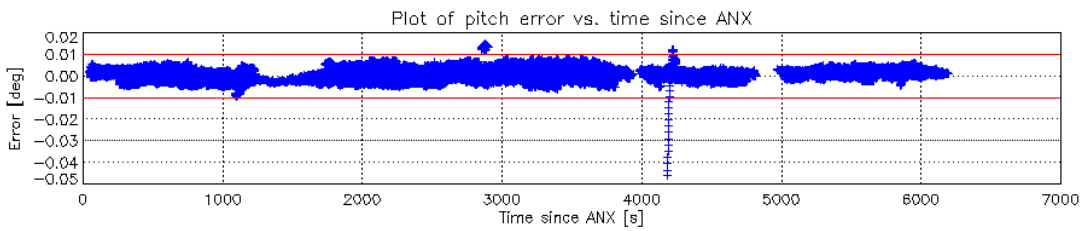
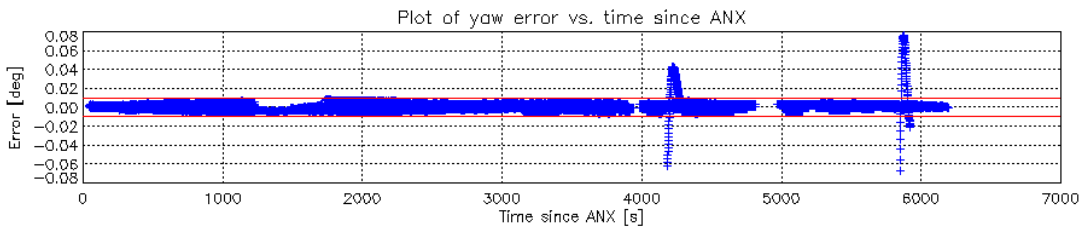
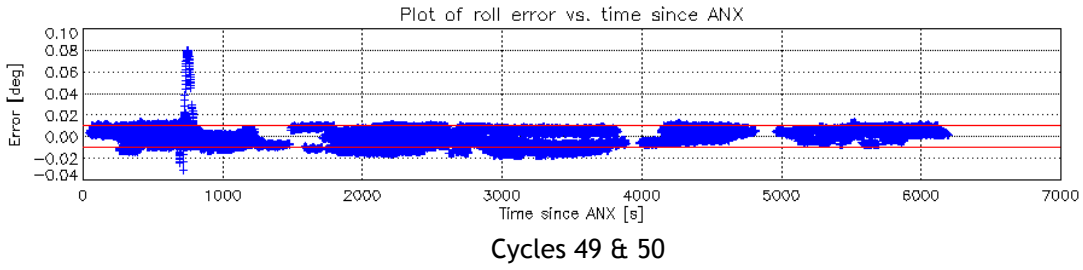


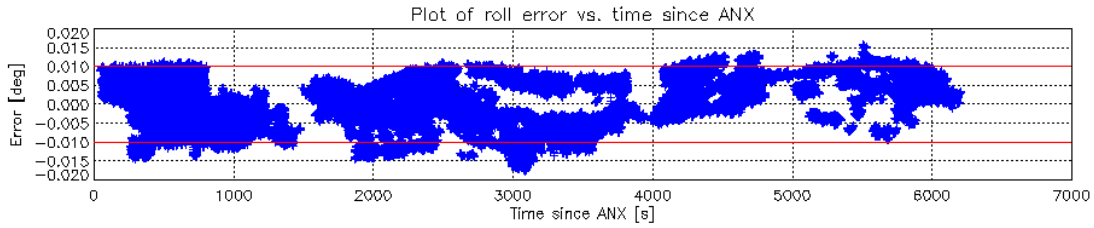
Cycles 45 & 46



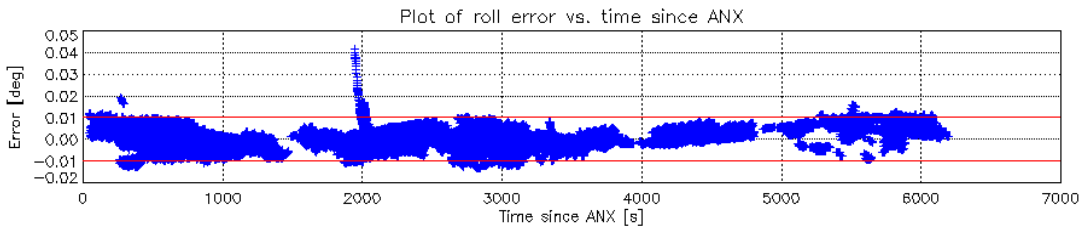
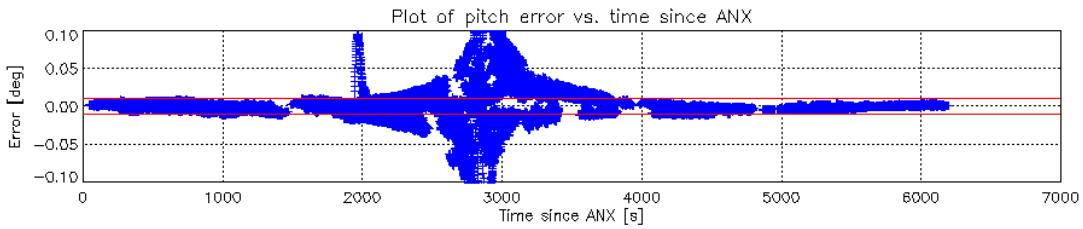
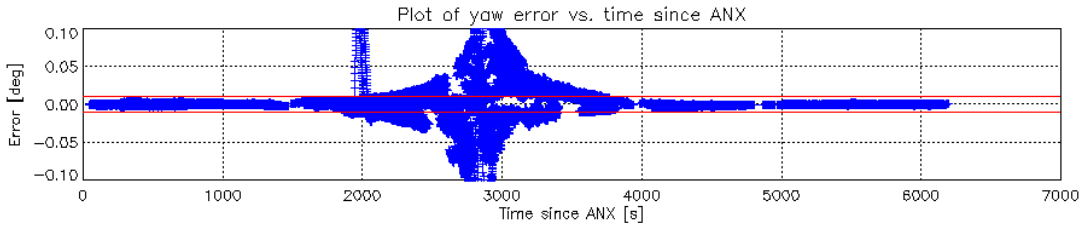
Cycles 47 & 48



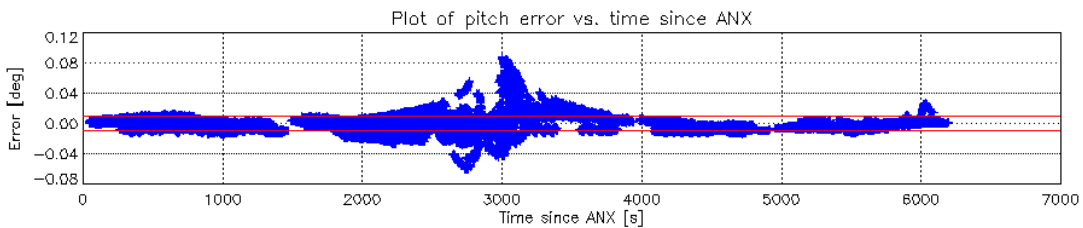
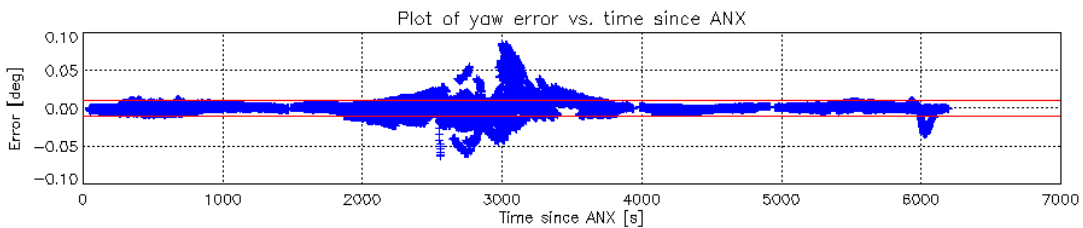


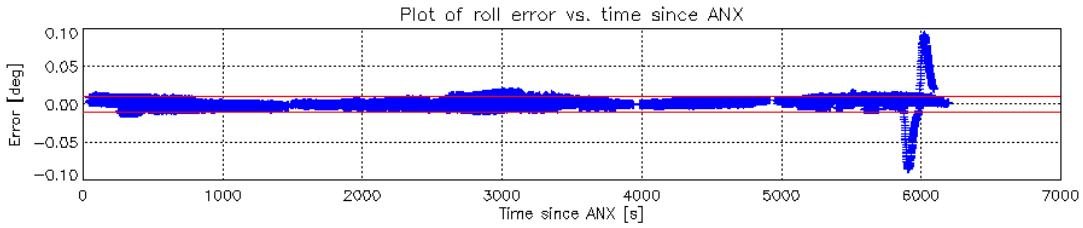


Cycles 53 & 54

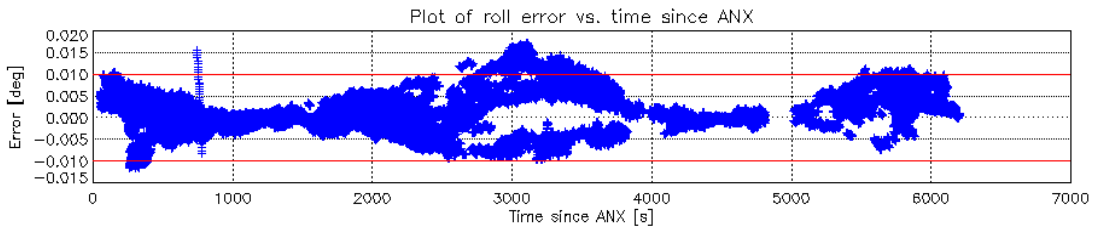
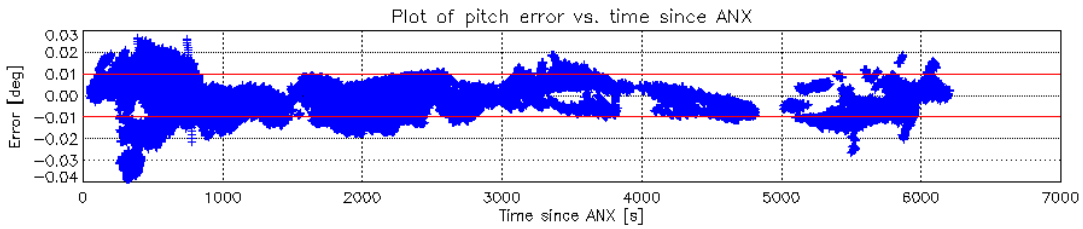
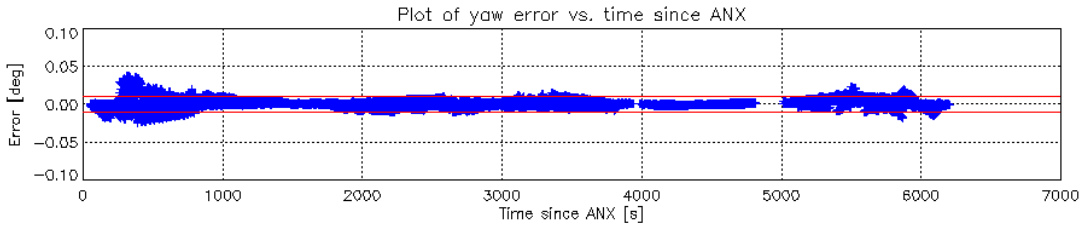


Cycles 55 & 56

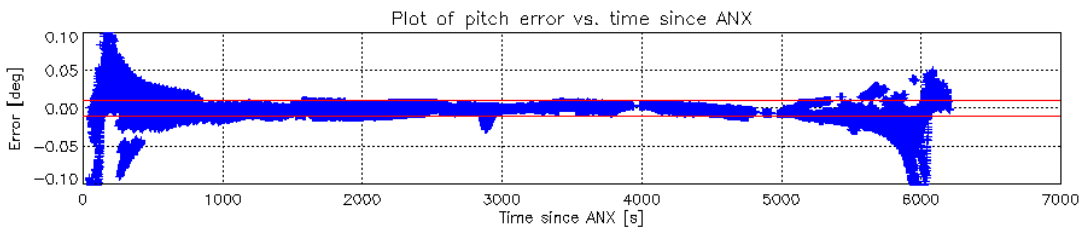
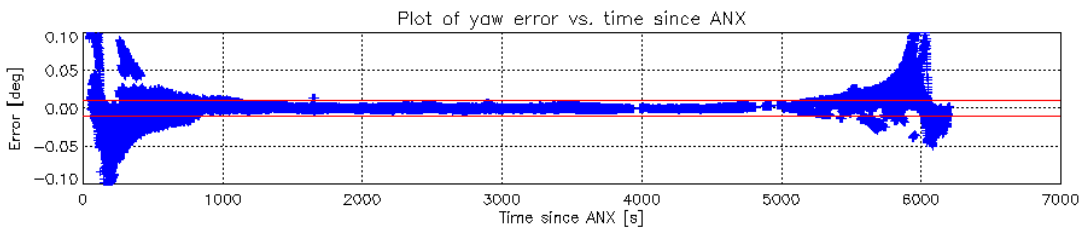


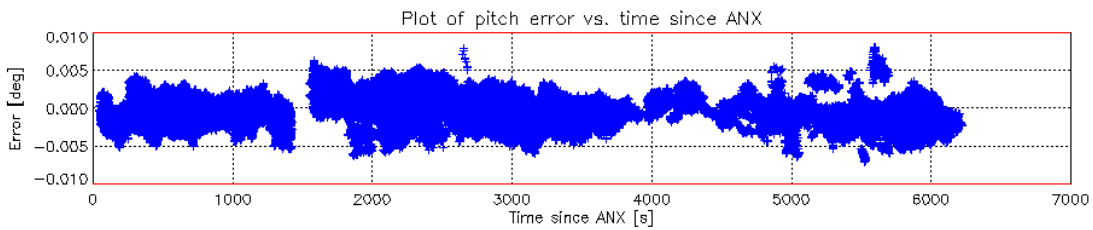
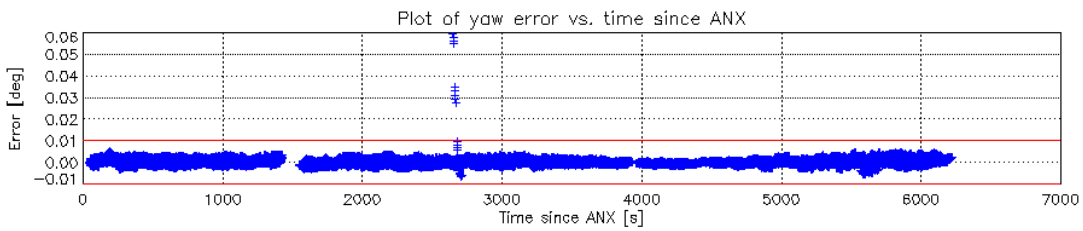
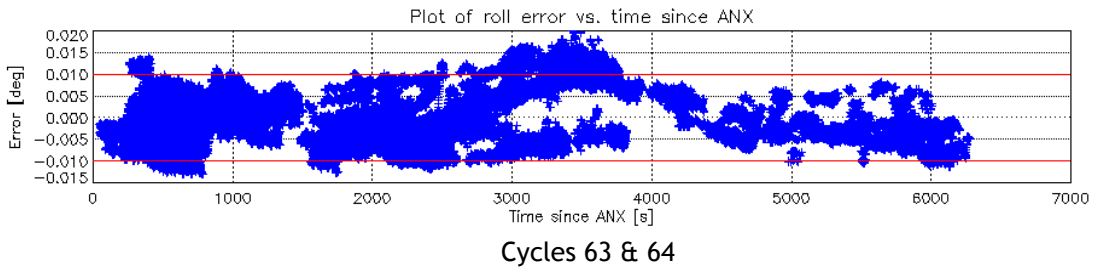
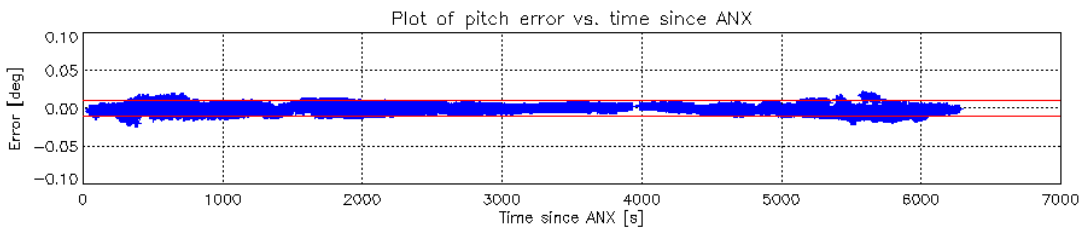
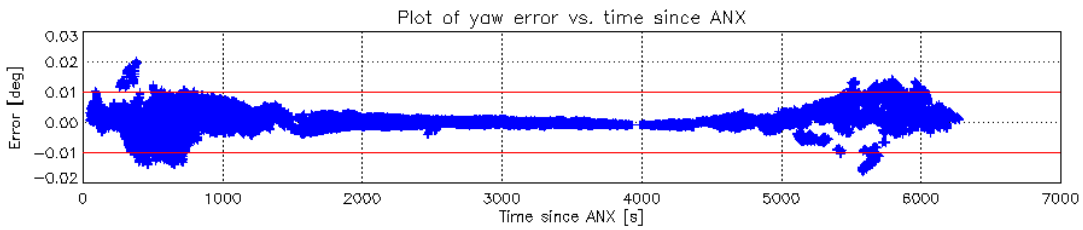
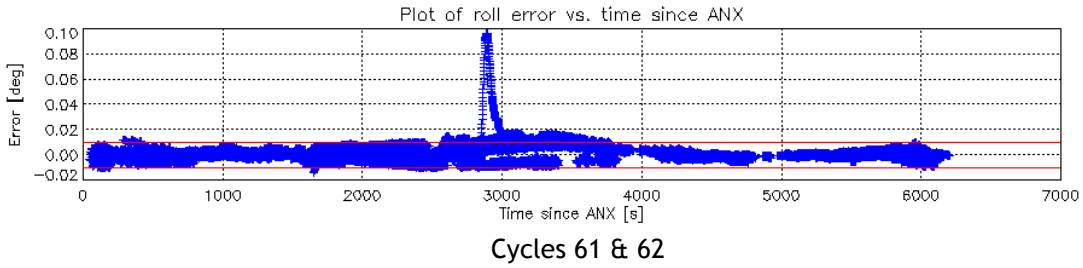


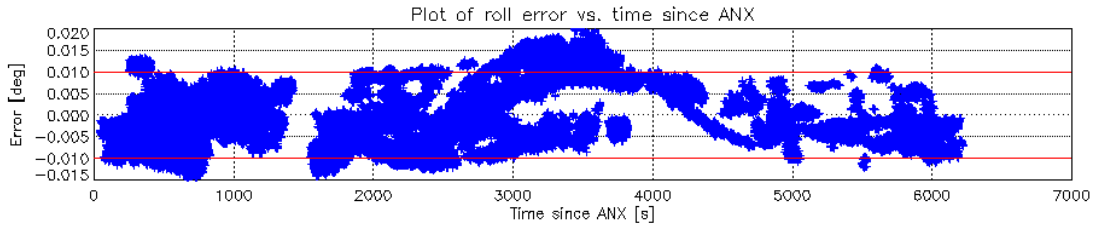
Cycles 57 & 58



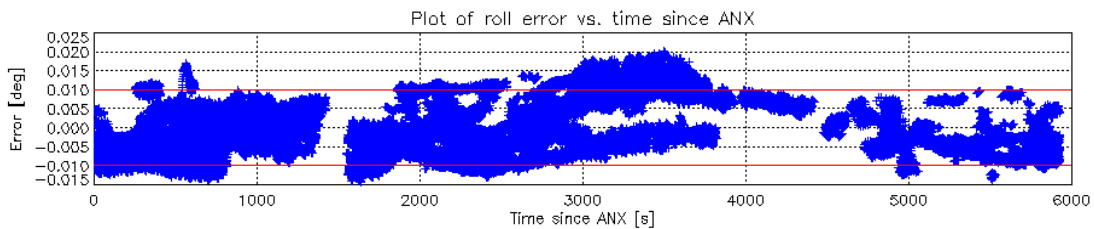
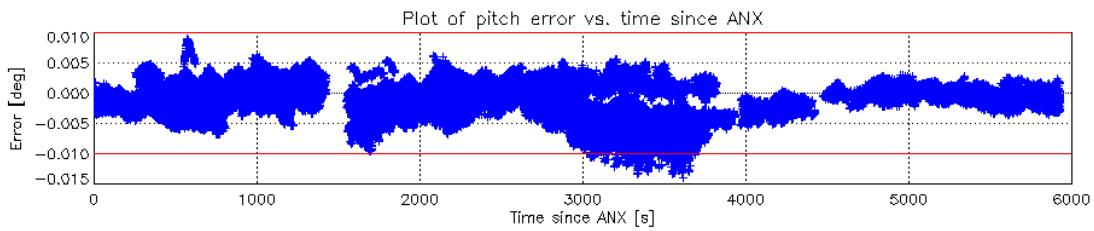
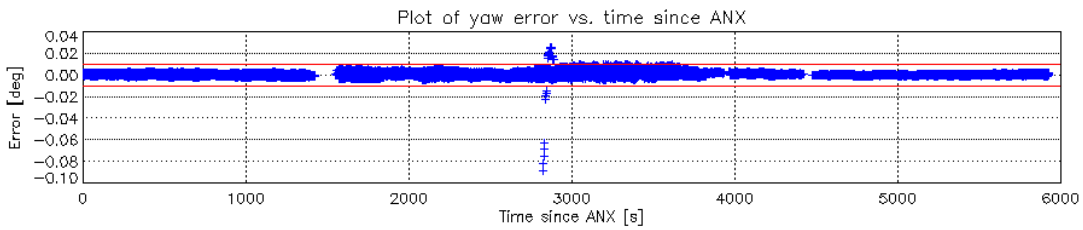
Cycles 59 & 60







Cycles 65 & 66



Cycles 67 & 68